Supporting Information for

A Pd_4L_2 Cage Containing Brønsted-Base Active Sites for One-Pot Photooxidation/Knoevenagel Condensation Reaction

Yan-Fang Zhou[a, b], Dan-Ni Yan[b], Shao-Jun Hu[b], Li-Peng Zhou[b], Li-Xuan Cai*[, a, b], Qing-Fu Sun*[, a, b]

a. College of Chemistry, Fuzhou University, Fuzhou 350108, People's Republic of China.

b. Fujian College, University of Chinese Academy of Sciences, State Key Laboratory of Structural Chemistry, Fujian Institute of Research on the Structure of Matter, Chinese Academy of Sciences, Fuzhou 350002, People's Republic of China.

Table of Content

1. Single crystal X-ray diffraction studies:

X-ray diffraction studies for cage **2** and ligand L^1 were carried out on micro-focus metaljet diffractometer using Ga Kα radiation (λ = 1.3405 Å). Data reduction was performed with the CrysAlisPro package.[S1] The structures were solved by direct method and refined by full-matrix least-squares on F^2 with anisotropic displacement using the SHELX software package.[S2] In these two case, solvent molecules were highly disordered and could not be reasonably located. These residual intensities were removed by PLATON/SQUEEZE routine. [S3]

Yellow block-shaped single crystals were obtained by vapor diffusion of THF into an aqueous solution of the complex cage **2** over two months. Since the crystals of cage **2** immediately lost solvent after removal from the mother liquor, rapid handling in the NVH oil prior to flash cooling was required to collect data. The crystals of this giant supramolecular assembly usually diffract very weekly in nature, and the crystals were small and subject to rapid beam damage during data collection on micro-focus metaljet diffractometer using Ga Kα radiation (λ = 1.3405 Å). Compared with the diffraction image at the first run, the diffraction image at the last run showed a significant drop-off in diffraction intensity after around 1.08 Å resolution, resulting in a low ratio of observed/unique reflections (or low redundancy) (Figure S71). The quality of single crystal is damaged by radiation. With increasing resolution, the data become weak and somewhat less accurate. At resolutions higher than 1.03 Å, the R_{int} values grow to be higher than 0.2. Even though we optimized the measurement based on synchrotron radiations, the data was not getting better. Considering that the overall completeness of 99% is fine and an average redundancy of 3.4 and merge R_{int} of 0.105 is acceptable (Table S2), we tried to refine the model. We removed unreasonable NO_3^- ions and remained only the SiF_6^{2-} ions. We also removed some of the rigid group constraints, such as AFIX 66, FLAT and EADP, as well as SADI restraint.

PLATON/SQUEEZE routine was used to remove the contribution of the electron density associated with the remaining anions and highly disordered solvents. This gave a total potential solvent accessible void of 9169 $Å^3$ per unit cell and a total of approximately 3885 electron count. In principle, co-existence of three types of anions are possible in the systems: NO_3^- introduced by the Pd salt, BF_4^- introduced by the pyridinium ligand, as well as SiF_6^{2-}, which is a consequence of decomposition of BF_4^- in water in the glass vial. After accounting for the unresolved anions (let's suppose they are six nitrates), the remaining masked electrons may correspond to 78 THF or 311 H_2O molecules per Pd_4L_2 cage, or more likely a mixture of these two solvents. Moreover, the crystals were found to be highly unstable and lost crystallinity quickly after they were token out from the mother liquor, TGA won't help to assess the nature of the SQUEEZED solvents in this case. In short, the identity of the masked anions and solvents could not be conclusively determined, these molecules were not included in the molecular formula. Consequently, the molecular weight and density given are underestimated.

Due to the limited resolution of the data for cage **2**, thermal parameter restraints (SIMU, DELU) were applied to some atoms of the framework and one SiF_6^{2-} to obtain the chemical-reasonable models and reasonable atomic displacement parameters. Due

to significant thermal motion within the structure, bond length of C4-C5 in tmenPd units were restrained to 1.54 Å by DFIX restraints. However even with these restraints, the U_{eq} values of the following atoms are larger than 0.15: C14_1, C17_1, C1_3, F7_7, Si1_8-F7_8, O3_10, and O4_10, all of which result from thermal motion (or minor unresolved disorder) of the framework. CheckCIF gives two alert level A and one alert level B errors. These alerts result from the poor diffraction ability of such a cage complex and the existence of a large amount of amorphous solvents and counter anions, or the ghost peaks near the palladium heavy atoms.

Single crystals of ligand L^1, suitable for X-ray crystallography, were obtained by vapor diffusion of ethyl acetate into a DMSO solution of ligand L^1 over one month. Few reflections at greater than 1.08 Å resolution were observed and the data were trimmed accordingly (Figure S72). As there were no significant diffractions at high angles, we decided to apply a high-resolution cutoff at 1.10 Å. The SQUEEZE function of PLATON was employed to remove the contribution of the electron density associated with highly disordered solvent, which gave a potential solvent accessible void of 329 $Å^3$ per unit cell an a total of approximately 71 electrons. Based on the squeeze calculation, about 7 water molecules in each unit cell are calculated. A plot showing F(obs) vs F(calc) has to be added. The refinement details are as follows: Two BF_4^- counter ions are refined in disorder with thermal parameter restraints (SIMU, DELU) to obtain reasonable atomic displacement parameters. EXYZ was used to constrain the two B atoms to share identical coordinates, and EADP was applied to constrain the two B atoms to have identical anisotropic displacement parameters. Due to significant thermal motion within the structure, bond lengths and angles within the ions were restrained to be similar to each other using SADI. However even with these restraints, the Ueq values of the fluorine atoms from BF_4^- are extremely large (U_{eq} = > 0.15), due to high thermal motion of the anions. CheckCIF then gave one alert level A error and two alert level B errors. These alerts all result from the limited resolution of the data (low resolution, low bond precision, and poor data/parameter ratio). The resolution of the data is poor even when we collected the data on micro-focus metaljet diffractometer using Ga radiation (wavelength = 1.3405 angstrom).

Crystal data for cage **2**: Formula $C_{224}H_{256}F_{30}N_{66}O_6Pd_8Si_5$ [+ solvent]. Space group $P2_1/c$, a = 19.77341(8) Å, b =58.059(2) Å, c = 18.5454(7) Å, V = 19340.8(14) $Å^3$, Z = 2, T = 100(2) K. Anisotropic least-squares refinement on 39474 independent merged reflections (Rint =0.1088) converged at residual wR_2 = 0.4092 for all data; residual R_1 = 0.1544 for 26022 observed data [I > 2σ (I)], and goodness of fit (GOF) =1.482. (CCDC number: 2246529)

Crystal data for ligand L^1: Formula $C_{43}H_{38}B_2F_8N_{13}O_{3.50}$. Space group *P*-1, a = 12.9685(6) Å, b =12.9815(6) Å, c = 15.4846(8) Å, V = 2315.6(2) $Å^3$, Z = 2, T = 293(2) K. Anisotropic least-squares refinement on 3799 independent merged reflections (R_{int} =0.0533) converged at residual wR_2 = 0.2684 for all data; residual R_1 = 0.0855 for 2863 observed data [$I > 2\sigma(I)$], and goodness of fit (GOF) =1.070. (CCDC number: 2246530)

2. Supplemental figures for synthesis of ligands and assemblies

2.1 Synthesis of ligand L^1

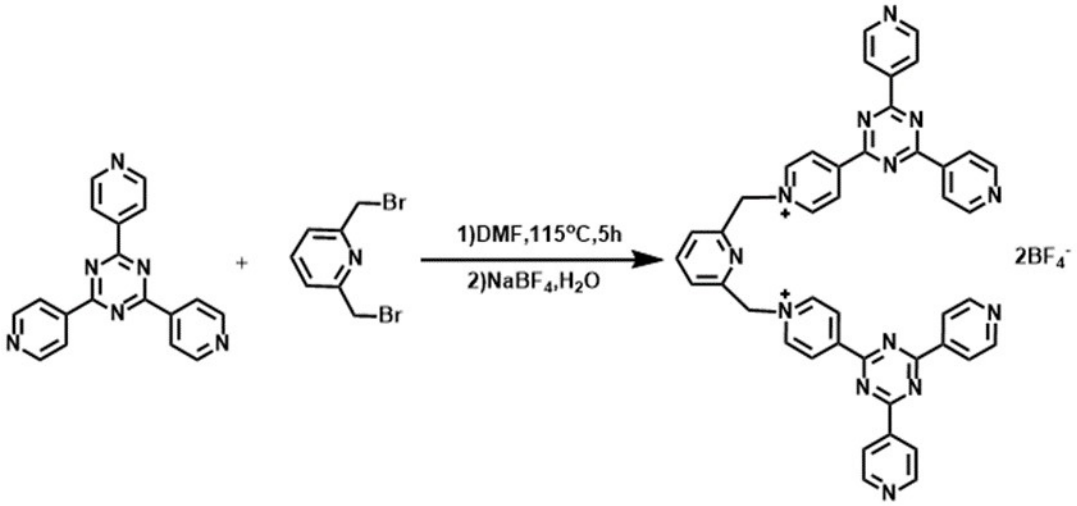

Scheme S1. Synthesis of ligand $L^1 \cdot (BF_4)_2$.

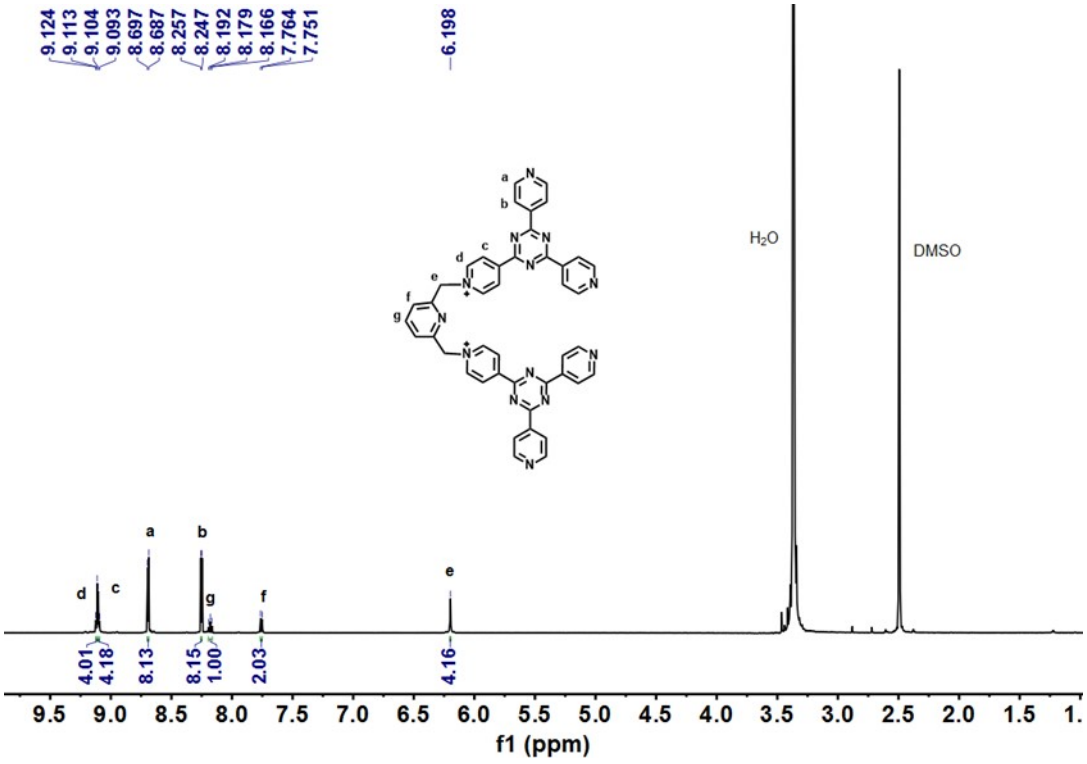

Figure S1. ^{1}H NMR spectrum (600 MHz, DMSO-d_6, 298 K) of $L^1 \cdot (BF_4)_2$.

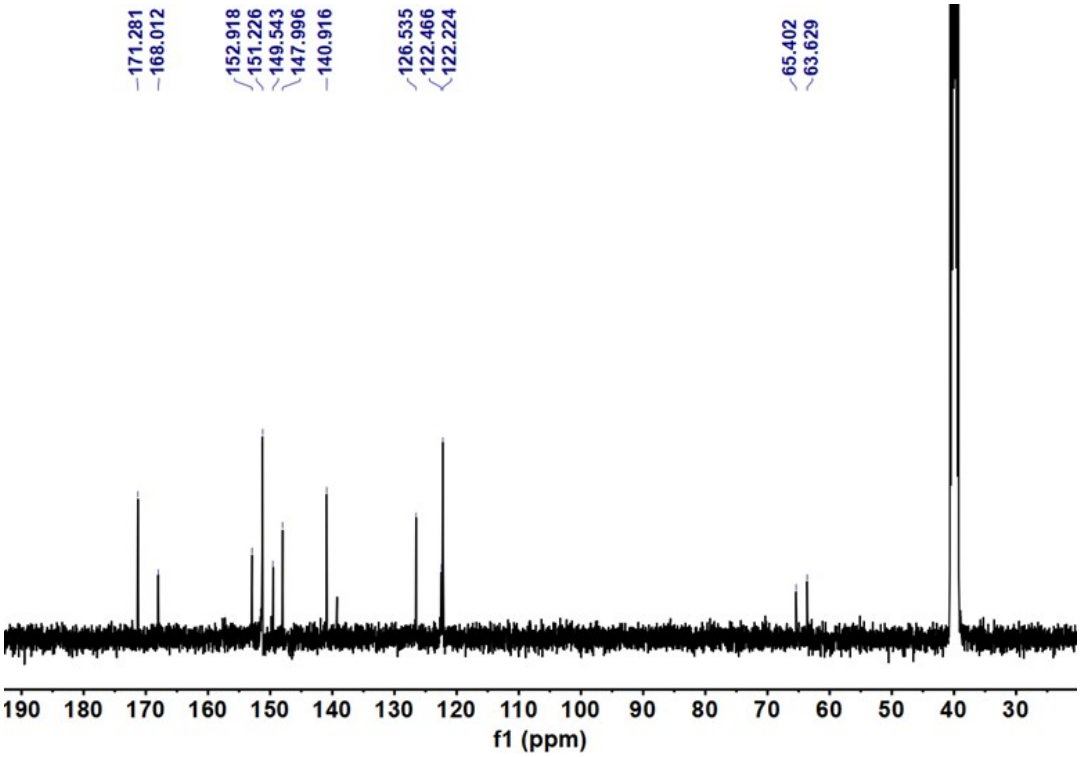

Figure S2. ^{13}C NMR spectrum (101 MHz, DMSO-d_6, 298 K) of ligand $L^1 \cdot (BF_4)_2$.

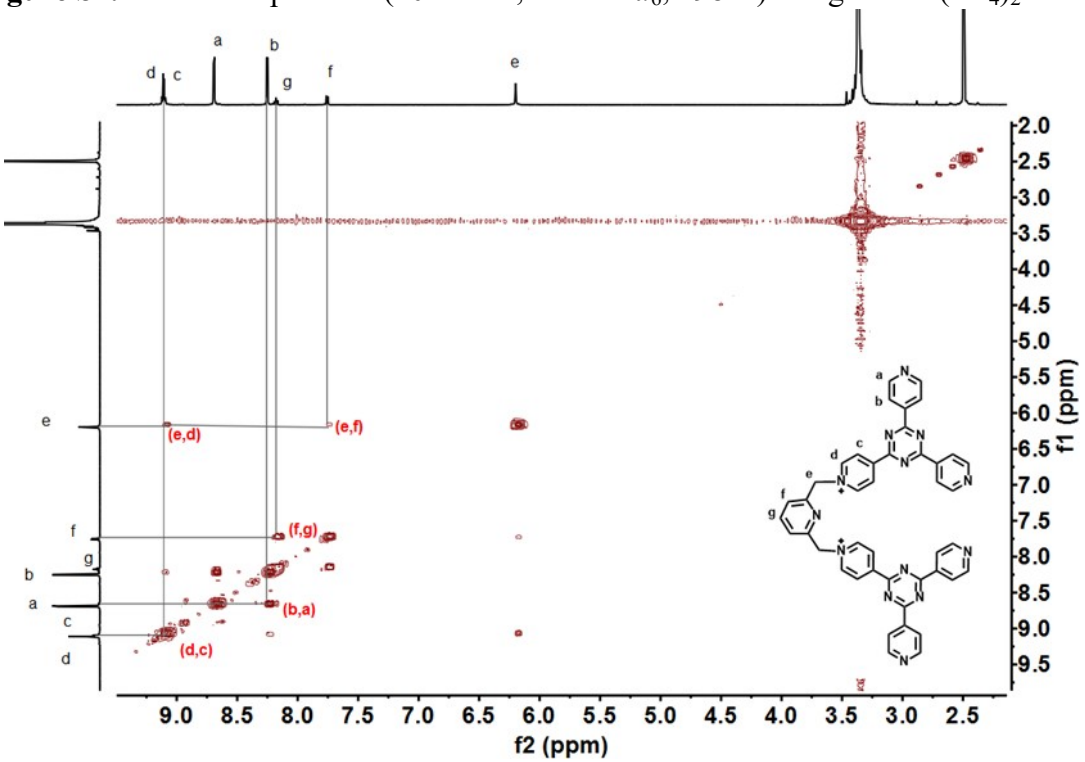

Figure S3. ^{1}H-^{1}H COSY NMR spectrum (600 MHz, DMSO-d_6, 298 K) of ligand $L^1 \cdot (BF_4)_2$.

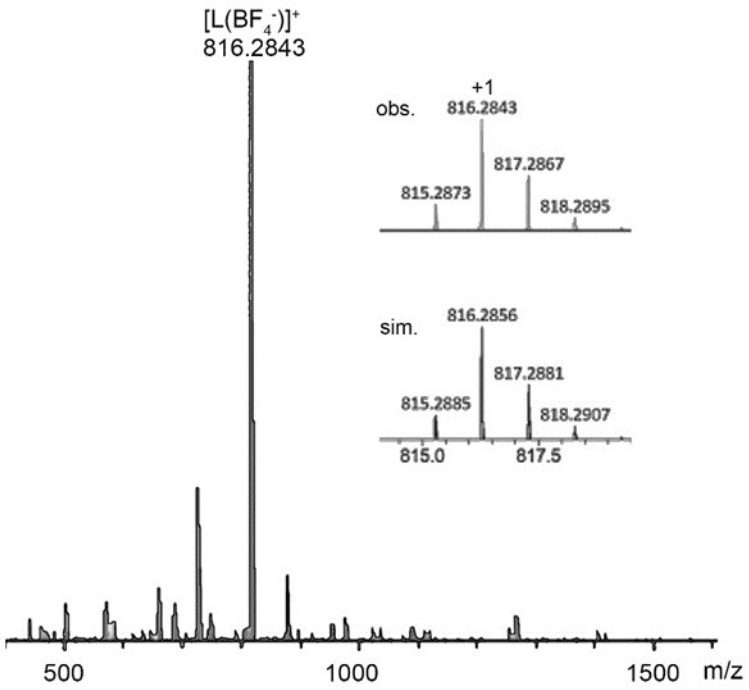

Figure S4. ESI-TOF-Mass spectrum of ligand $L^1 \cdot (BF_4)_2$; below: simulated and observed isotopic distribution of the 1+ peaks.

2.2 Synthesis of cage 1 ($Pd_4L^1_2$)

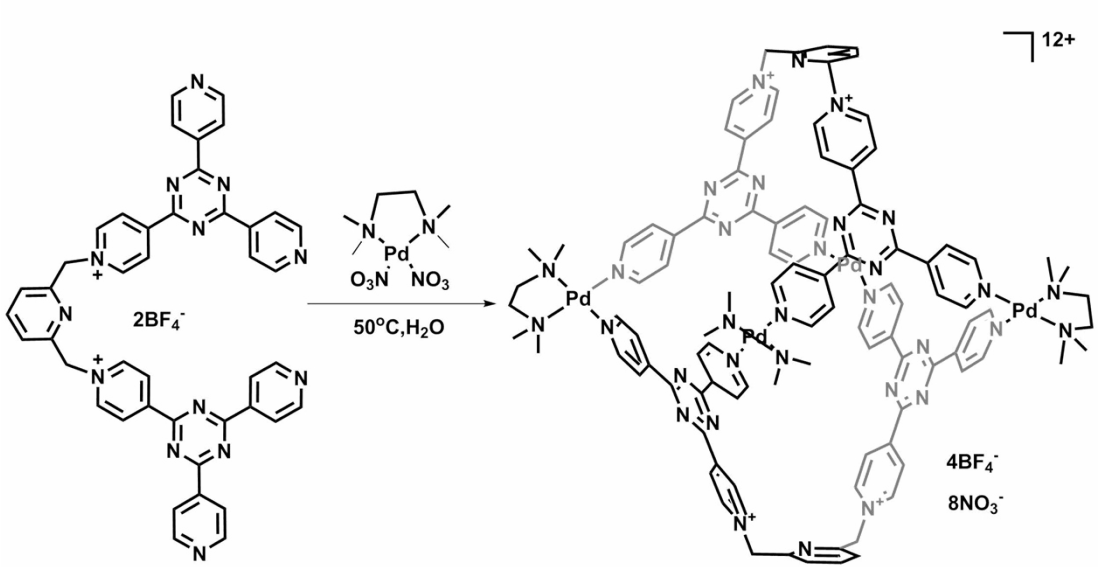

Scheme S2. The synthetic route of cage **1**.

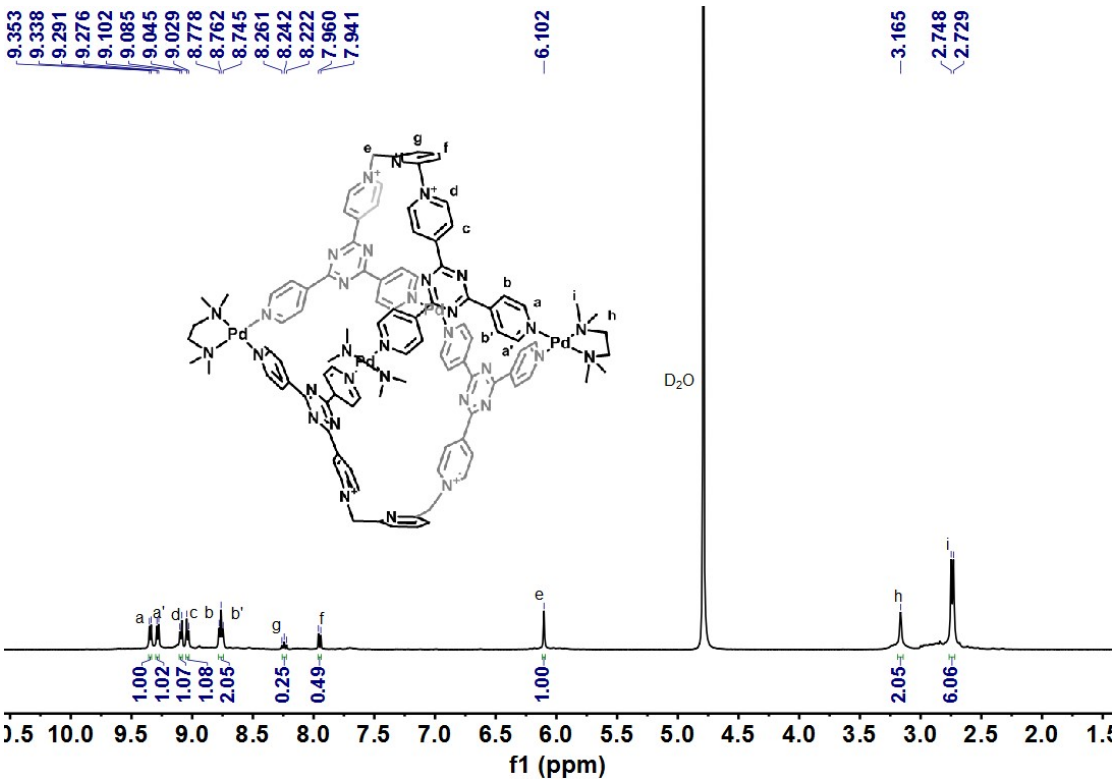

Figure S5. ^{1}H NMR spectrum (600 MHz, D_2O, 298 K) of cage **1**.

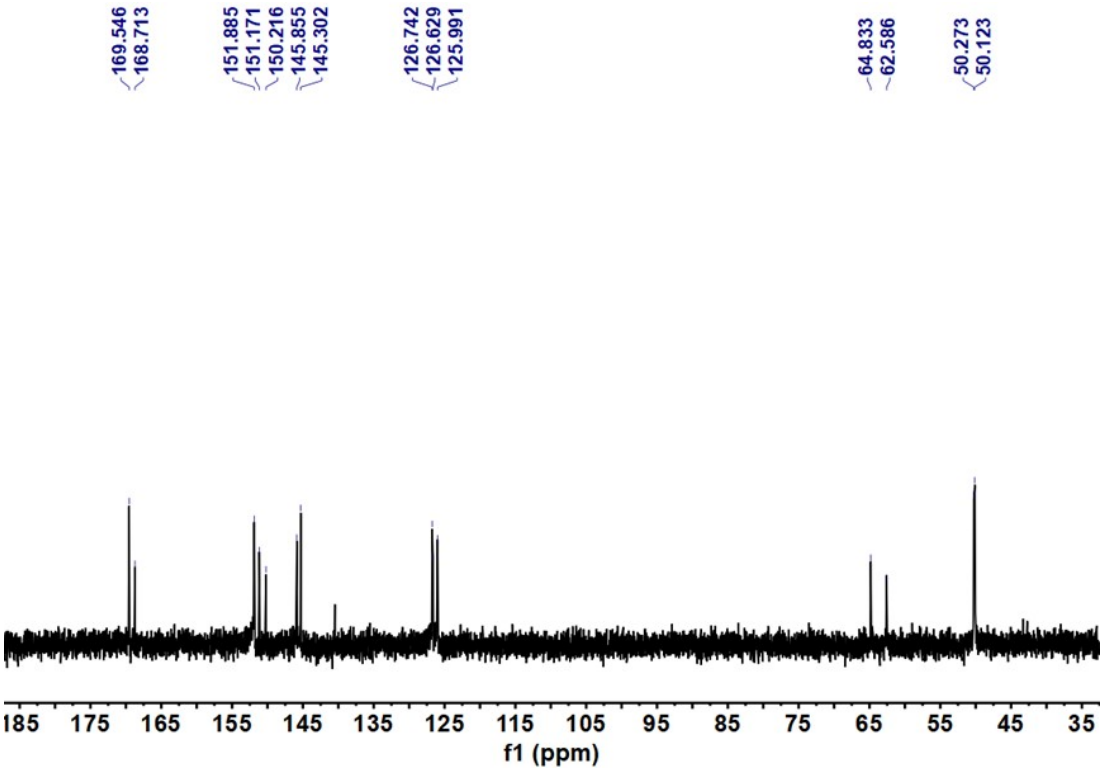

Figure S6. ^{13}C NMR spectrum (101 MHz, D_2O, 298 K) of cage **1**.

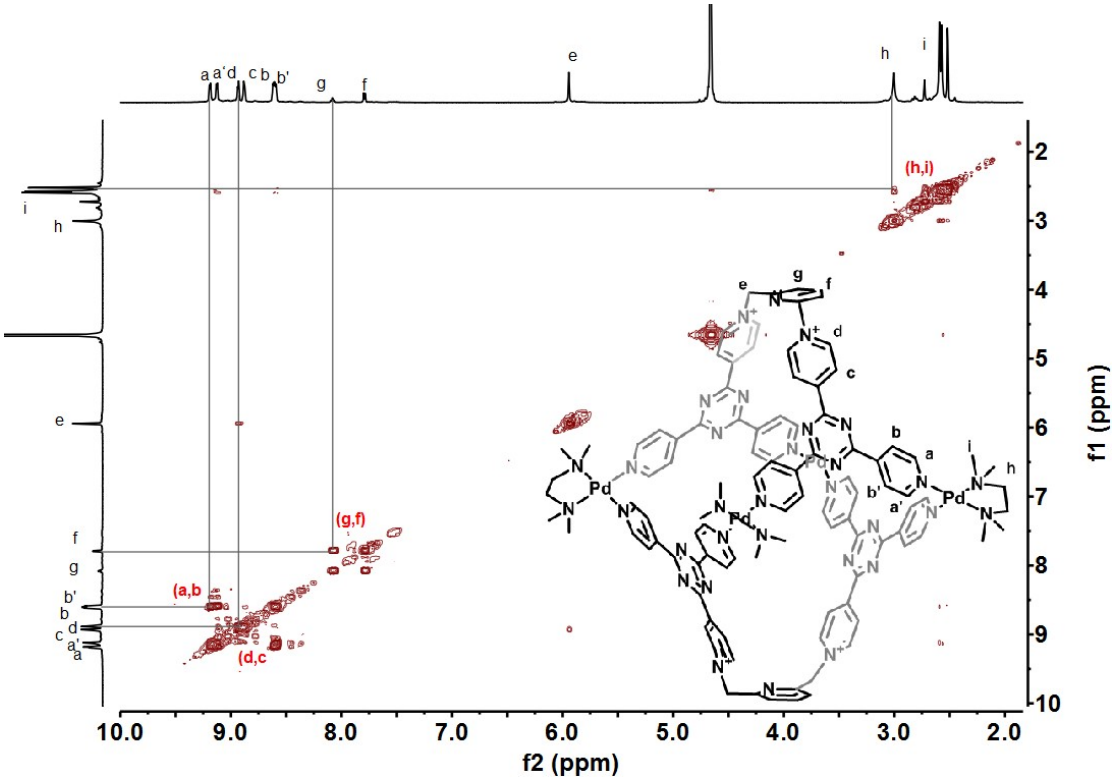

Figure S7. ^{1}H-^{1}H COSY NMR spectrum (600 MHz, D_2O, 298 K) of cage **1**.

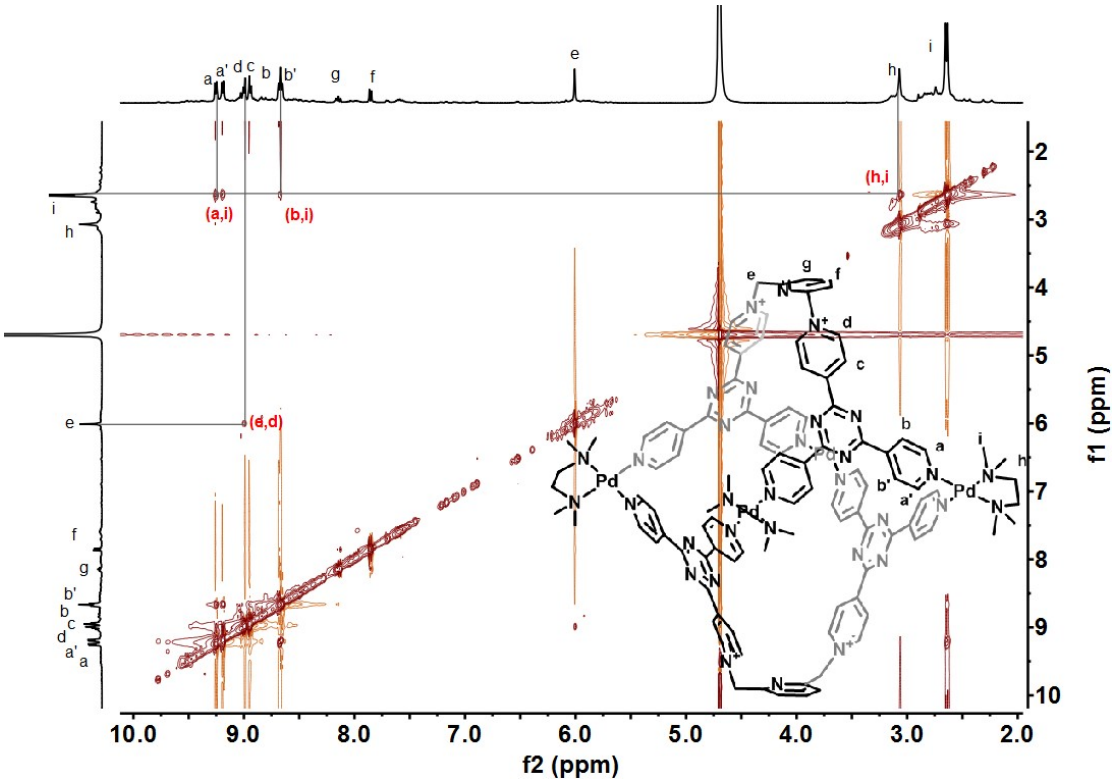

Figure S8. ^{1}H-^{1}H NOESY NMR spectrum (600 MHz, D_2O, 298 K) of cage **1**.

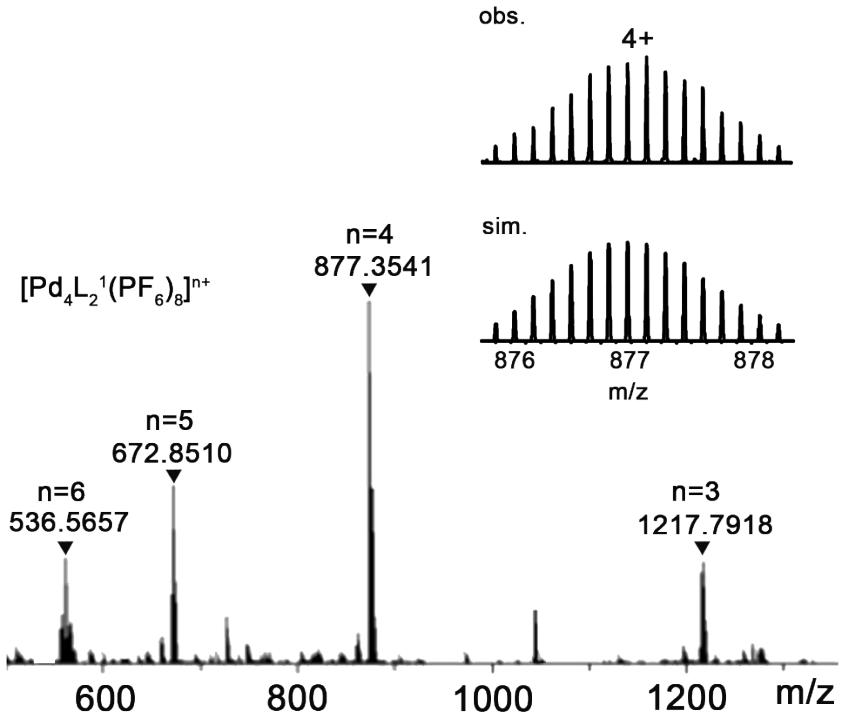

Figure S9. The ESI-TOF-Mass spectrum of cage **1**·$(PF_6)_{12}$ with inset showing the observed (Obs.) and simulated (Sim.) isotopic distribution of the 4+ peaks.

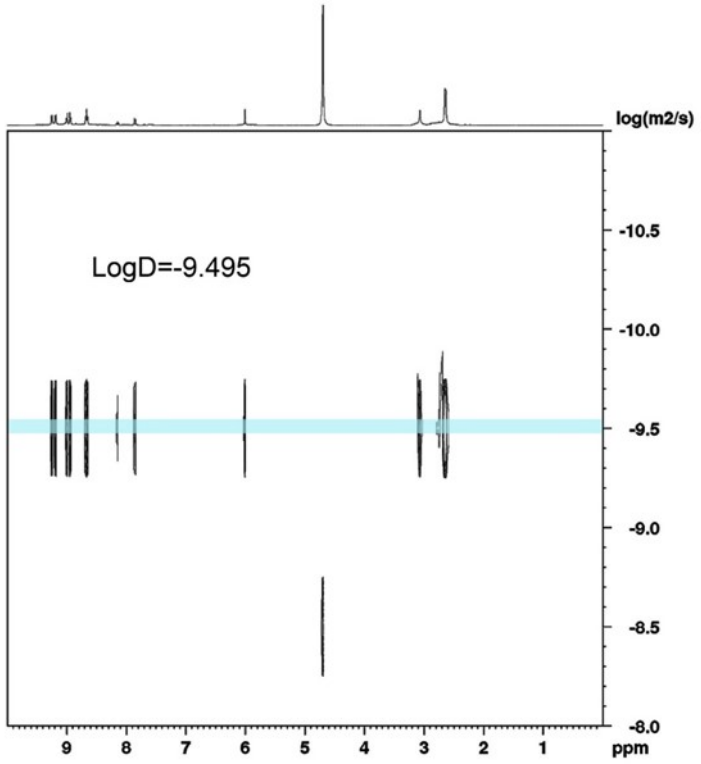

Figure S10. ^{1}H DOSY spectrum (400 MHz, D_2O, 298 K) of cage **1**. (Diffusion Constant = 3.20E^{-10} m^2/S, d = 1.53 nm)

2.3 Synthesis of ligand L^2

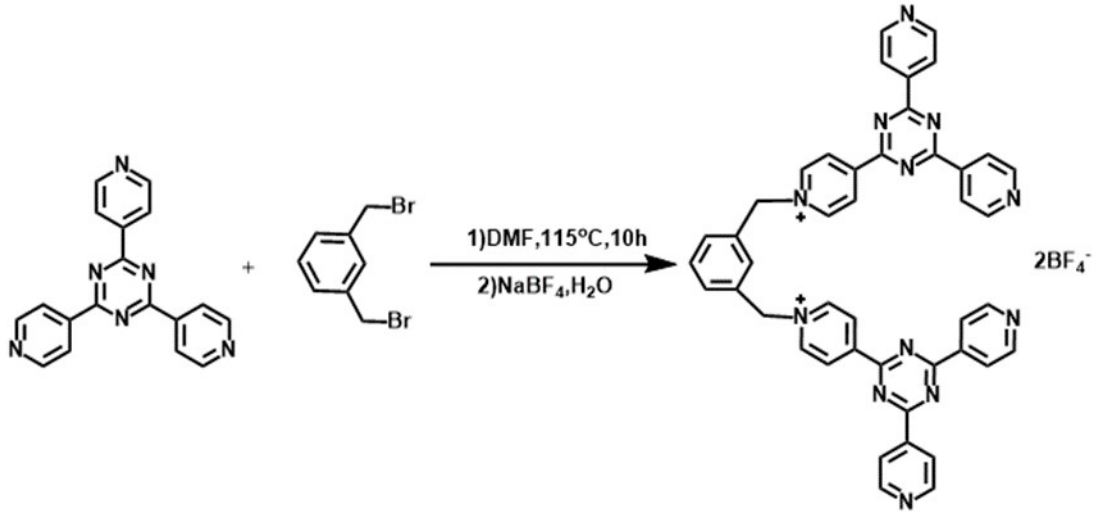

Scheme S3. Synthesis of ligand $L^2 \cdot (BF_4)_2$.

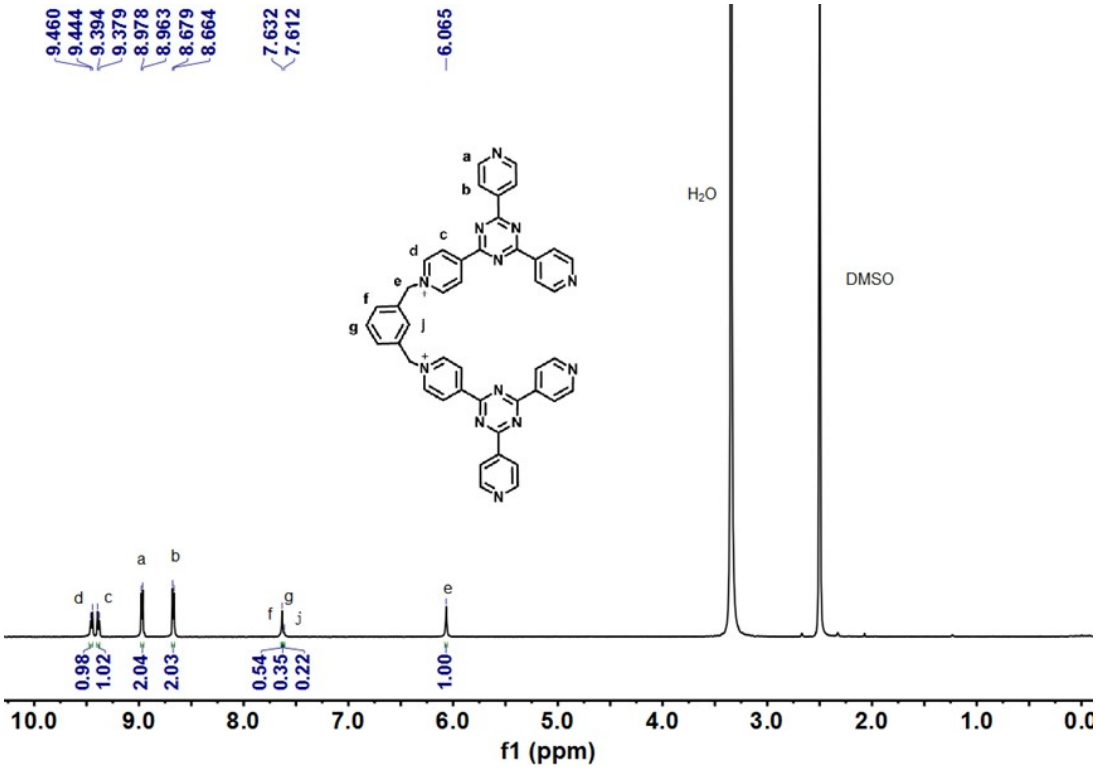

Figure S11. ^{1}H NMR spectrum (600 MHz, DMSO-d_6, 298 K) of $L^2 \cdot (BF_4)_2$.

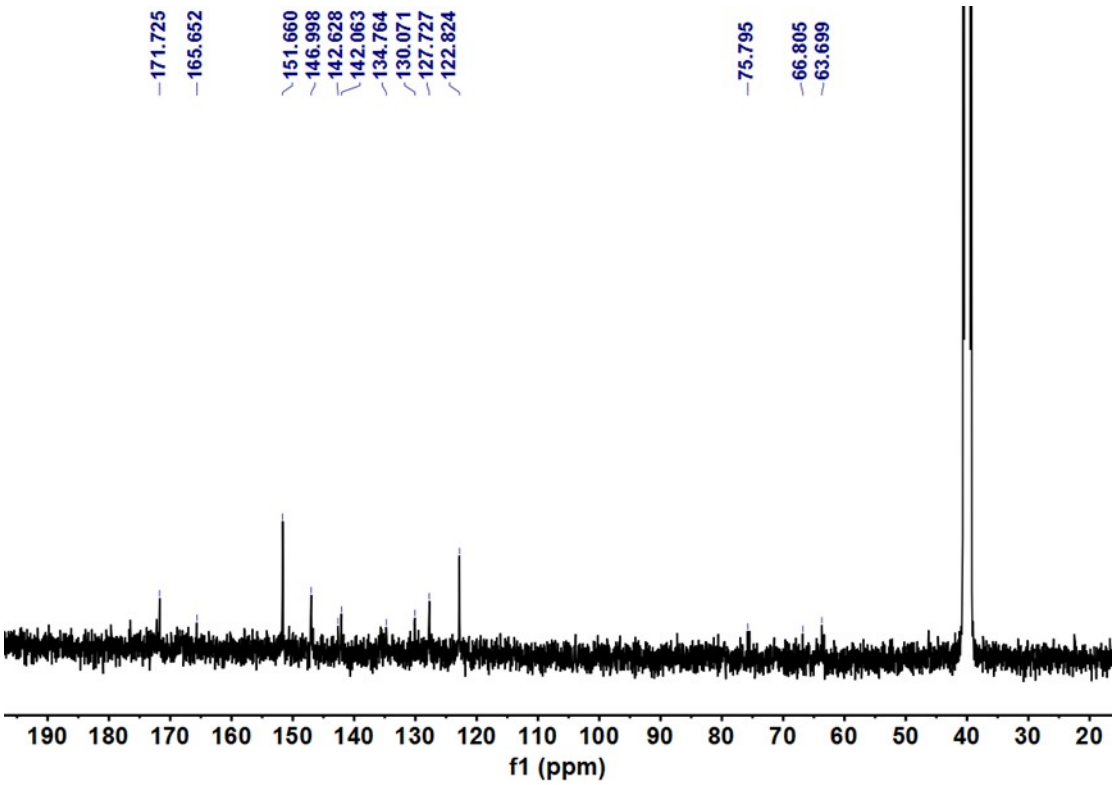

Figure S12. ^{13}C NMR spectrum (101 MHz, DMSO-d_6, 298 K) of ligand $L^2 \cdot (BF_4)_2$.

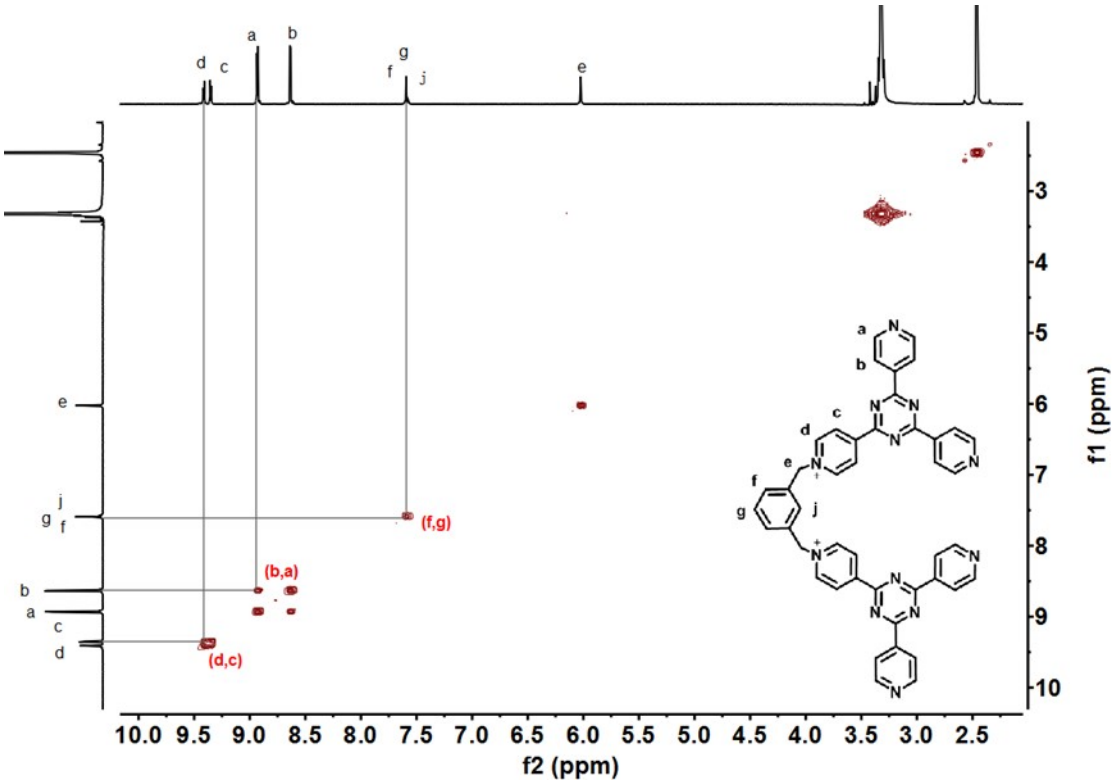

Figure S13. ^{1}H-^{1}H COSY NMR spectrum (600 MHz, DMSO-d_6, 298 K) of ligand $L^2 \cdot (BF_4)_2$.

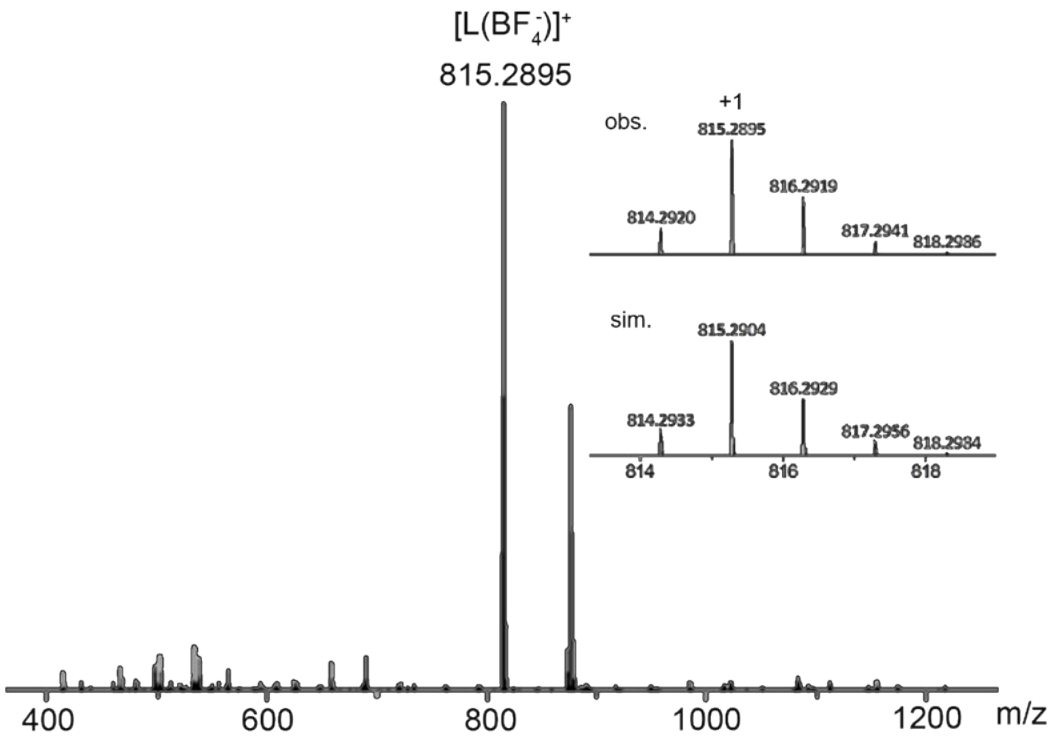

Figure S14. Top: ESI-TOF-Mass spectrum of ligand $L^2 \cdot (BF_4)_2$; below: simulated and observed isotopic distribution of the 1+ peaks.

2.4 Synthesis of cage 2 ($Pd_4L^2_2$)

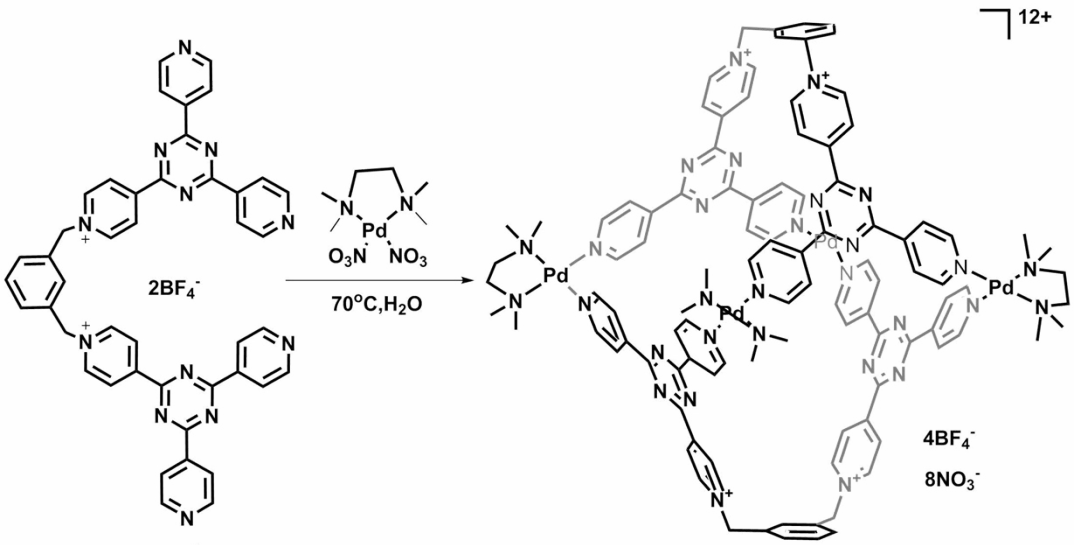

Scheme S4. The synthetic route of cage **2**.

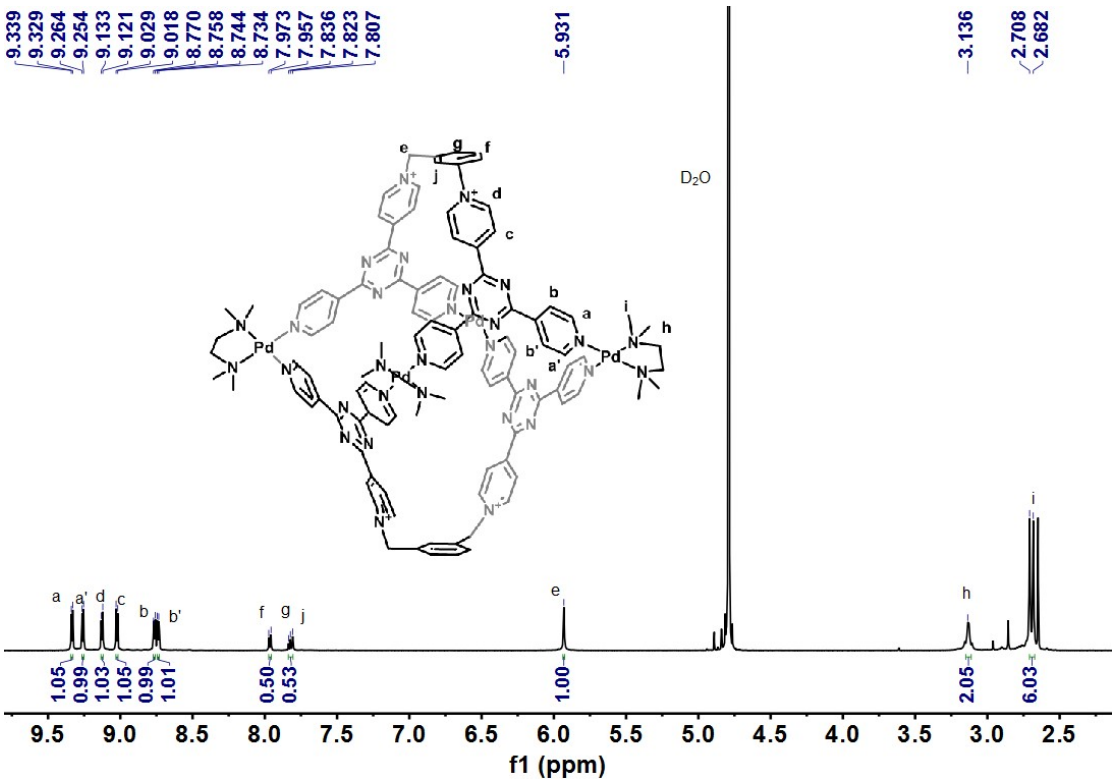

Figure S15. ^{1}H NMR spectrum (400 MHz, D_2O, 298 K) of cage **2**.

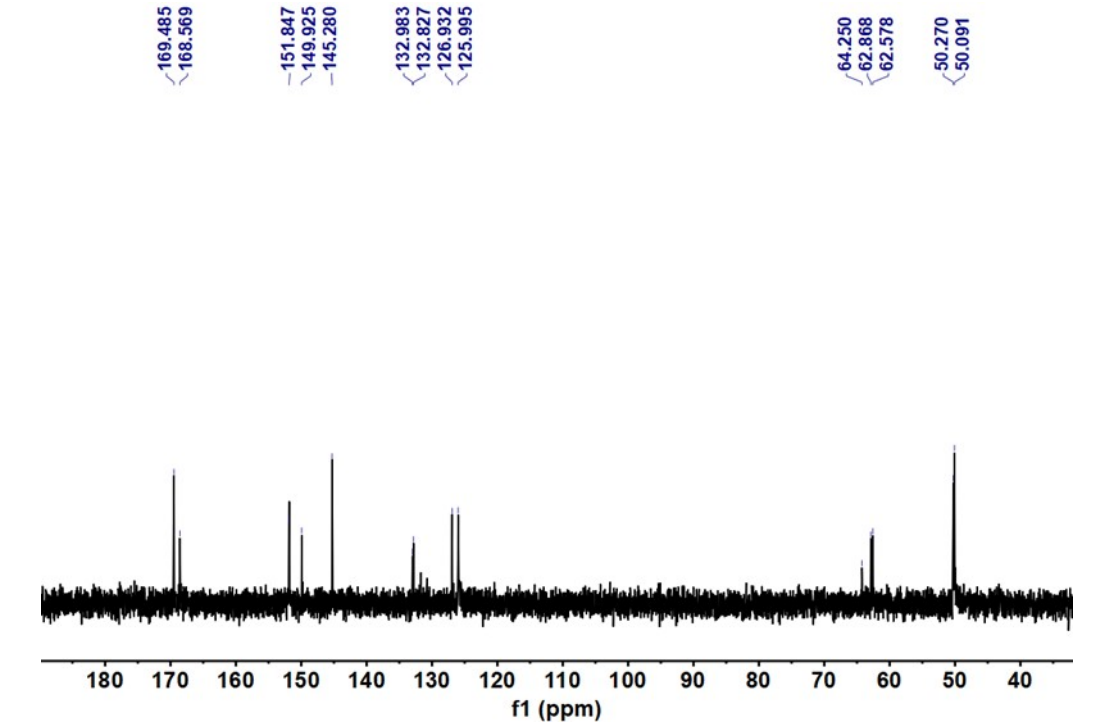

Figure S16. ^{13}C NMR spectrum (101 MHz, D_2O, 298 K) of cage **2**.

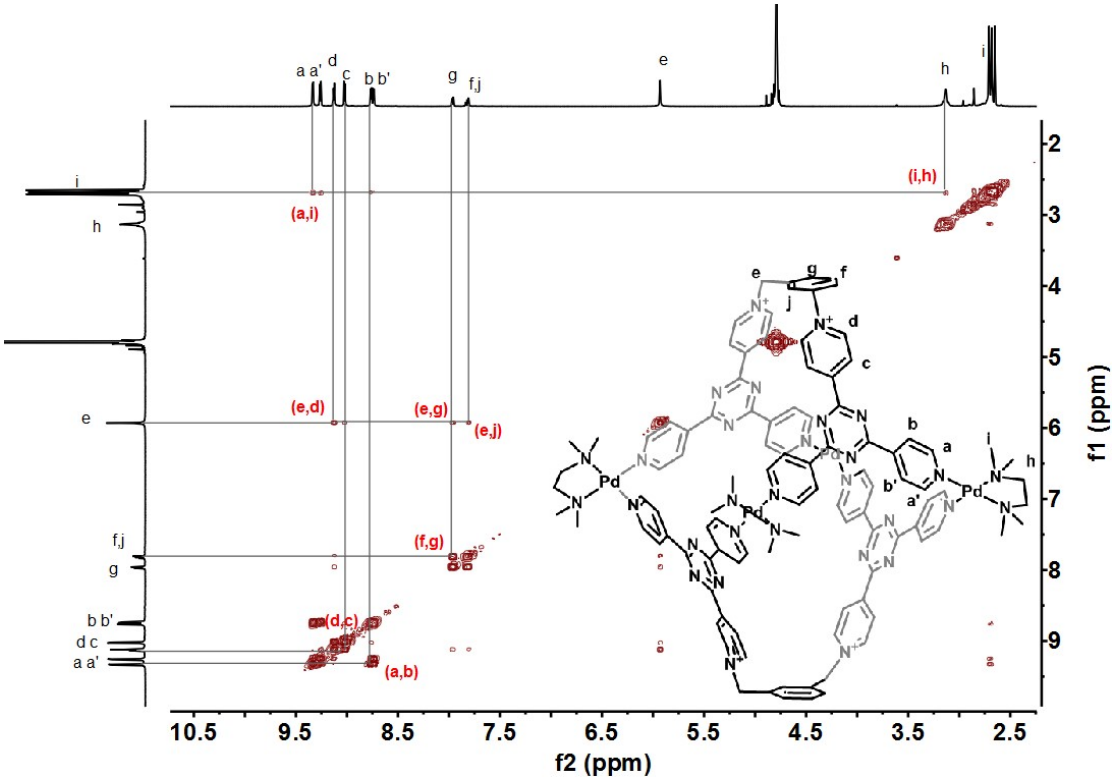

Figure S17. ^{1}H-^{1}H COSY NMR spectrum (600 MHz, D_2O, 298 K) of cage **2**.

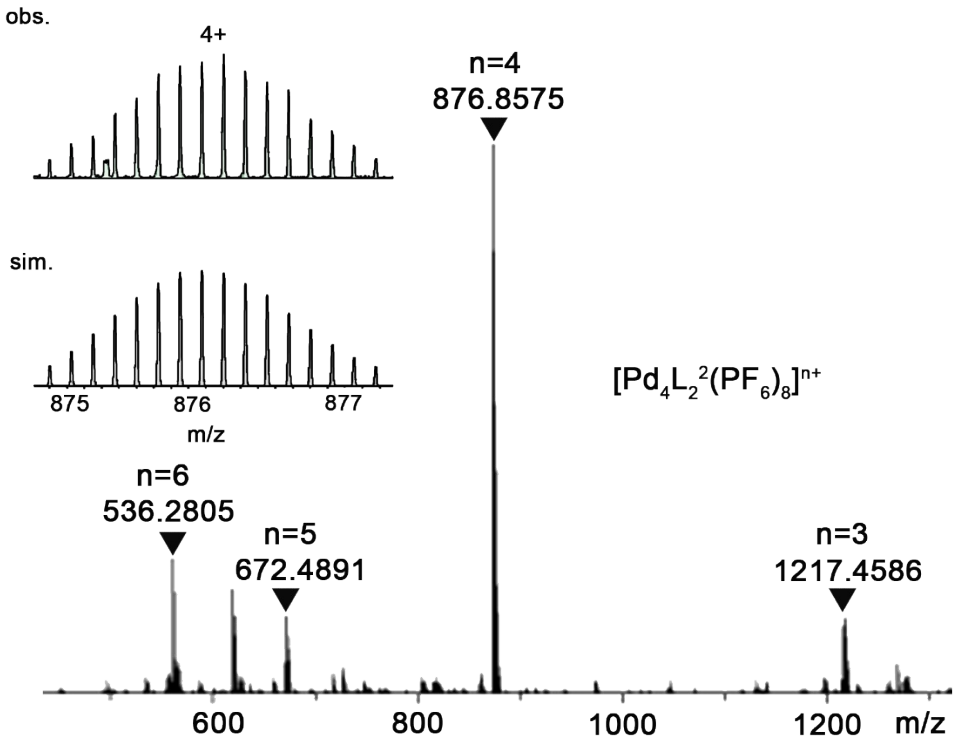

Figure S18. The ESI-TOF-Mass spectrum of cage **2**·$(PF_6)_{12}$ with inset showing the observed (Obs.) and simulated (Sim.) isotopic distribution of the 4+ peaks.

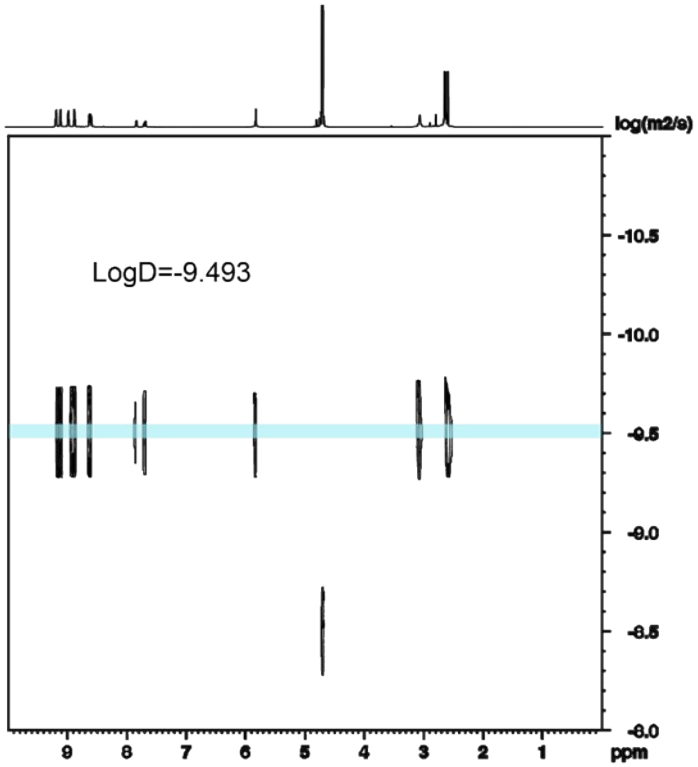

Figure S19. ^{1}H DOSY spectrum (400 MHz, D_2O, 298 K) of cage **2**. (Diffusion Constant = 3.21E^{-10} m^2/S, d = 1.52 nm)

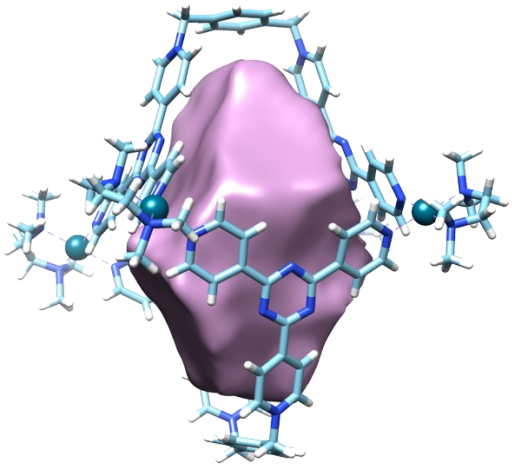

View Volume in Jmol

Volume Information	
Voxel size:	0.5 Å
Volume:	806 Å^3
Surface area:	694 Å^2
Sphericity, Ψ:	0.60
Effective radius:	3.49 Å
Center of Mass:	(-24.4, -20.8, -19.1) Å

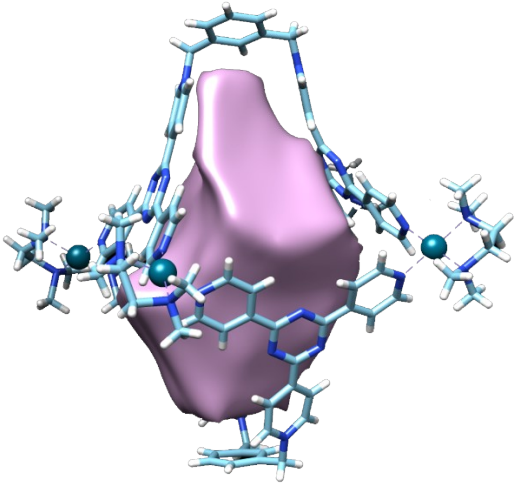

View Volume in Jmol

Volume Information	
Voxel size:	0.5 Å
Volume:	834 Å^3
Surface area:	892 Å^2
Sphericity, Ψ:	0.48
Effective radius:	2.80 Å
Center of Mass:	(-18.3, -18.7, -15.7) Å

Figure S20. The crystal structures of the cage previously reported (left) and cage **2** (right). And their corresponding cavity shapes and volumes. (Coordinates from the crystal structures were used. The outer and inner probe radius were 10 Å and 0.2 Å, respectively.

3. Photophysical and redox properties of cage 1:

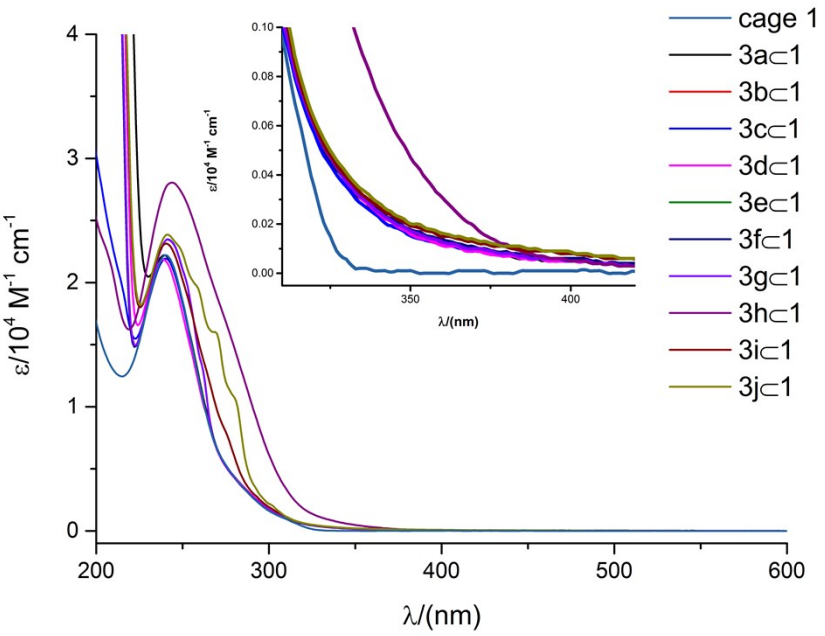

Figure S21. UV/Vis spectra of cage **1** and corresponding inclusion complex in H_2O.

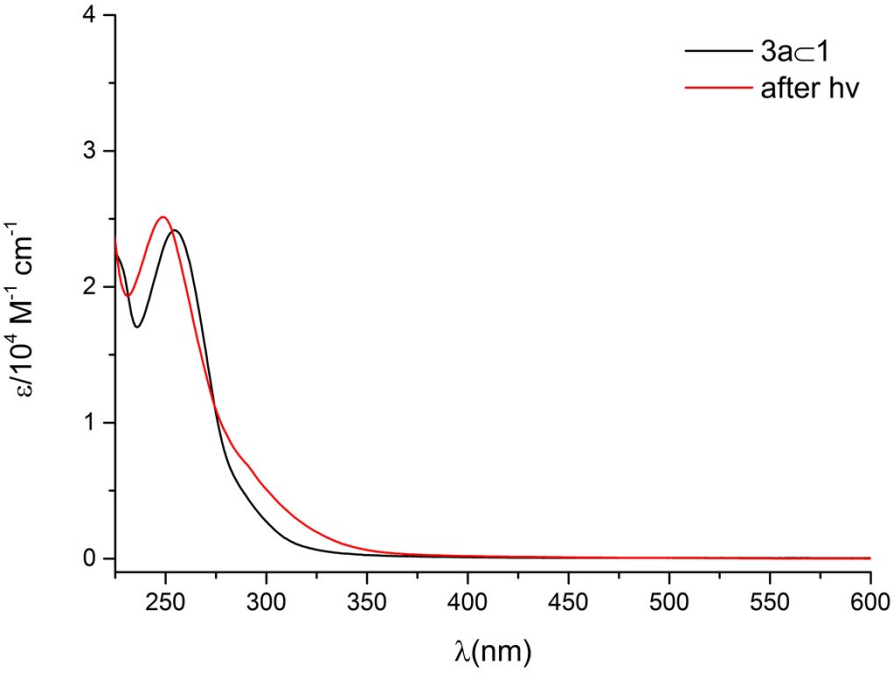

Figure S22. UV-vis absorption spectra of 10 equivalents of **3a** added to cage **1** in H_2O solution before (black line) and after (red line) irradiation.

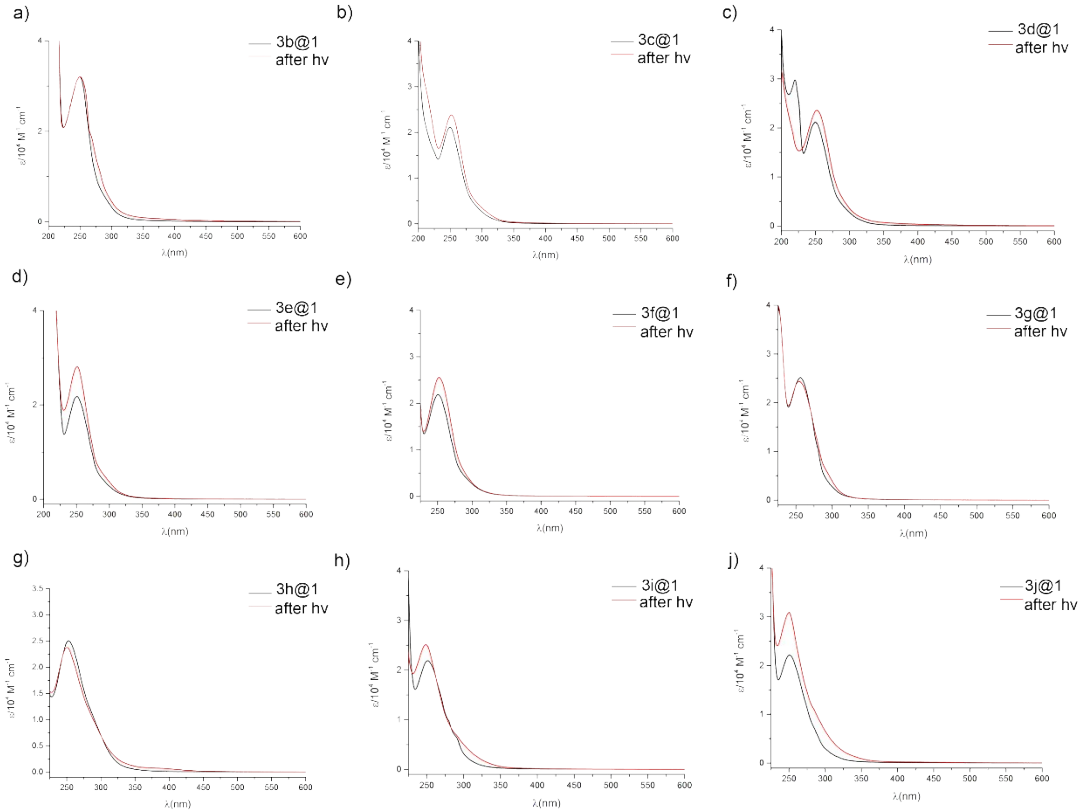

Figure S23.UV-vis absorption spectra of 10 equivalents of **3b-3j** added to cage **1** in H_2O solution before (black line) and after (red line) irradiation.

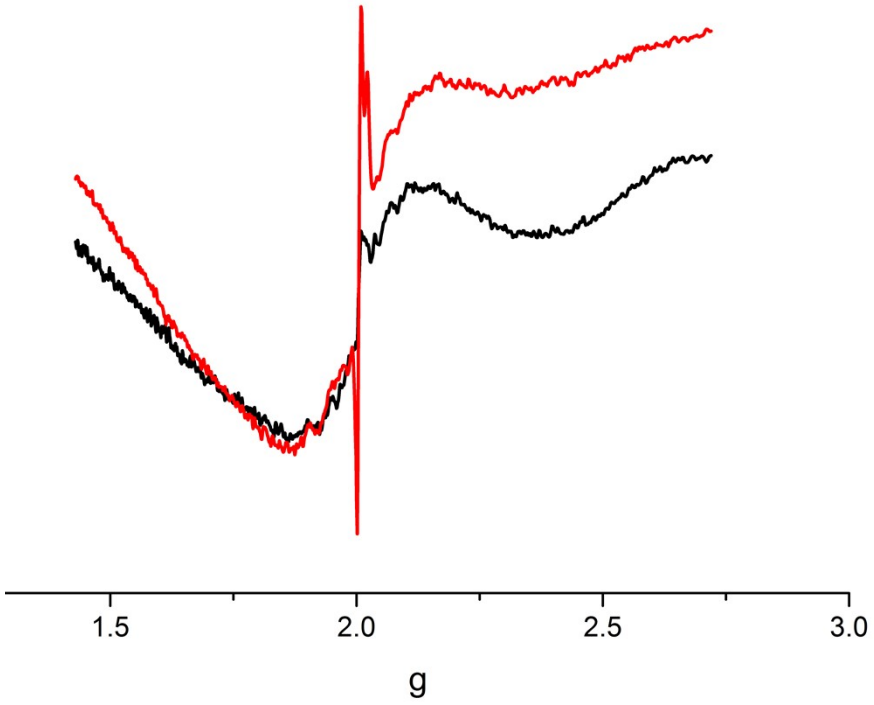

Figure S24. The ESR spectra (H_2O, 100 K) of **3i@1** before (black line) and after (red line) irradiation for 30 minutes (395 nm LEDs, 6 W) under nitrogen.

4. Procedure for photocatalysis experiment:

The photocatalytic reactivity of cage **1** was tested with (4-bromophenyl) methanol (**3a**), phenylmethanol (**3b**), (2-bromophenyl) methanol (**3c**), (4-chlorophenyl) methanol (**3d**), (3-chlorophenyl) methanol (**3e**), p-tolylmethanol (**3f**), (4-methoxyphenyl) methanol (**3g**), (4-nitrophenyl) methanol (**3h**), naphthalen-1-ylmethanol (**3i**), naphthalen-2-ylmethanol (**3j**), pyren-1-ylmethanol (**3k**) as substrates candidates. Generally, benzyl alcohols (10 equiv.) and malononitrile (excess) were added into the D_2O solution (1 mL) containing catalysts (0.001 mmol, 1.0 equiv.).This mixture solution was directly treated under purple LEDs ($\lambda > 395$ nm, 6 W) with a magnetic stirring bar in air at r.t. The reaction solution was monitored by thin layer chromatography method. After reaction, the products were extracted with CH_2Cl_2 (3×5 mL) which were dried under reduce pressure and subjected to ^1H NMR without further purification. The conversion and selectivity of Photooxidation-Knoevenagel condensation reactions of benzyl alcohols are determined using 1,3,5-trimethoxybenzene as the internal standard (0.003 mM).

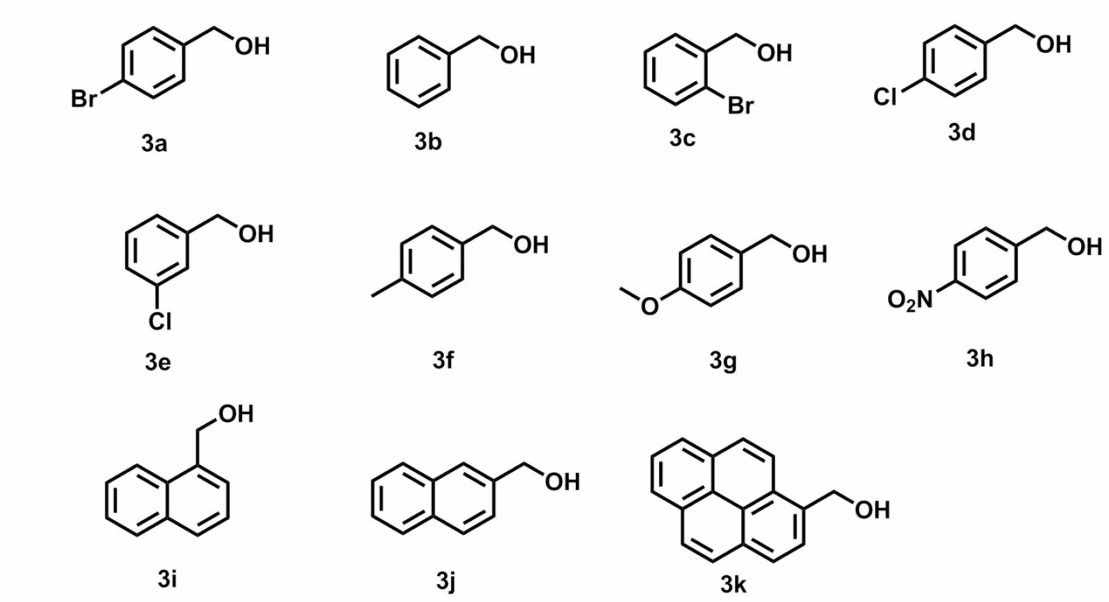

Scheme S5. The benzyl alcohol substrates scope selected for photooxidation-Knoevenagel condensation reactions.

4.1 The photocatalysis performance of cage 1.

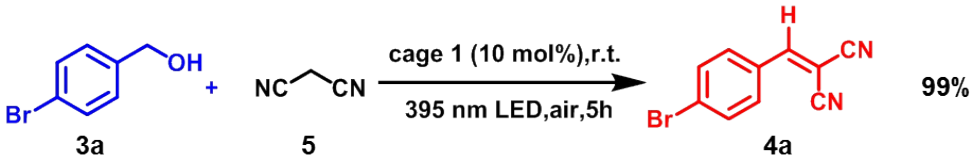

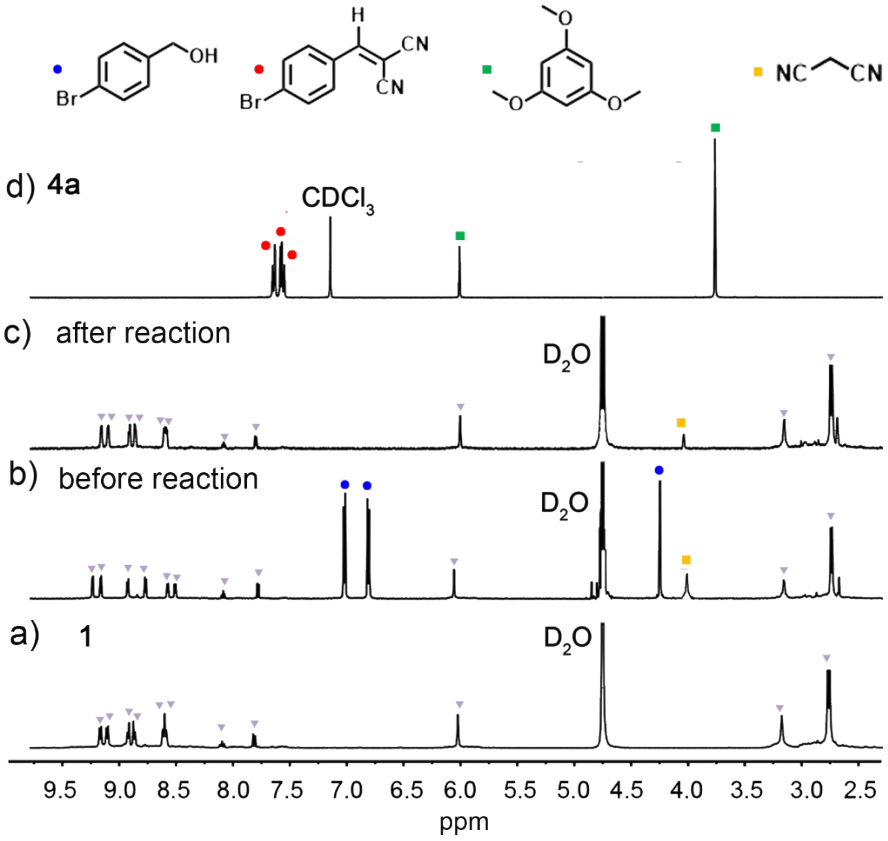

Figure S25. One-pot photooxidation/Knoevenagel condensation of **3a** with malononitrile (**5**) catalyzed by cage **1**. ^{1}H NMR spectra (400 MHz, D_2O, 298 K) of 1 mM cage **1** (a); after addition of **3a** and **5** to cage **1** (b); after sequential reaction for 5h. (c); crude product **4a** obtained by extraction and dissolved in $CDCl_3$ with 1,3,5-trimethoxybenzene as an internal standard (labelled by ■). The signals of were labelled with. The signals of cage **1, 3a** and product **4a** are labelled by ▲, ● and ●, respectively.

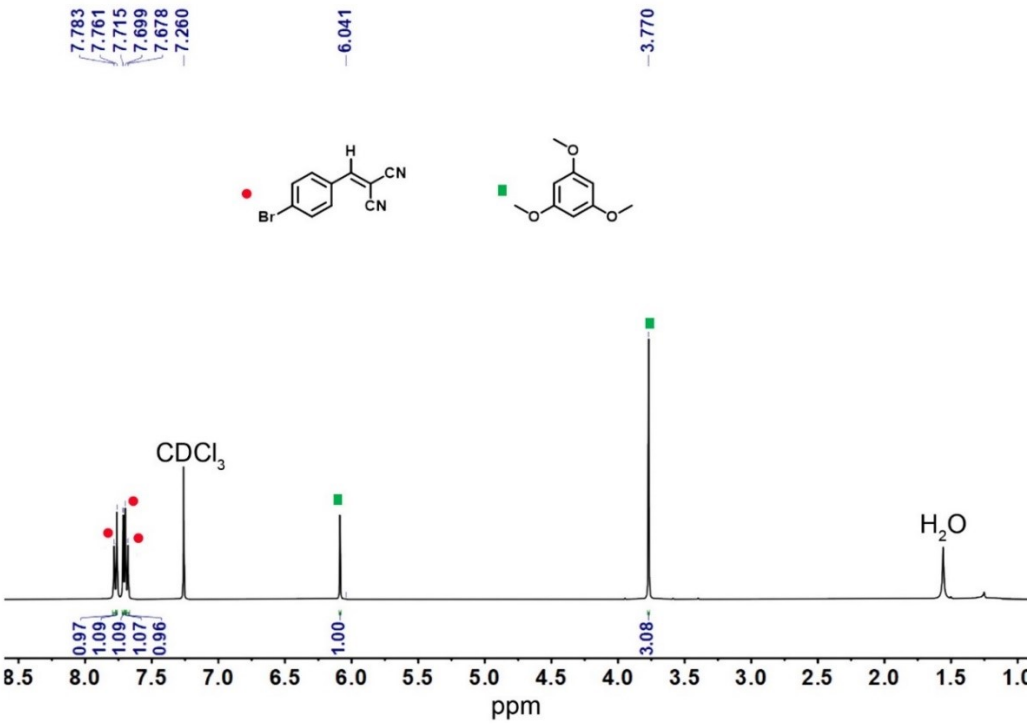

Figure S26. ^{1}H NMR spectrum (400 MHz, 298 K, $CDCl_3$) of the product **4a**, corresponding to entry 1 in table 1. 1,3,5-trimethoxybenzene was used as internal standard.

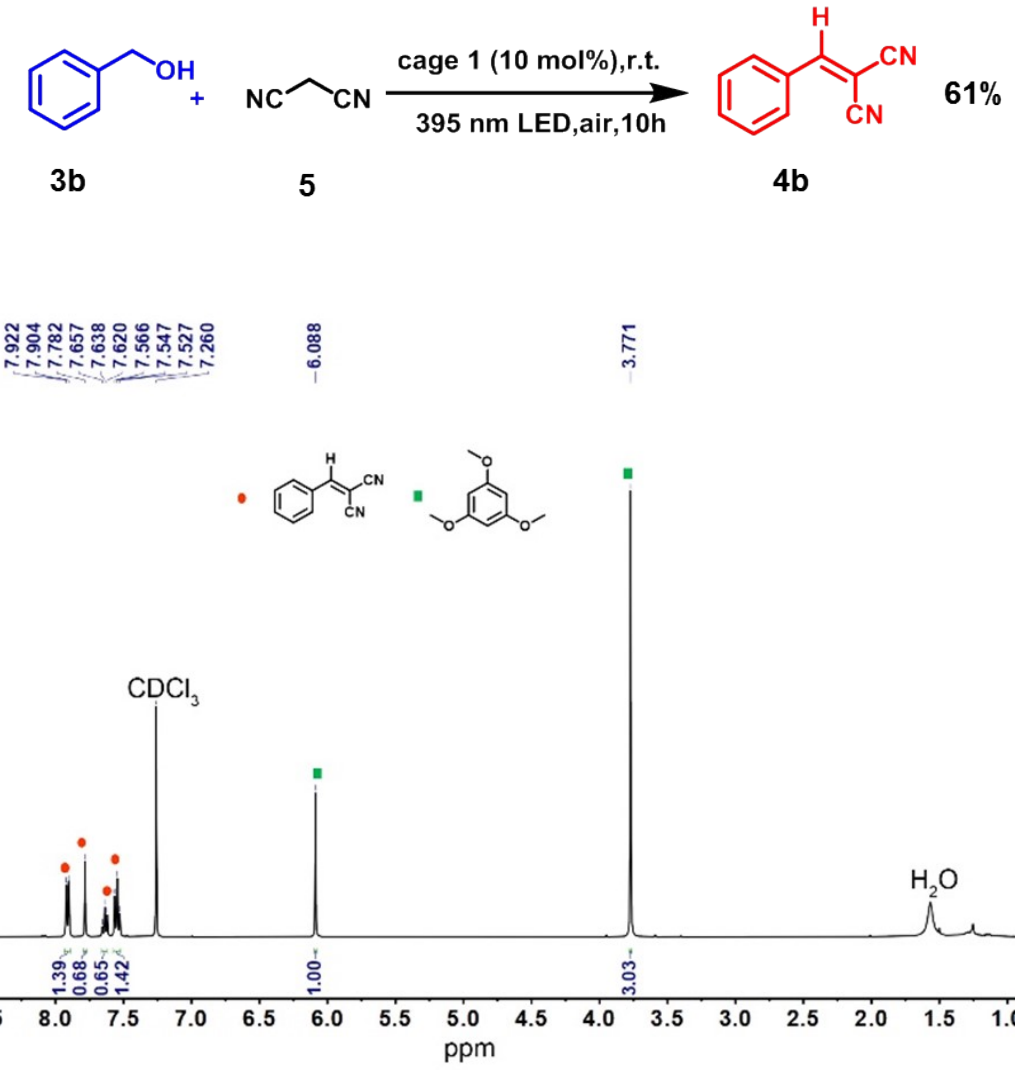

Figure S27. ^{1}H NMR spectra (400 MHz, 298 K, $CDCl_3$) of the product **4b**, corresponding to entry 8 in table 1. 1,3,5-trimethoxybenzene was used as internal standard.

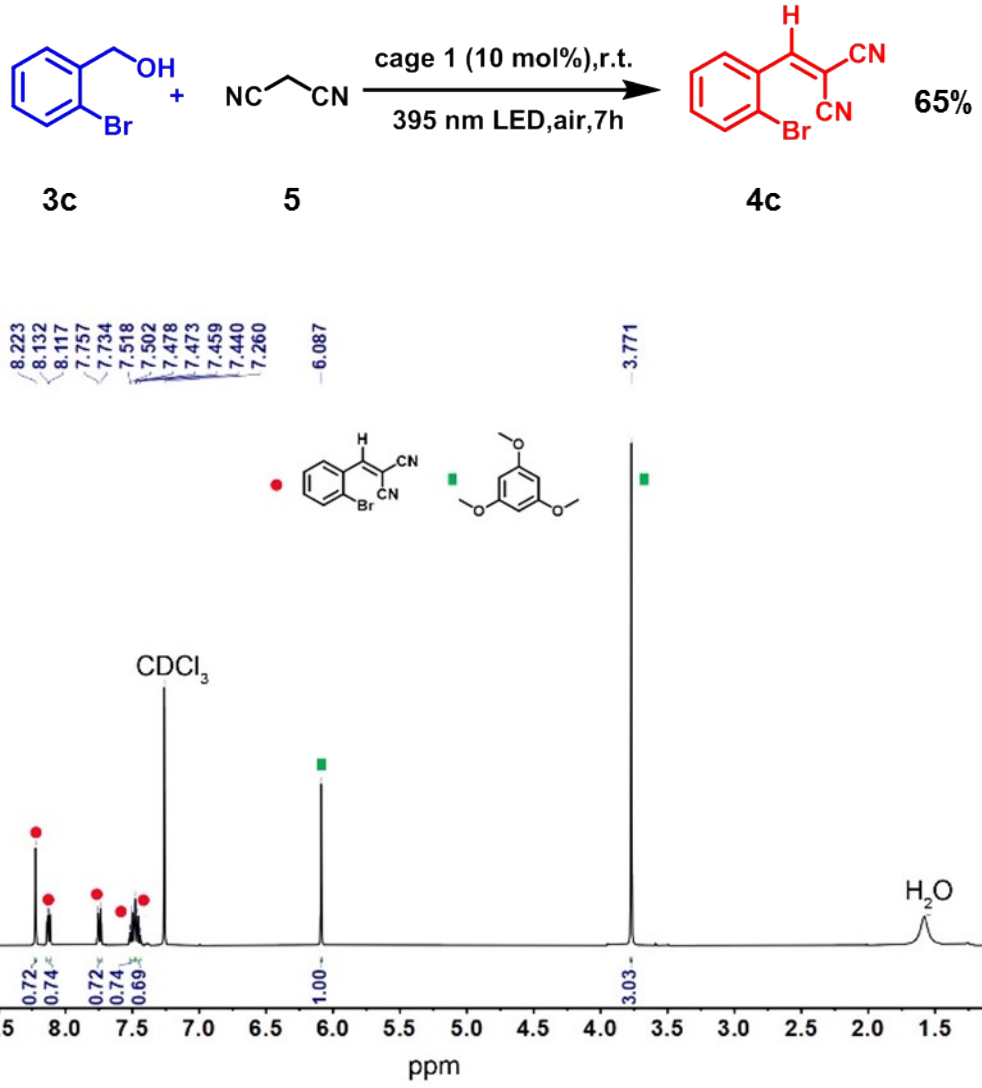

Figure S28. ^{1}H NMR spectra (400 MHz, 298 K, $CDCl_3$) of the product **4c**, corresponding to entry 9 in table 1. 1,3,5-trimethoxybenzene was used as internal standard.

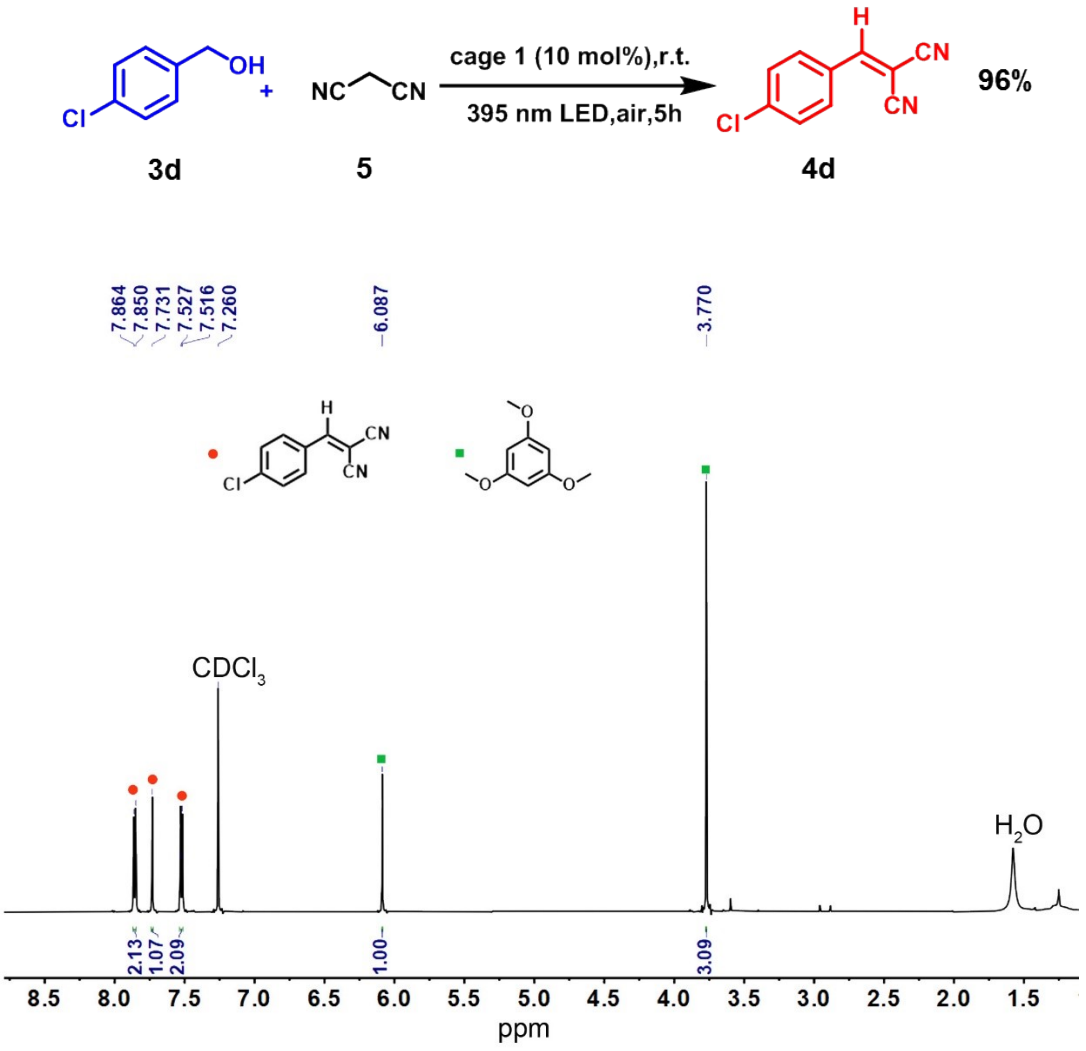

Figure S29. ^{1}H NMR spectra (400 MHz, 298 K, $CDCl_3$) of the product **4d**, corresponding to entry 10 in table 1. 1,3,5-trimethoxybenzene was used as internal standard.

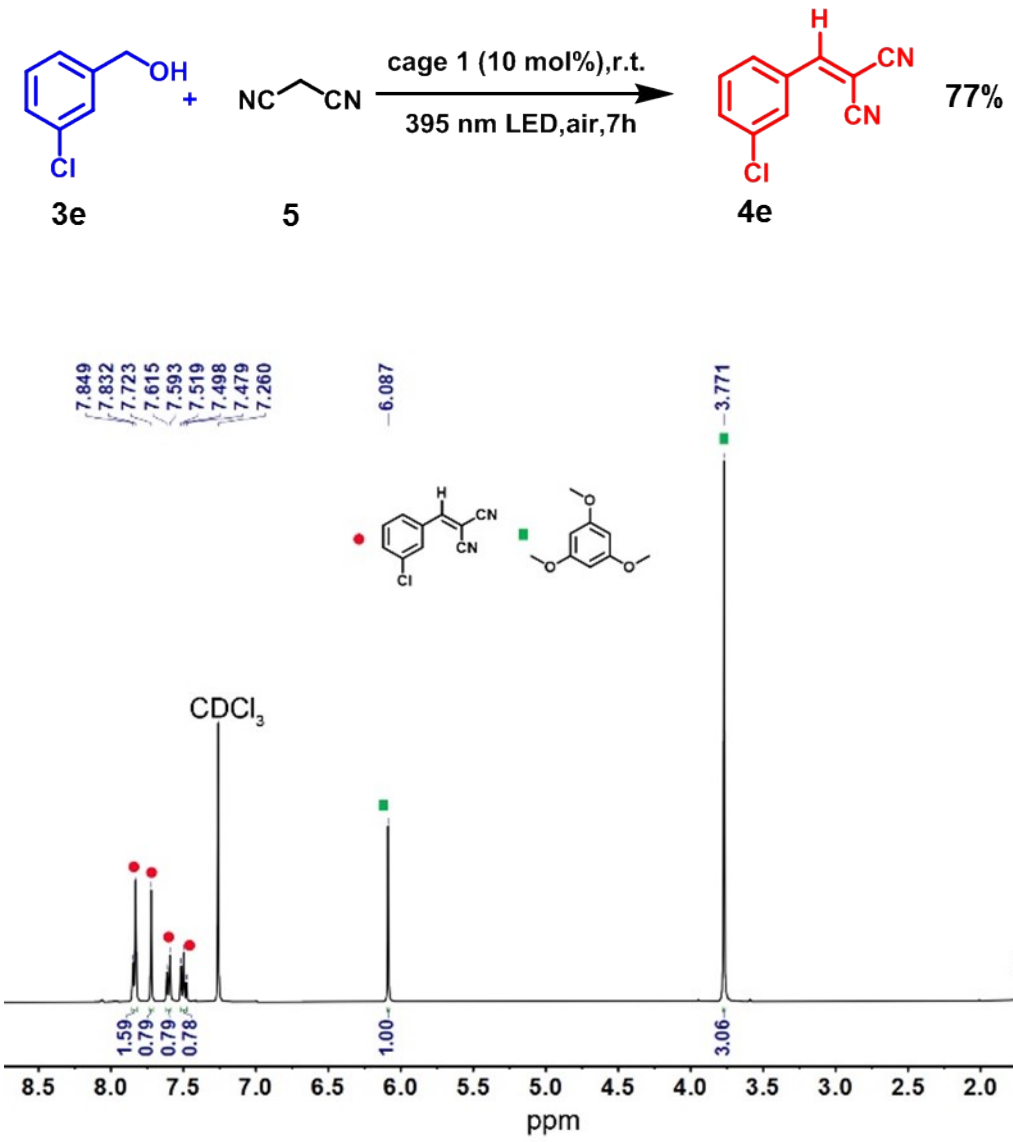

Figure S30. ^{1}H NMR spectra (400 MHz, 298 K, $CDCl_3$) of the product **4e**, corresponding to entry 11 in table 1. 1,3,5-trimethoxybenzene was used as internal standard.

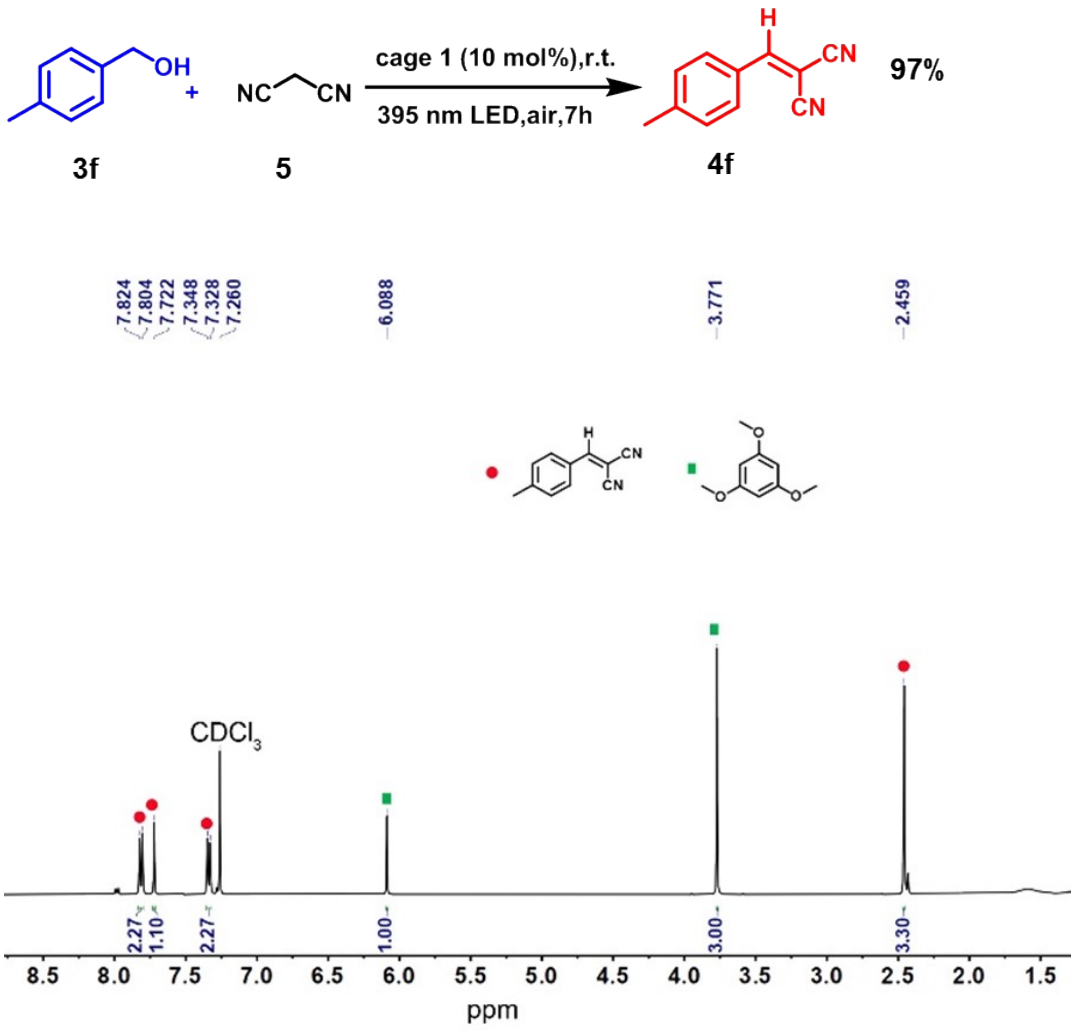

Figure S31. ^{1}H NMR spectra (400 MHz, 298 K, $CDCl_3$) of the product **4f**, corresponding to entry 12 in table 1. 1,3,5-trimethoxybenzene was used as internal standard.

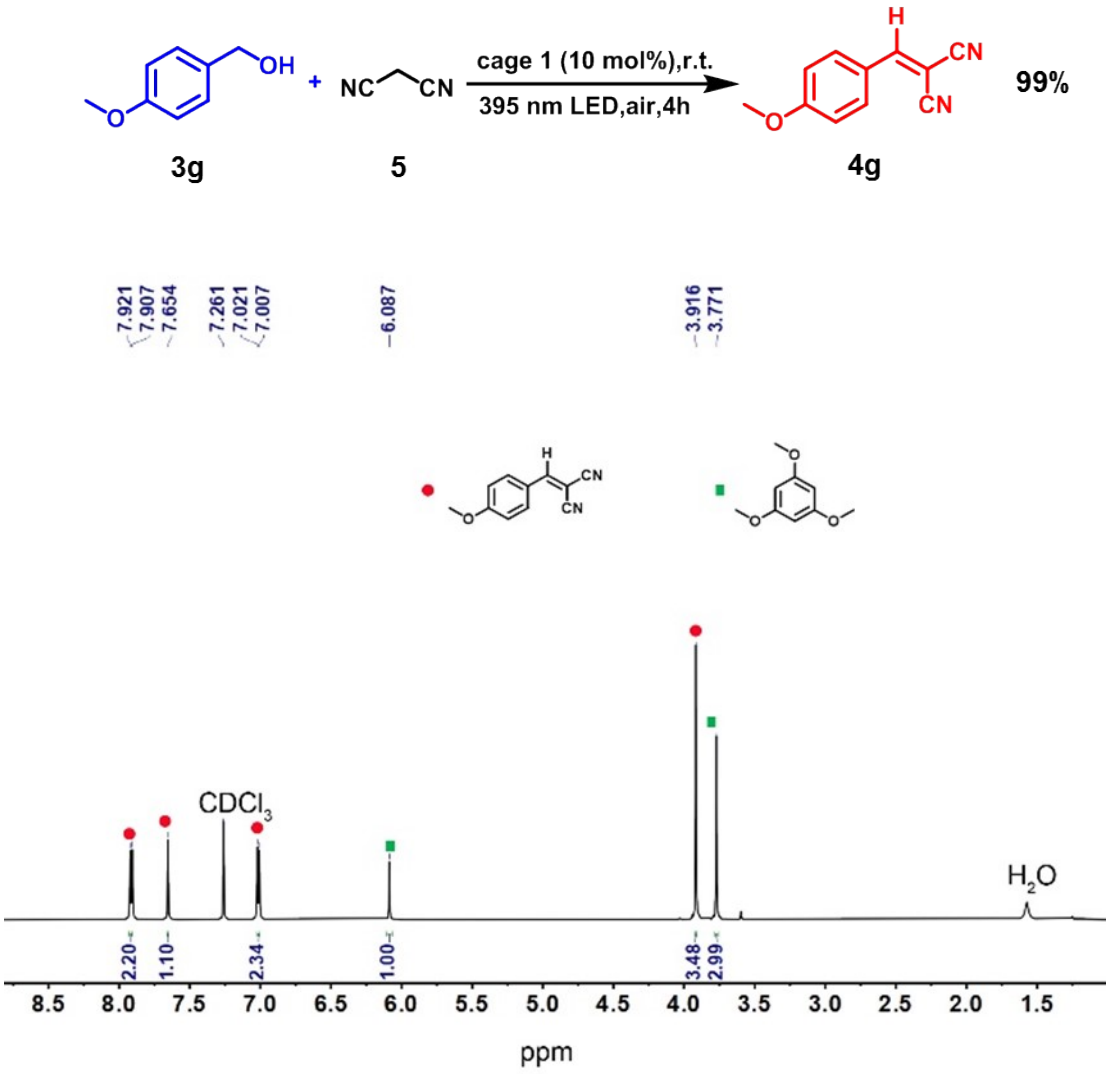

Figure S32. ^{1}H NMR spectra (400 MHz, 298 K, $CDCl_3$) of the product **4g**, corresponding to entry 13 in table 1. 1,3,5-trimethoxybenzene was used as internal standard.

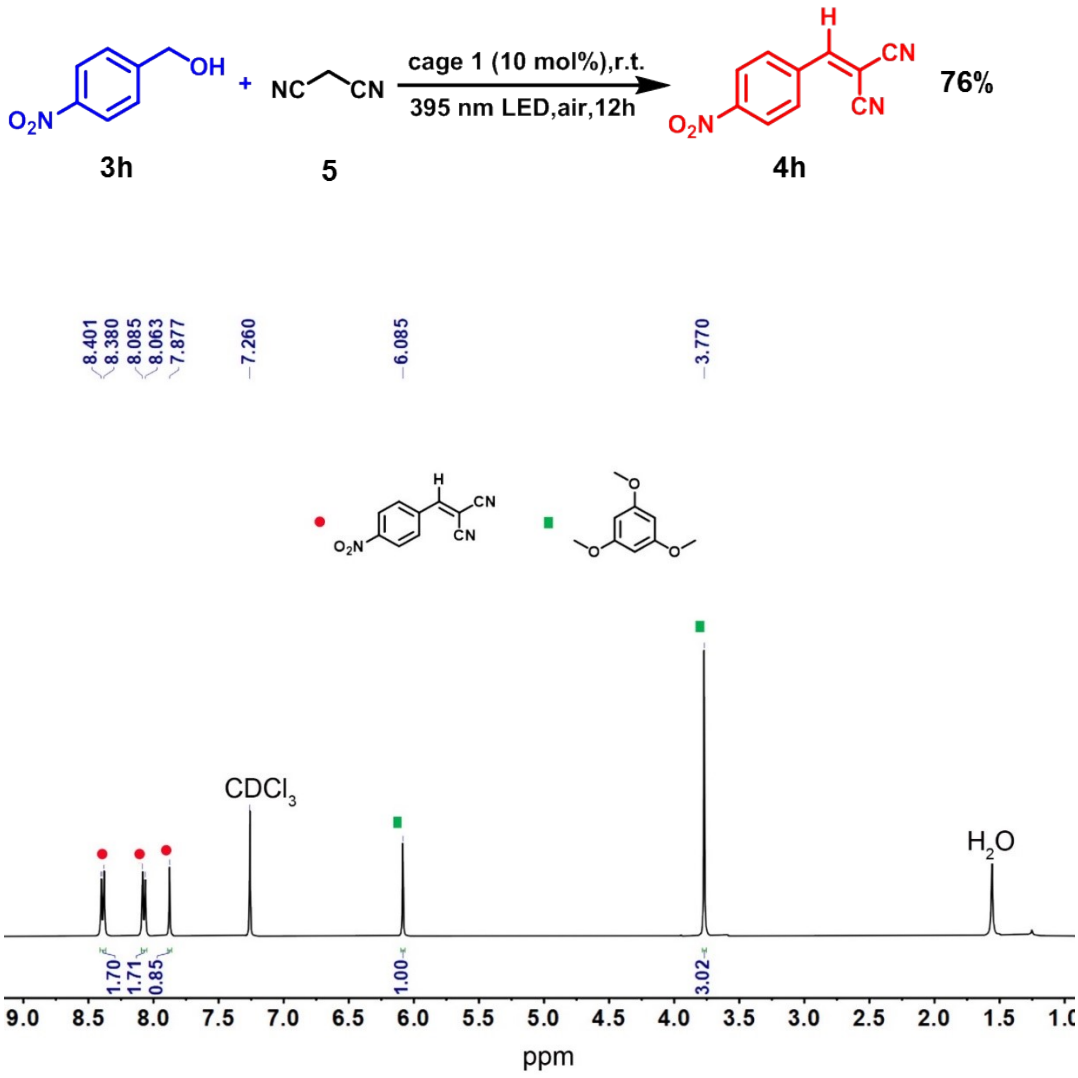

Figure S33. ^{1}H NMR spectra (400 MHz, 298 K, $CDCl_3$) of the product **4h**, corresponding to entry 14 in table 1. 1,3,5-trimethoxybenzene was used as internal standard.

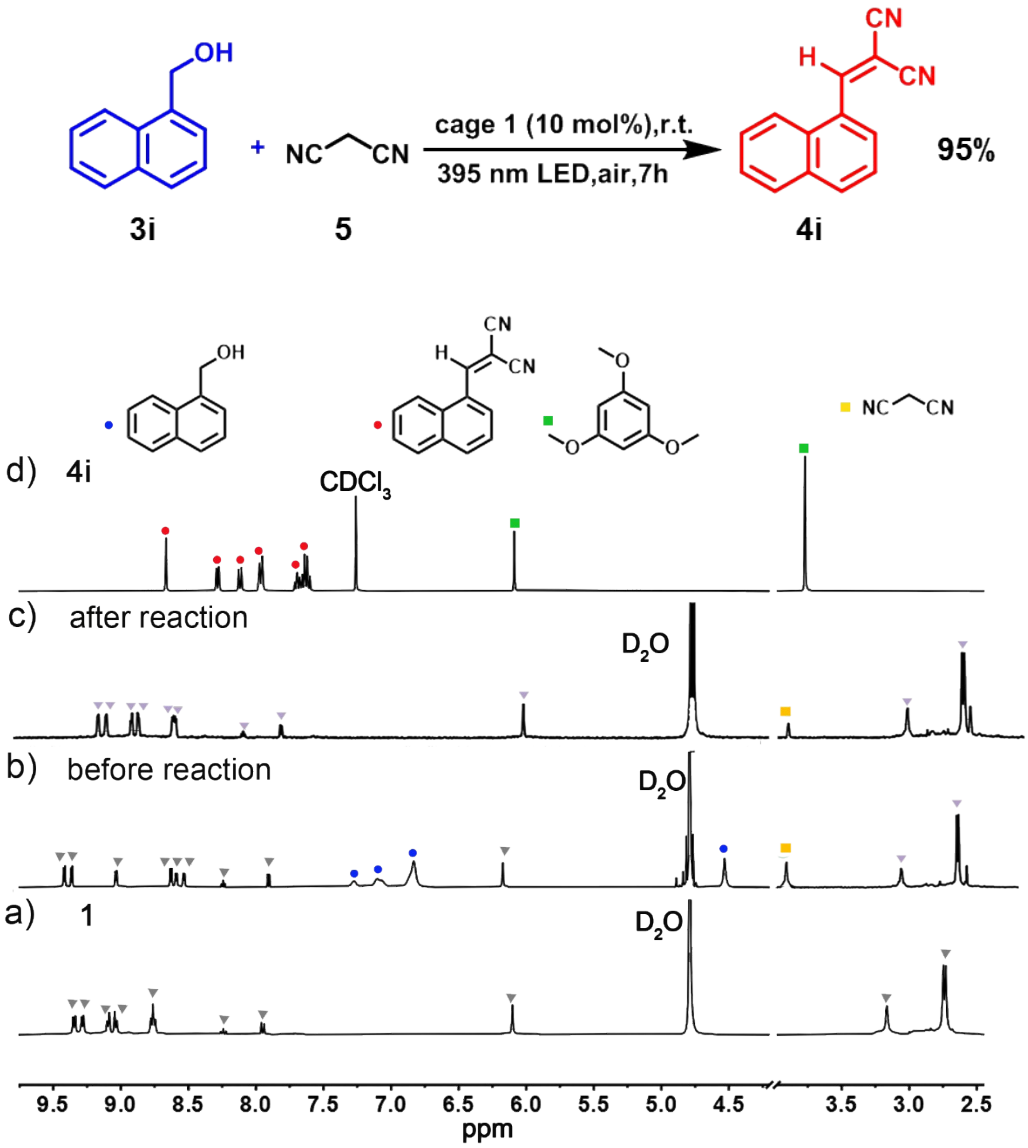

Figure S34. One-pot photooxidation/Knoevenagel condensation of **3i** with malononitrile (**5**) catalyzed by cage **1**. ^{1}H NMR spectra (400 MHz, D_2O, 298 K) of (A) free cage **1**, (B) after addition of **3i** and **5** to cage **1**, (C) after sequential reaction, (D) crude product **4i** obtained by extraction and dissolved in $CDCl_3$ with 1,3,5-trimethoxybenzene as an internal standard (labelled by ■). The signals of cage **1**, **3i** and product **4i** were labelled with ▲, ● and ●, respectively.

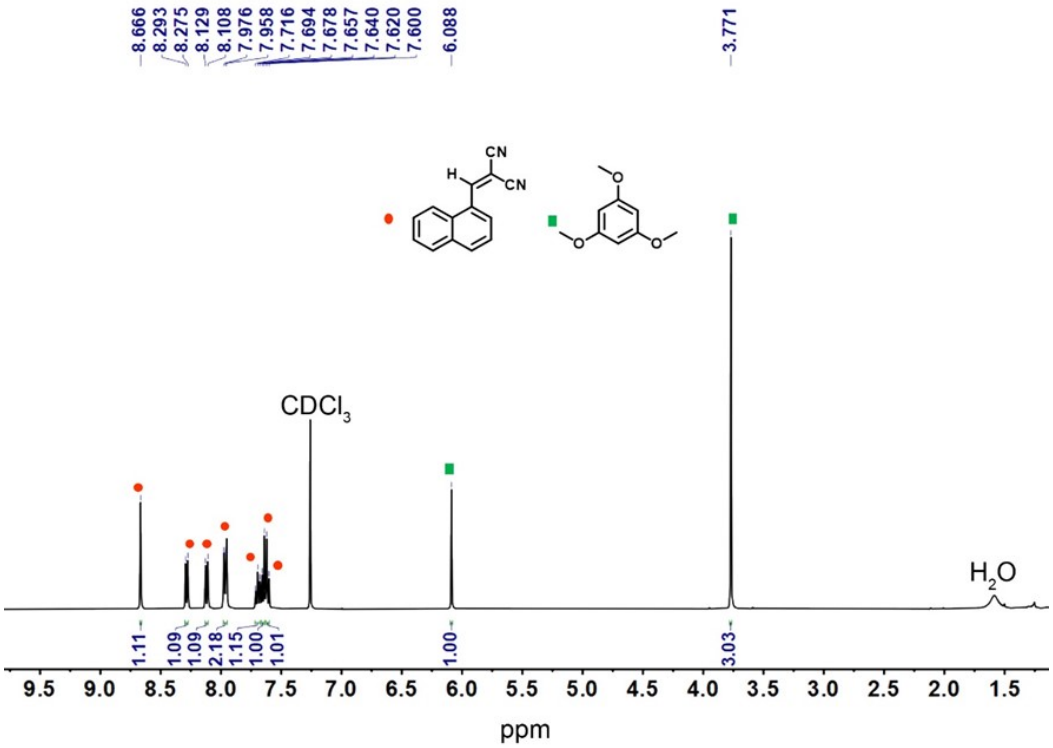

Figure S35. ^{1}H NMR spectra (400 MHz, 298 K, $CDCl_3$) of the product **4i**, with the cage **1** (10 mol% catalysis loading), corresponding to entry 15 in table 1. 1,3,5-trimethoxybenzene was used as internal standard.

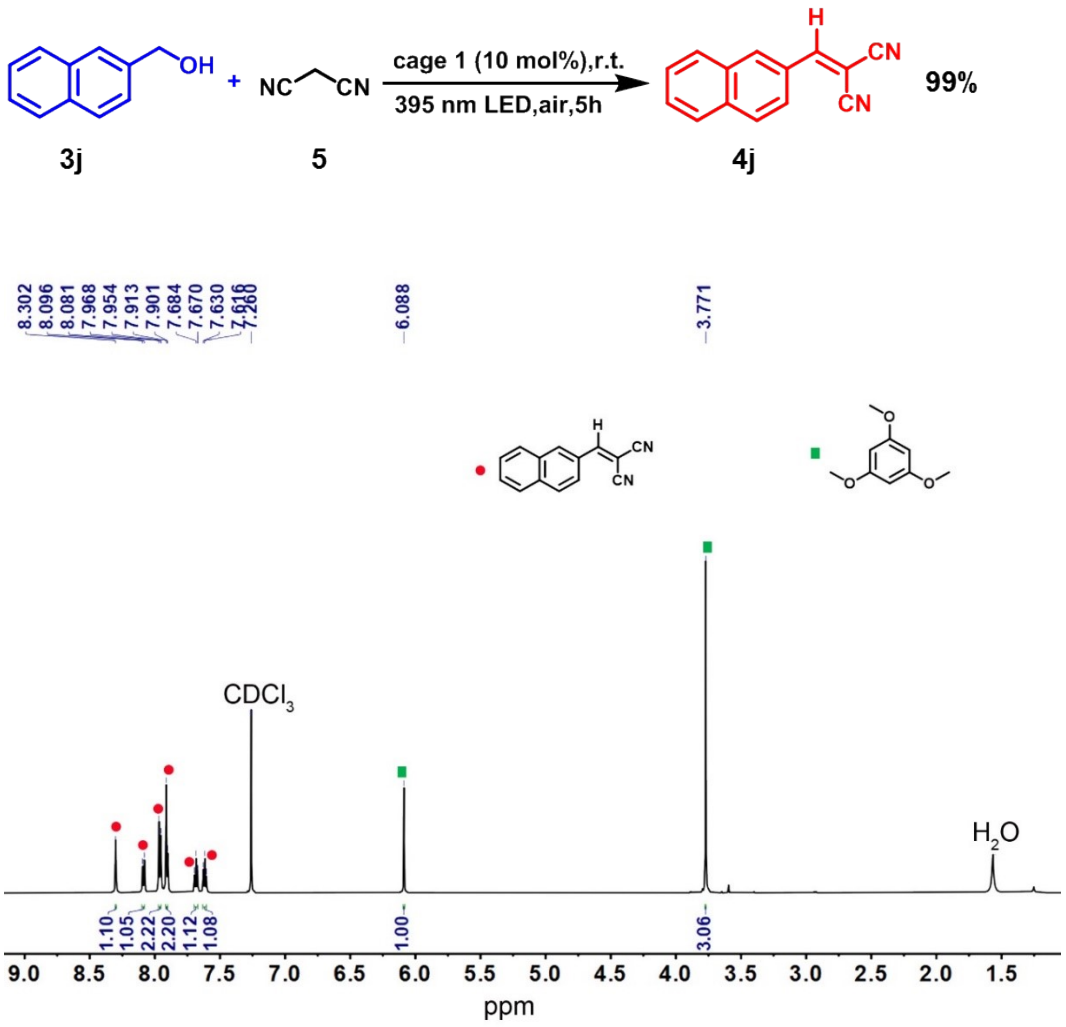

Figure S36. ^{1}H NMR spectra (400 MHz, 298 K, $CDCl_3$) of the product **4j**, corresponding to entry 16 in table 1. 1,3,5-trimethoxybenzene was used as internal standard.

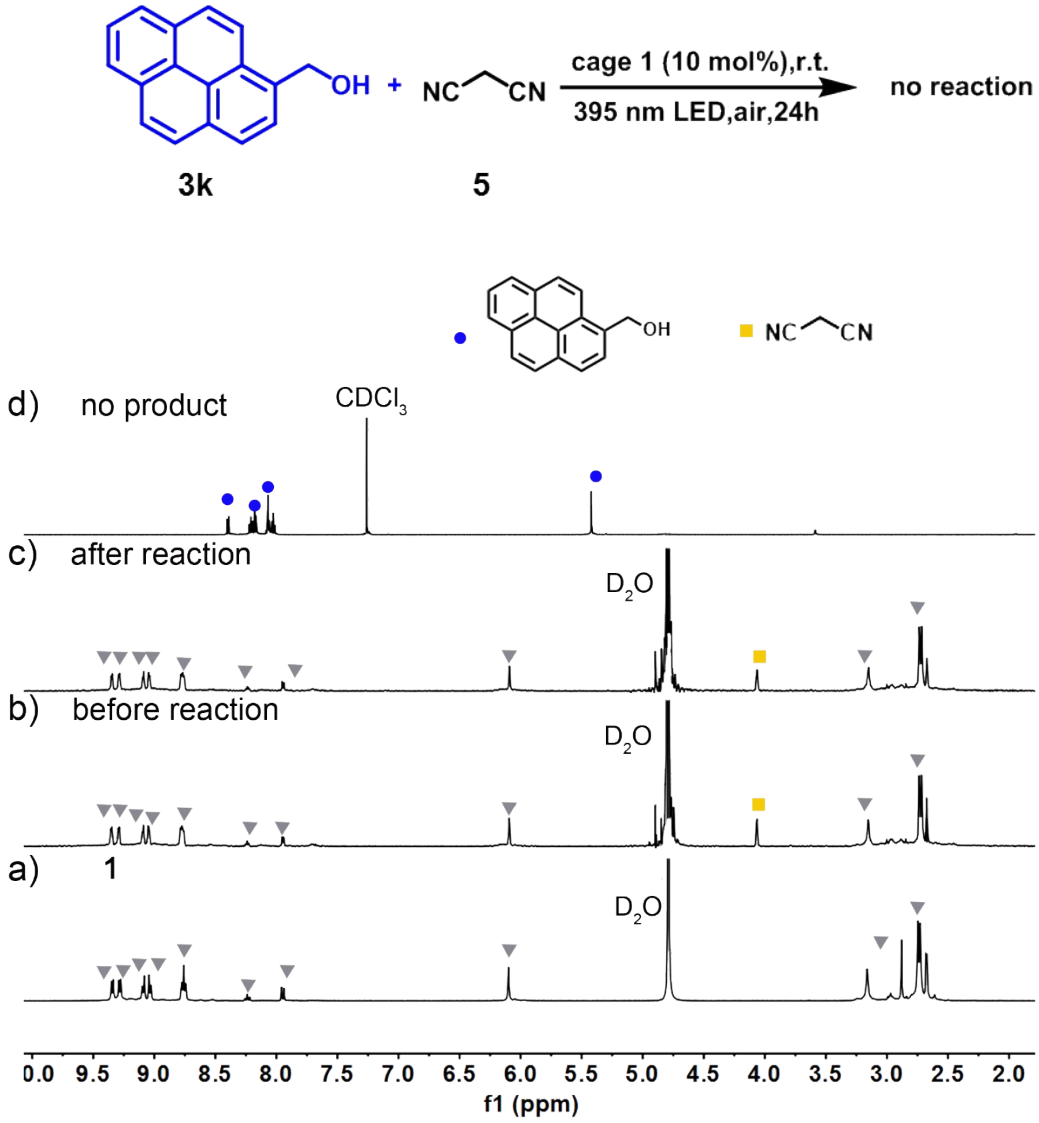

Figure S37. One-pot photooxidation/Knoevenagel condensation of **3k** with malononitrile (**5**) catalyzed by cage **1,** corresponding to entry 17 in table 1. ^{1}H NMR spectra (400 MHz, D_2O, 298 K) of (A) free cage **1**, (B) after addition of **3k** and **5** to cage **1**, (C) after sequential reaction, (D) no crude product obtained by extraction and dissolved in $CDCl_3$. The signals of were labelled with. The signals of cage **1**, and **3k** are labelled by ▲, and ●, respectively.

4.2 The control and inhibited experiment:

Control experiments

To a white suspension of L^1•2BF_4 (1.81 mg, 2 μmol, 20 mol%) in 1 mL D_2O, a white solid of **3a** (1.87mg, 10 μmol) was added and stirred at room temperature for 5 h under purple LEDs. The resulting solution was extracted by CH_2Cl_2 (3×5 mL) then the solvent was evaporated in vacuum pump. The resulting product was characterized without further purification by ^{1}H NMR spectrometer (600 μL $CDCl_3$ with 0.003 mM 1, 3, 5-trimethoxybenzene as internal standard).

Other control experiments using (tmen)Pd(NO_3)$_2$, under N_2 atmosphere and under dark were performed and characterized in the same procedure as above. Detailed data was displayed in the Table 1.

The inhibitation experiment

To a light-orange solution of cage **1** (3.19 mg, 1 μmol), sodium tetraphenylboron $(Ph)_4BNa$ (0.684 mg, 2 μmol, 2 equiv.) and substrate **3a** (1.87mg, 10 μmol, 10 equiv.) were added and stirred at room temperature for 5 h under purple LEDs. After removal of the excess guest by filtration, the quantitative formation of the inclusion complex $(Ph)_4BNa$@**1** was observed by ^{1}H NMR analysis (Figure S41). There was no trace of substrate **3a** on the ^{1}H NMR spectrum. The resulting solution was extracted by CH_2Cl_2 (3×5 mL) then the solvent was evaporated. The resulting product was characterized without further purification by ^{1}H NMR spectrometer (600 μL $CDCl_3$ with 0.003 mM of 1, 3, 5-trimethoxybenzene as internal standard). Detailed data was displayed in the Table 1.

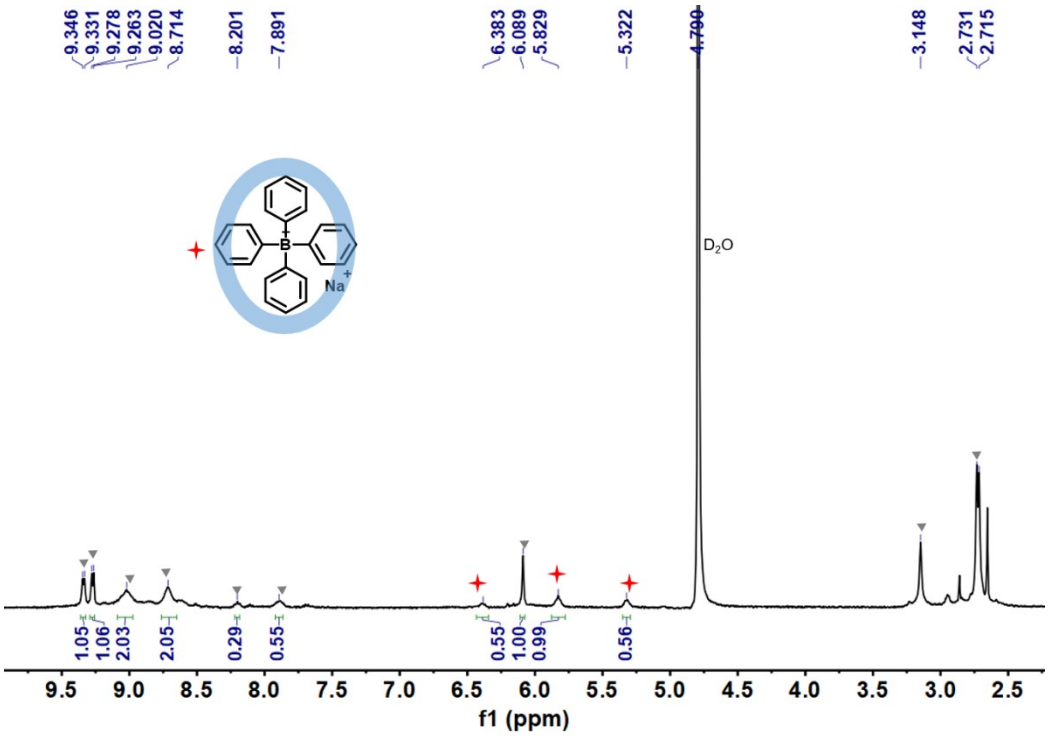

Figure S38. The ^{1}H NMR spectrum of the **[$(C_6H_5)_4B^-$]** @**1** (400 MHz, D_2O, 298 K).

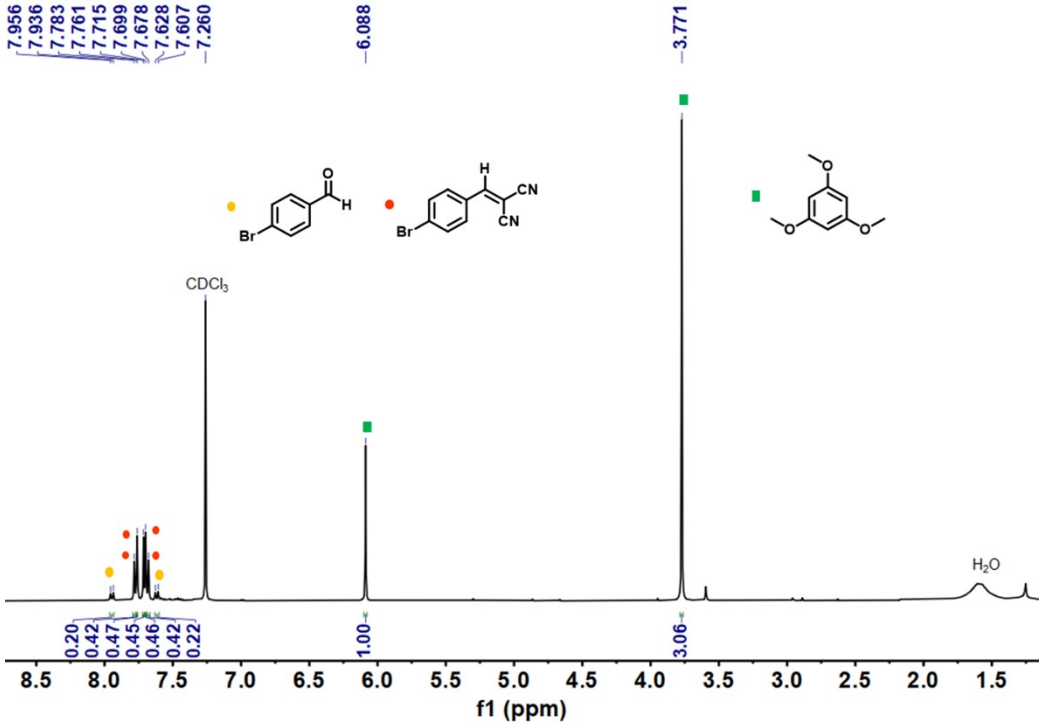

Figure S39. ^{1}H NMR spectra (400 MHz, 298 K, $CDCl_3$) of crude product with the addition of **[$(C_6H_5)_4$BNa]**, corresponding to entry 2 in table 1. 1,3,5-trimethoxybenzene was used as internal standard.

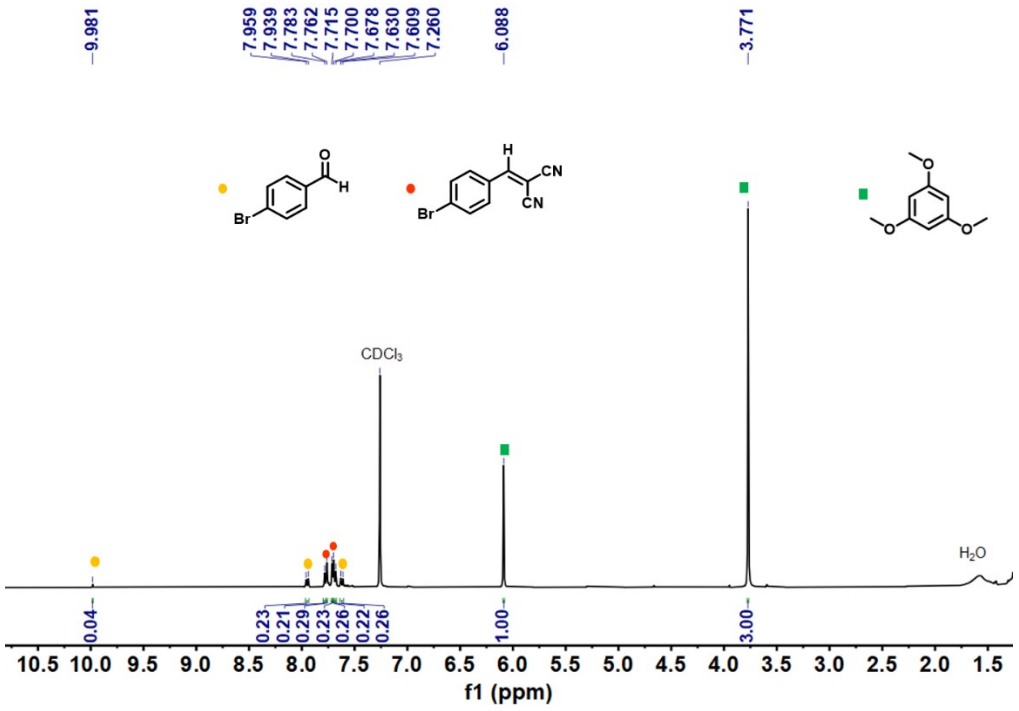

Figure S40. ^{1}H NMR spectra (400 MHz, 298 K, $CDCl_3$) of crude product with the addition of $L^1 \cdot 2BF_4$ (20 mol% catalysis loading), corresponding to entry 4 in table 1. 1,3,5-trimethoxybenzene was used as internal standard.

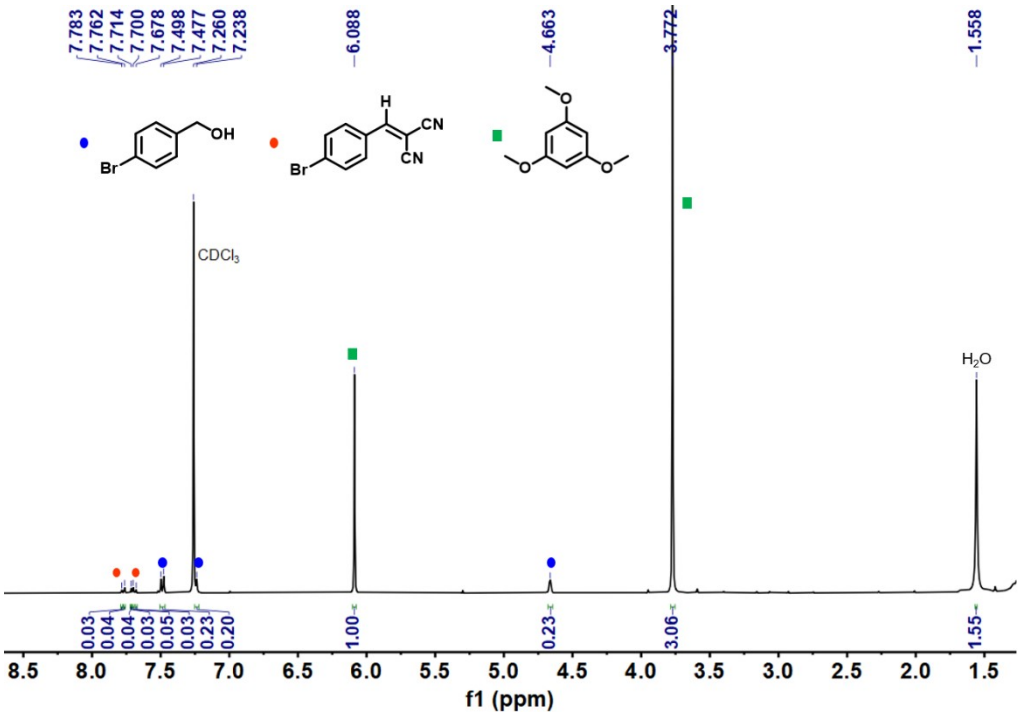

Figure S41. ^{1}H NMR spectra (400 MHz, 298 K, $CDCl_3$) of crude product with the addition of (tmen)Pd$(NO_3)_2$ (40 mol% catalysis loading), corresponding to entry 5 in table 1. 1,3,5-trimethoxybenzene was used as internal standard.

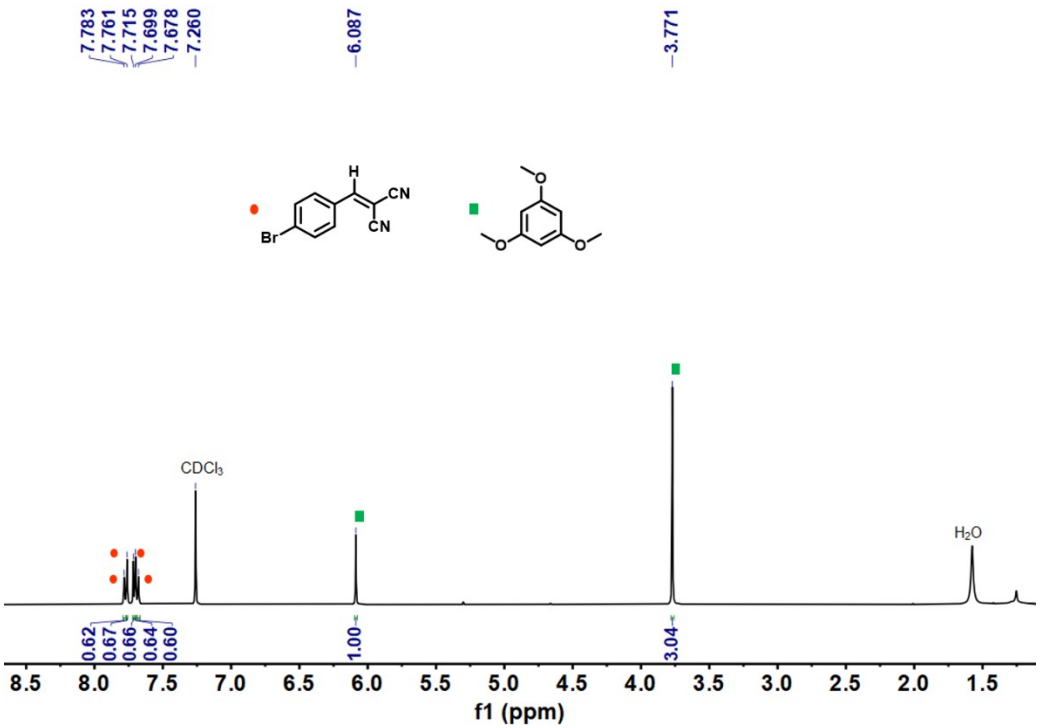

Figure S42. ^{1}H NMR spectra (400 MHz, 298 K, $CDCl_3$) of crude product with cage **1** (10 mol% catalysis loading) under N_2, corresponding to entry 3 in table 1. 1,3,5-trimethoxybenzene was used as internal standard.

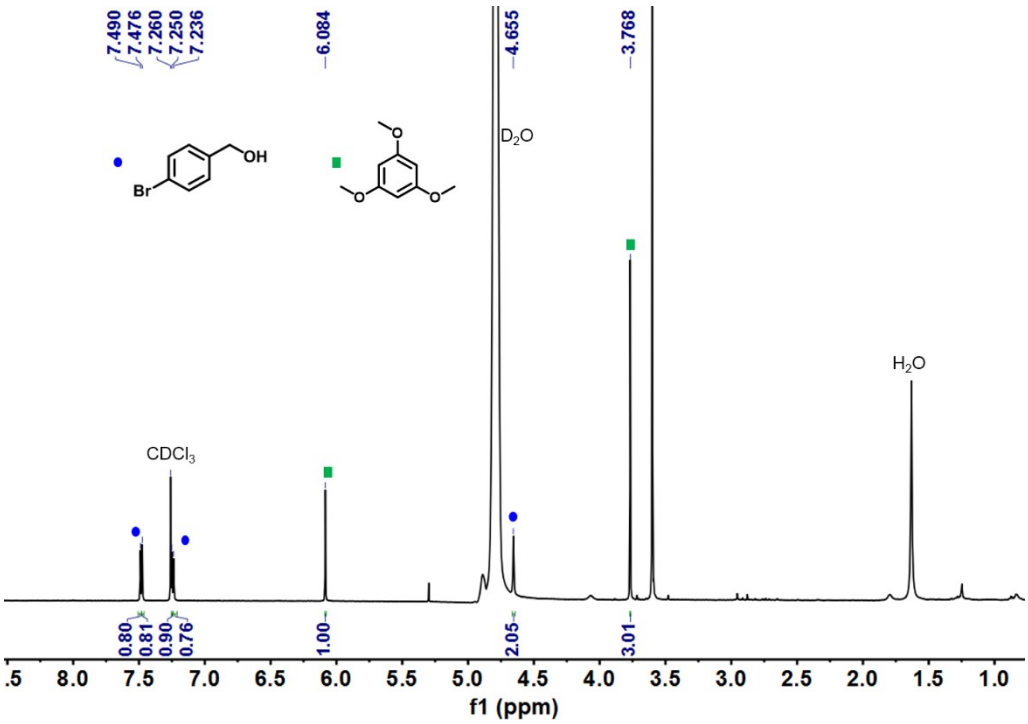

Figure S43. ^{1}H NMR spectra (400 MHz, 298 K, $CDCl_3$) of crude product with cage **1** (10 mol% catalysis loading) under dark, corresponding to entry 6 in table 1. 1,3,5-trimethoxybenzene was used as internal standard.

4.3 The catalytic cycle experiment:

3a (150 equiv.) and malononitrile (excess) were added into the D_2O solution (15 mL) containing catalysts (0.001 mM, 5 mL).This mixture solution was irradiated under purple LEDs (λ > 395 nm, 6 W) with a magnetic stirring bar in air at r.t. The reaction solution was monitored by thin layer chromatography method. After reaction, the products were extracted with CH_2Cl_2, which were dried under reduce pressure and subjected to ^1H NMR without further purification. The yield and selectivity were determined using 1,3,5-trimethoxybenzene as the internal standard (0.075 mM).

Table S1 The accumulative TON of substrate **3a** (150 equiv.) with reaction time.

Time	3h	6h	9h	12h	15h	20h	25h	30h	35h	40h
Yield	9%	19%	30%	41%	52%	60%	71%	79%	89%	89%
TON	14	28	44	62	77	90	106	119	133	134

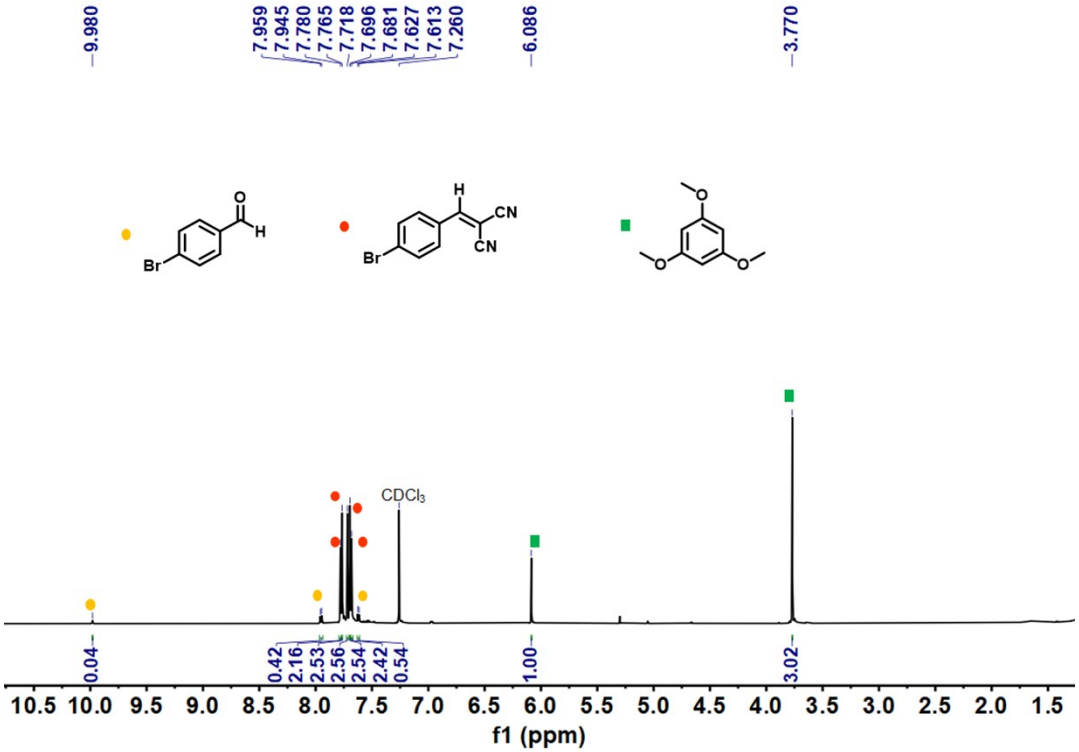

Figure S44. ^1H NMR spectra (400 MHz, 298 K, $CDCl_3$) of crude product of **3a** with the catalysis of cage **1** (0.67 mol% catalysis loading), offering 89% isolated yield of **4a**.

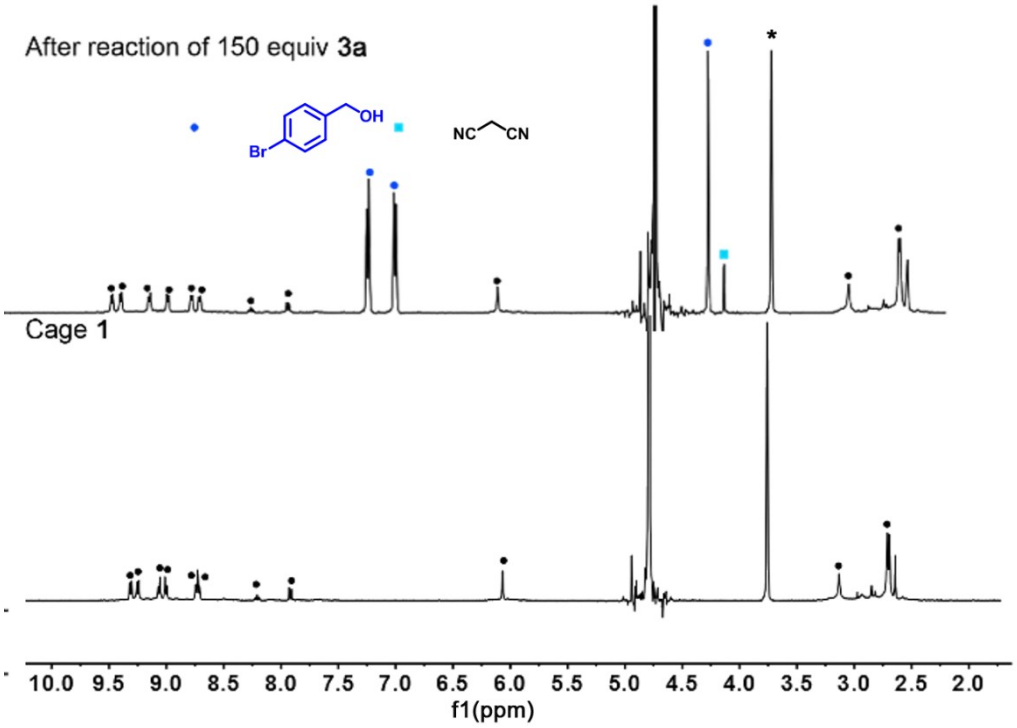

Figure S45. ^{1}H NMR spectra (400 MHz, D_2O, 298 K) of cage **1** with **3a** (150eq.) and excess malononitrile stirred for 40 h under purple LEDs. Signals labeled with star denote dioxane as internal standard.

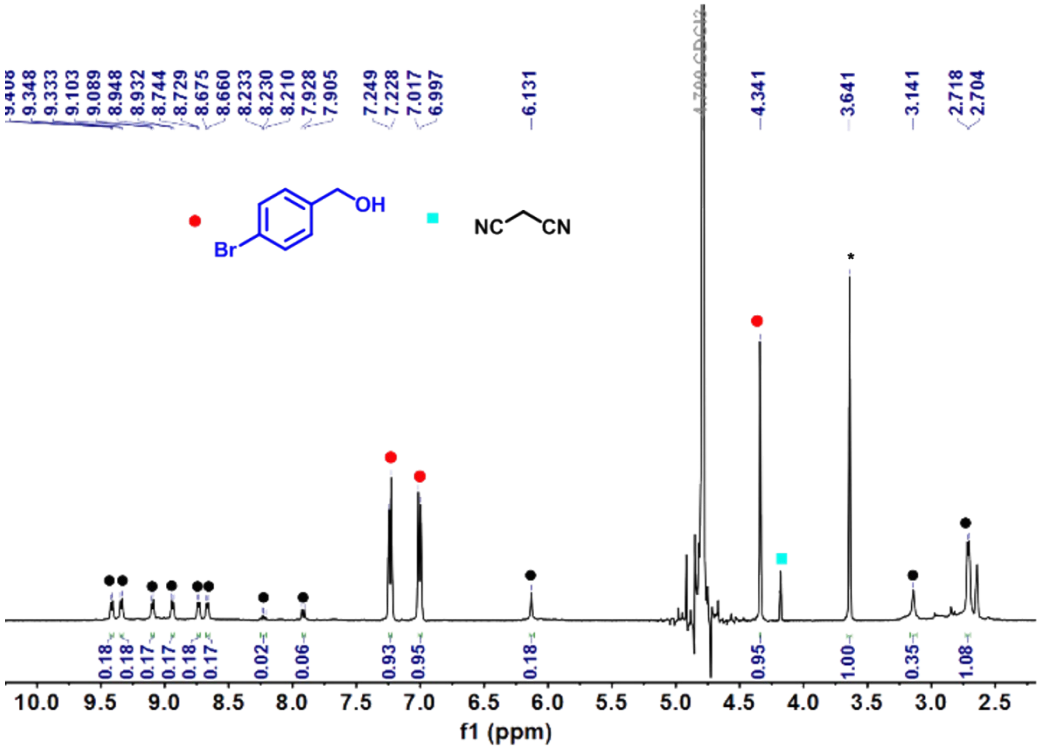

Figure S46. ^{1}H NMR spectrum (400 MHz, D_2O, 298 K) of cage **1** with **3a** (150eq.) and excess malononitrile stirred for 40 h under purple LEDs. Dioxane (10mM) was used as internal standard. Slight decrease of the cage's concentration from 1 mM to 0.9 mM was observed.

5. Comparison of photocatalytic experiments of cage 2

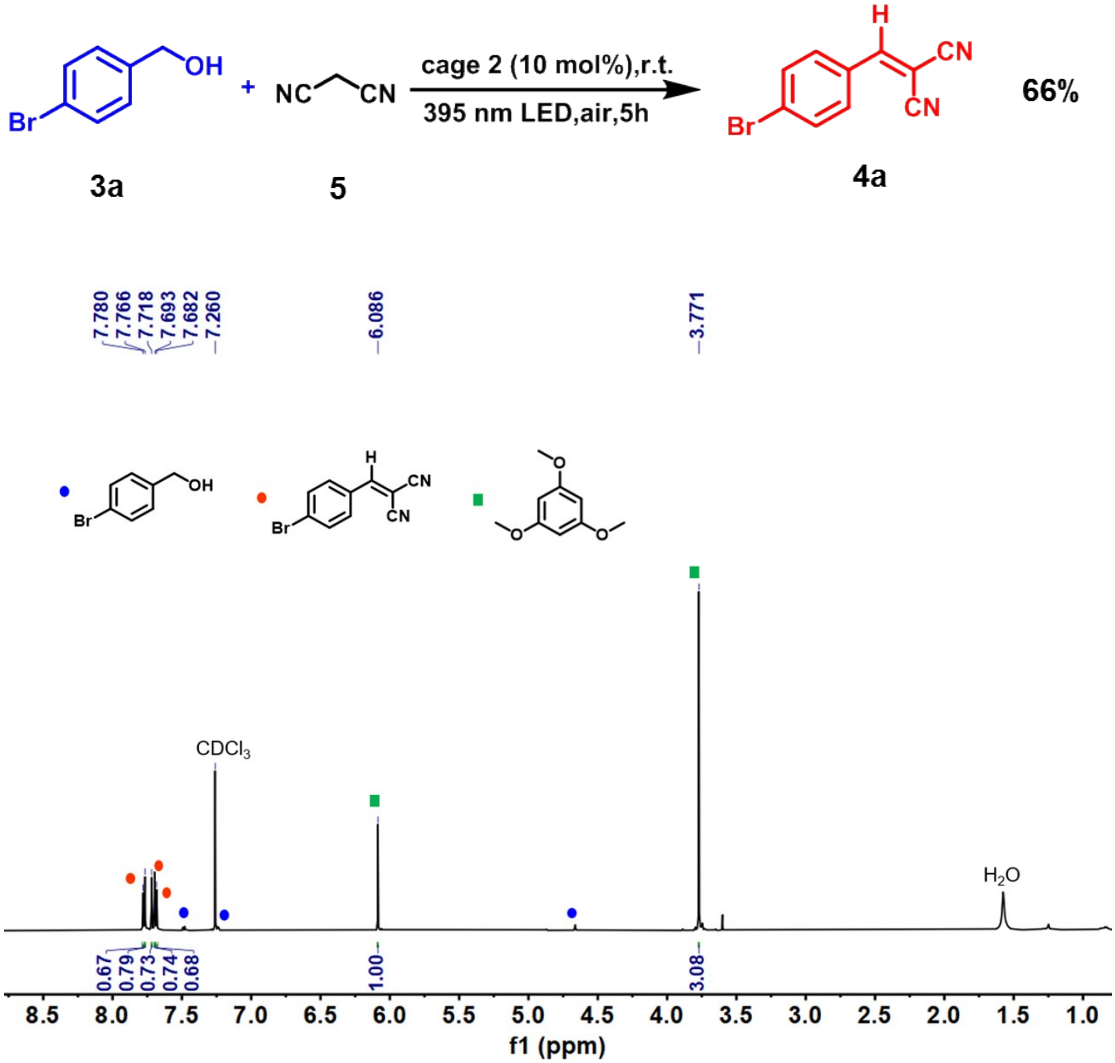

Figure S47. ^{1}H NMR spectra (400 MHz, 298 K, $CDCl_3$) of crude product, with the catalysis of cage **2** (10 mol% catalysis loading), corresponding to entry 7 in table 1. 1,3,5-trimethoxybenzene was used as internal standard.

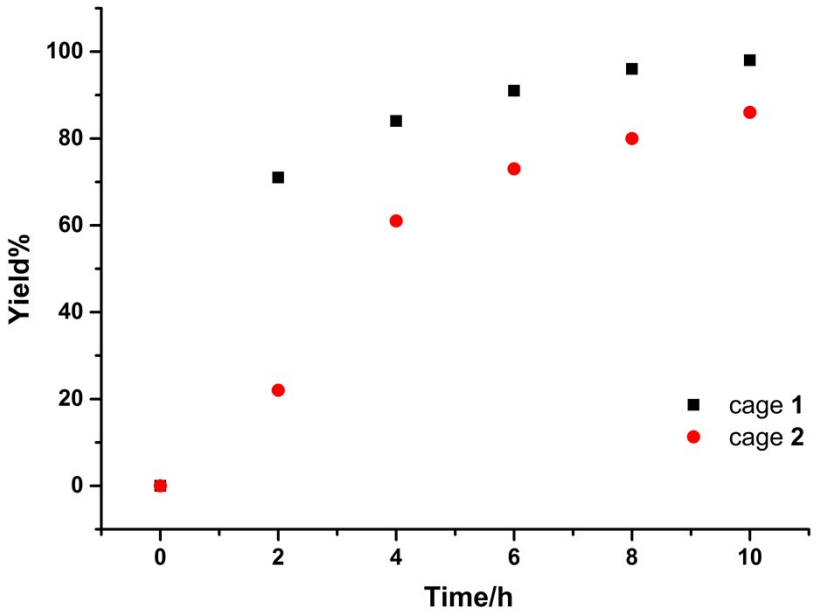

Figure S48.The comparison of the conversions for the photooxidation-Knoevenagel condensation of **3a** (15 equiv., under 6 W 395-nm LEDs) with either cage **2** or cage **1** as the catalysts.

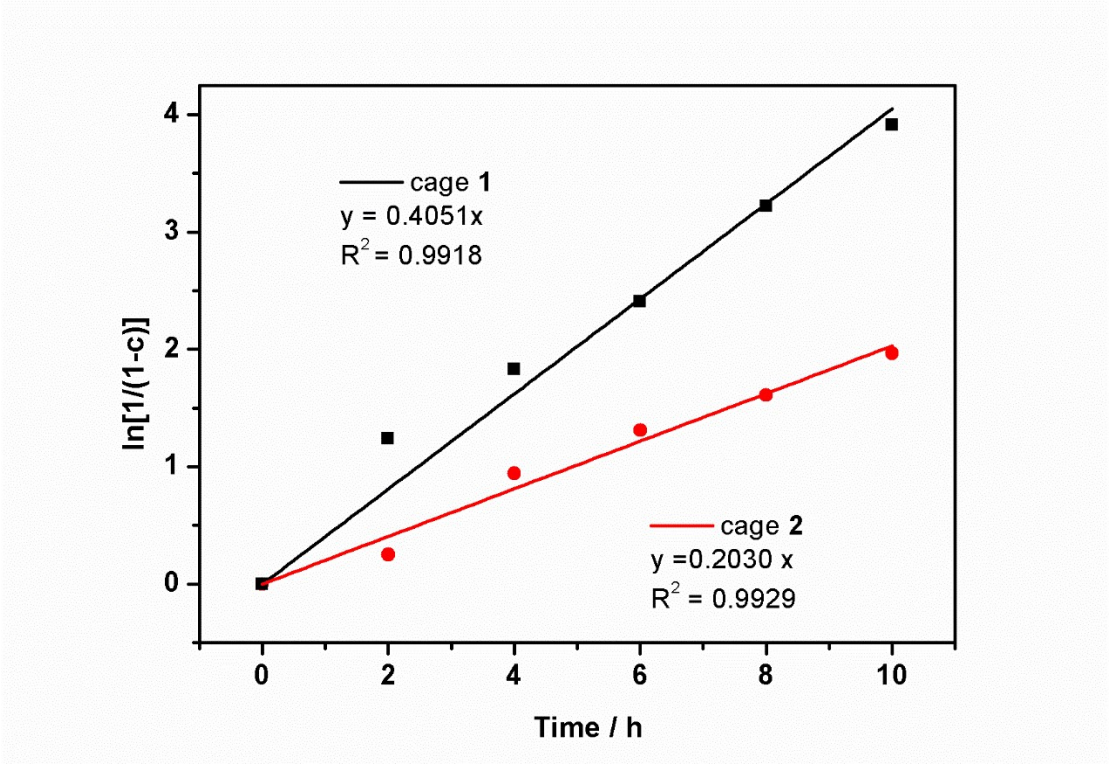

Figure S49. Pseudo-first-order kinetic plots for the photooxidation-Knoevenagel condensation of **3a** (15 equiv., under 6 W 395-nm LEDs) with either cage **2** or cage **1** as the catalysts.

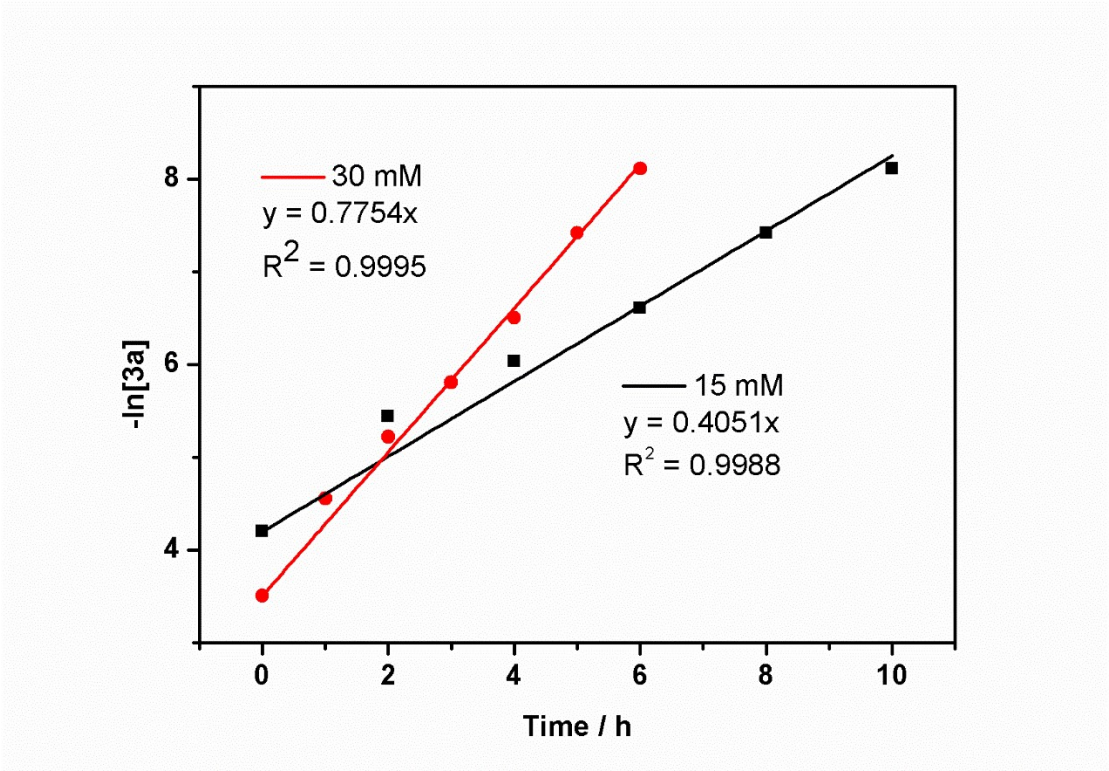

Figure S50. Pseudo-first-order kinetic plots for the cage **1** catalyzed photooxidation-Knoevenagel condensation of **3a** at the concentration of 15 mM and 30 mM.

6. Proposed mechanism:

The binding behavior of cage **1** for guests have been estimated by ^{1}H NMR titrations and fitted with a Hill function:[S4]

$$\log \frac{\theta}{1-\theta} = n \log [G] + n \log [K_a]$$

θ = saturated ratio.

$\theta_i = \Delta\delta_i / \Delta\delta_{max}$;

n = Hill coefficient;

[G]= concentration of guest;

K_a = apparent association constant.

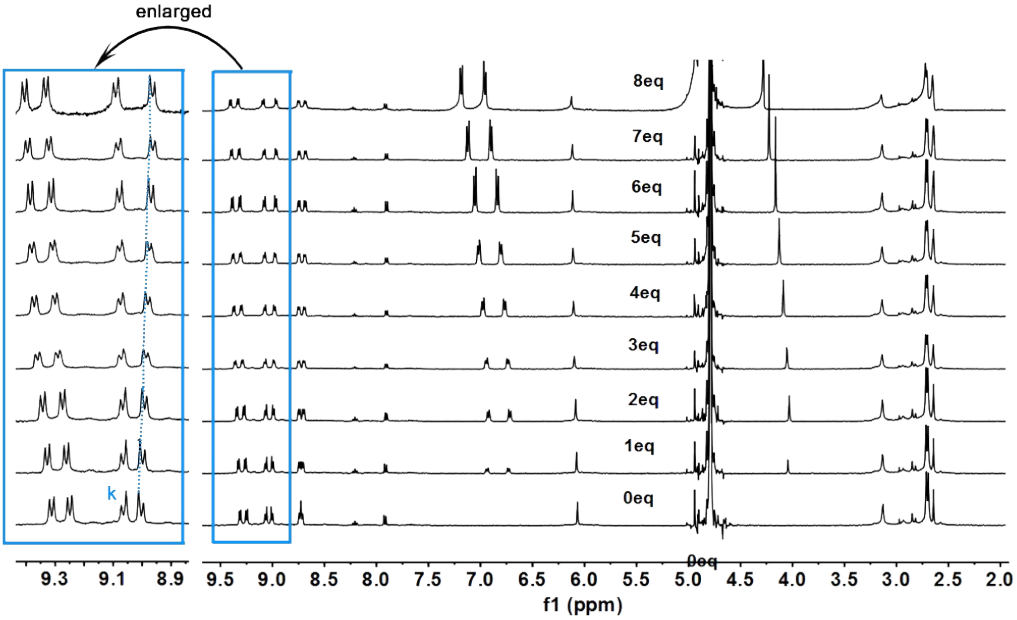

Figure 51. ^{1}H NMR titration (600 MHz, D_2O, 298 K) of cage **1** (1 mM) with (4-bromophenyl) methanol (**3a**).

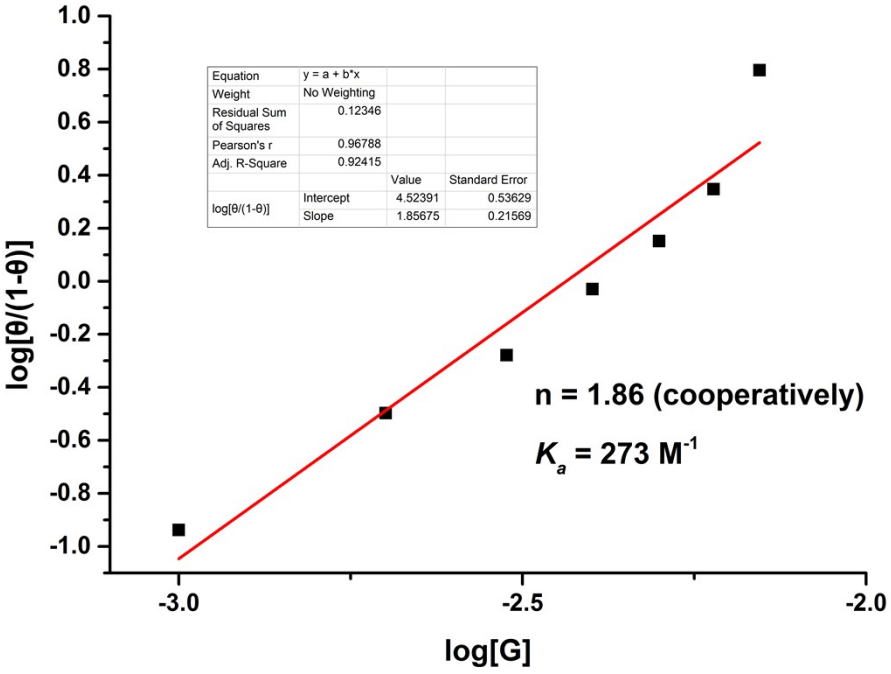

Figure 52. Titration curve fitting with Hill function for cage **1** and **3a**. The apparent binding constant was determined to be 273 M^{-1}.

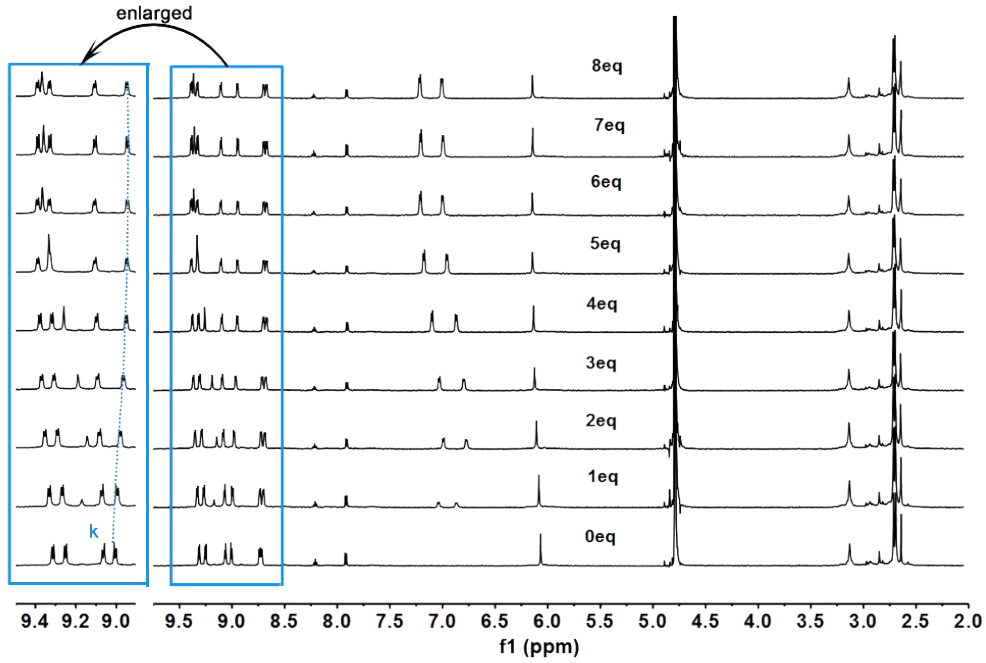

Figure S53. ^{1}H NMR titration (600 MHz, D_2O, 298 K) of cage **1** (1 mM) with 4-bromobenzaldehyde.

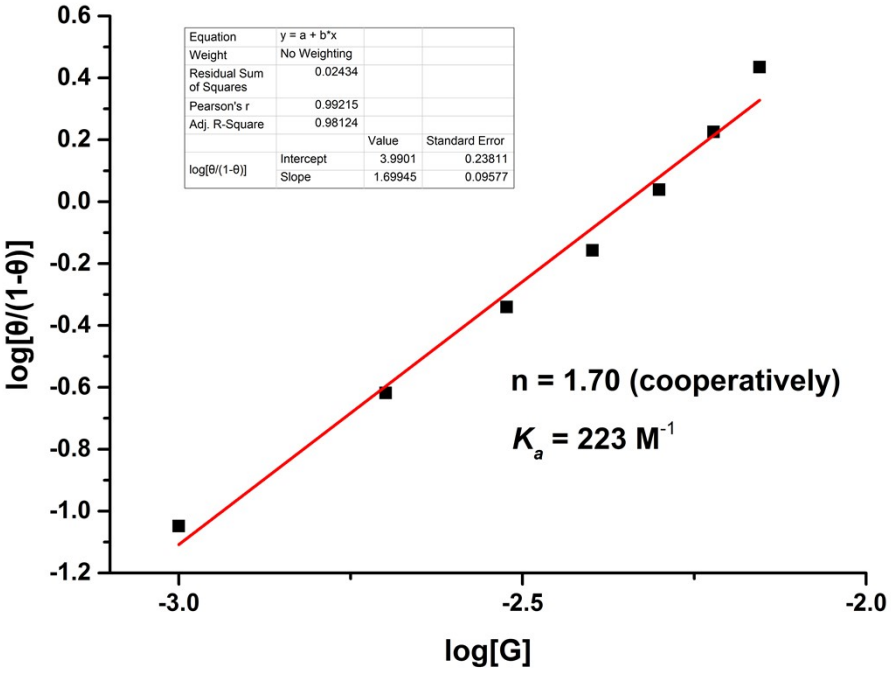

Figure S54. Titration curve fitting with Hill function for cage **1** and 4-bromobenzaldehyde. The apparent binding constant was determined to be 223 M^{-1}.

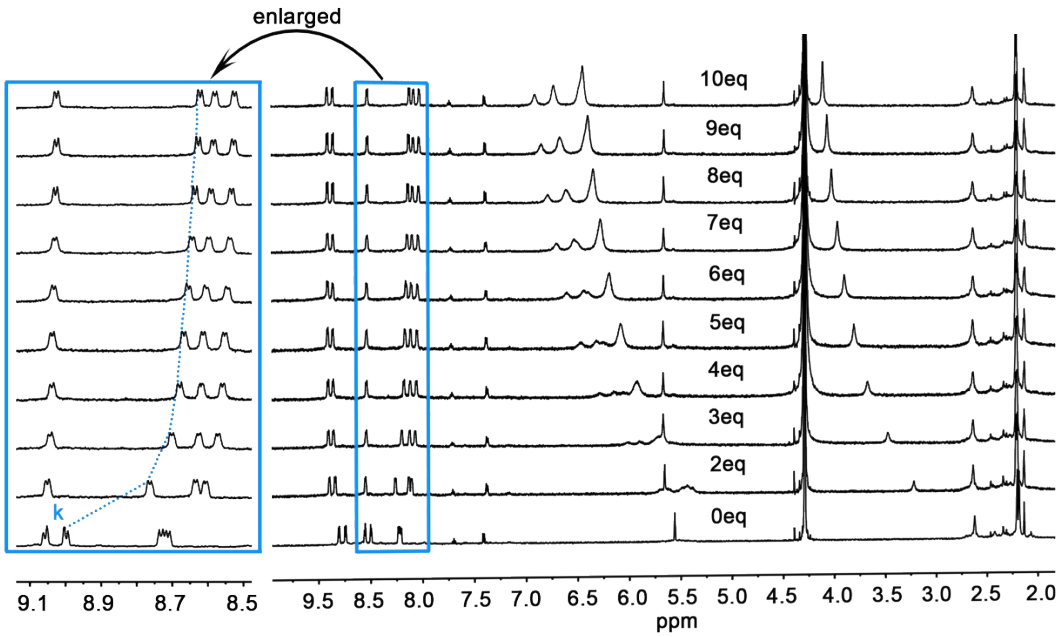

Figure S55. ^{1}H NMR titration (600 MHz, D_2O, 298 K) of cage **1** (1 mM) with **3i**.

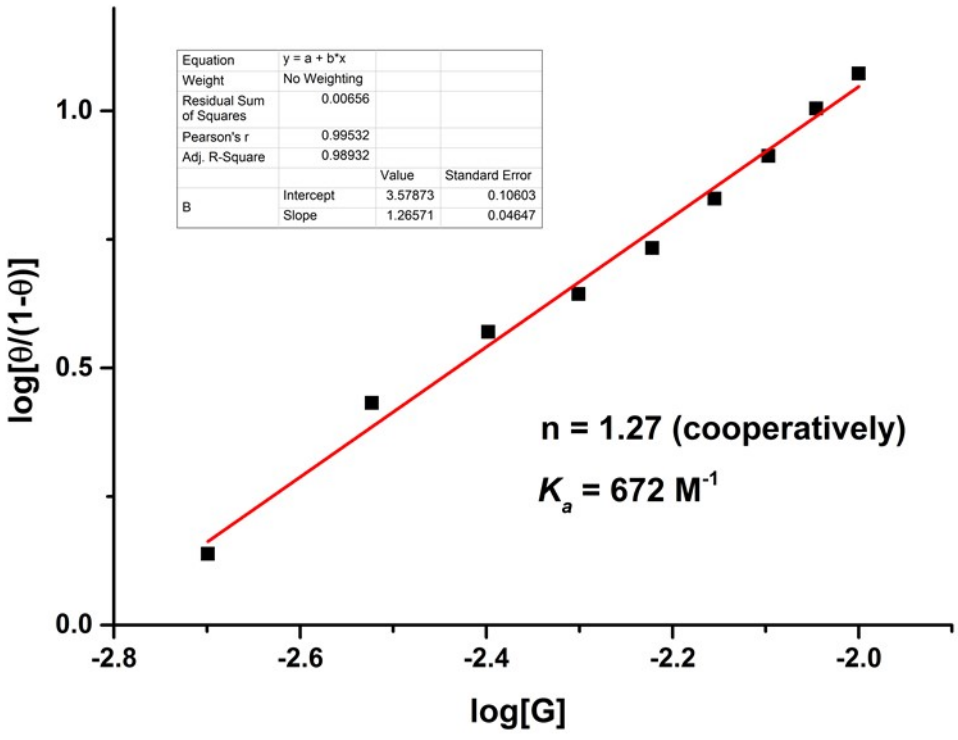

Figure S56. Titration curve fitting with Hill function for **3i**.

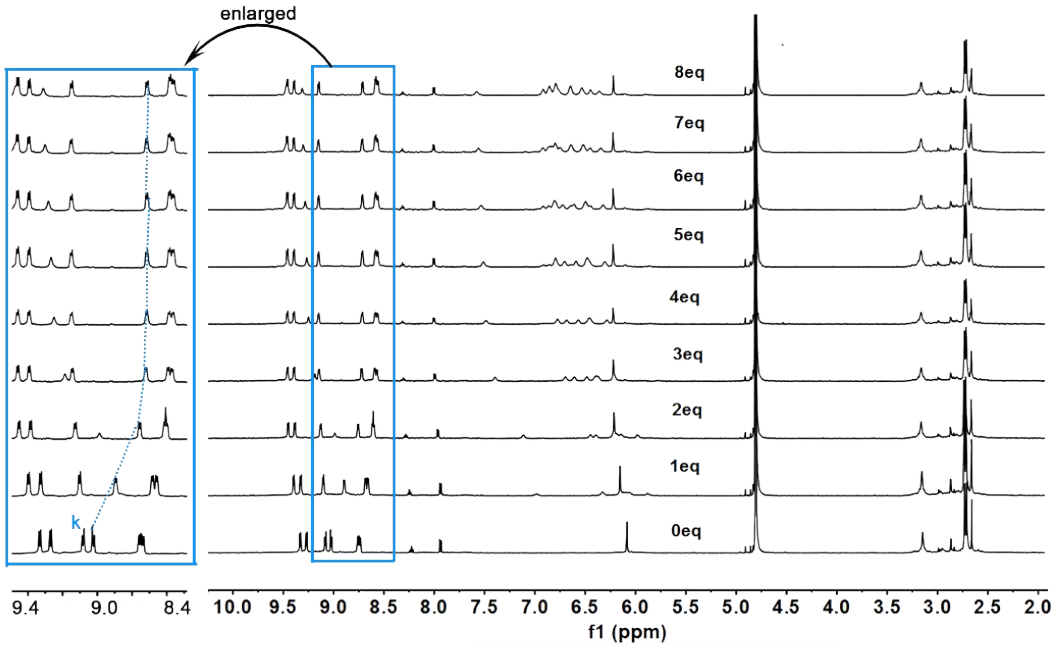

Figure S57. ^{1}H NMR titration (600 MHz, D_2O, 298 K) of cage 1 (1 mM) with 1-naphthaldehyde.

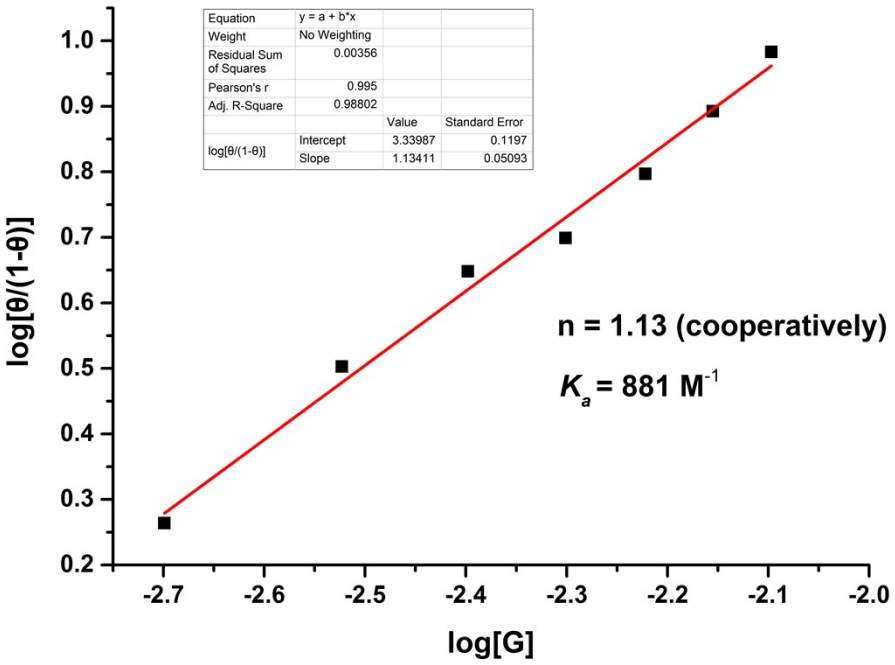

Figure S58. Titration curve fitting with Hill function for cage **1** and 1-naphthaldehyde. The apparent binding constant was determined to be 881 M^{-1}.

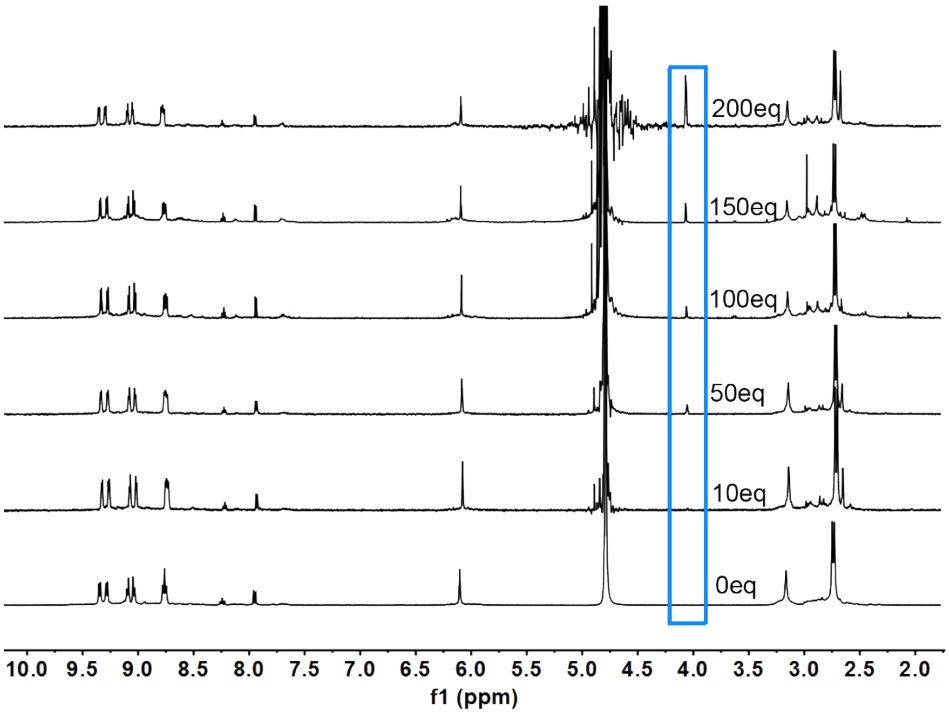

Figure S59. ^{1}H NMR (600 MHz, D_2O, 298 K) titration of cage **1** (1 mM) with malononitrile **5**.

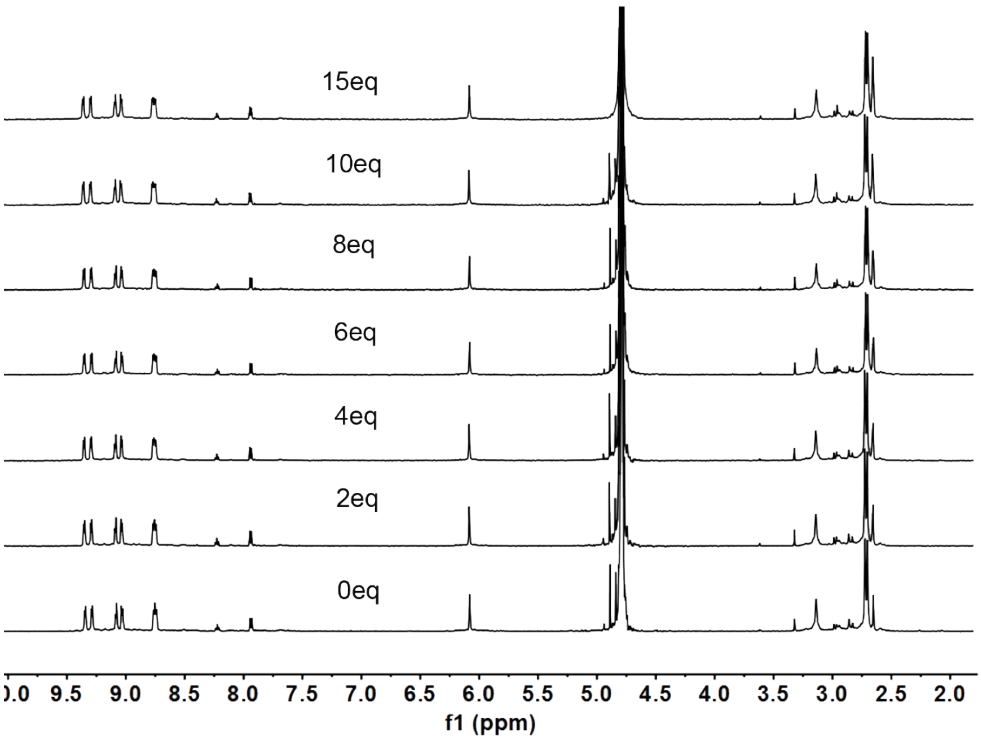

Figure S60. ^{1}H NMR (600 MHz, D_2O, 298 K) titration of cage **1** (1 mM) with **4a**.

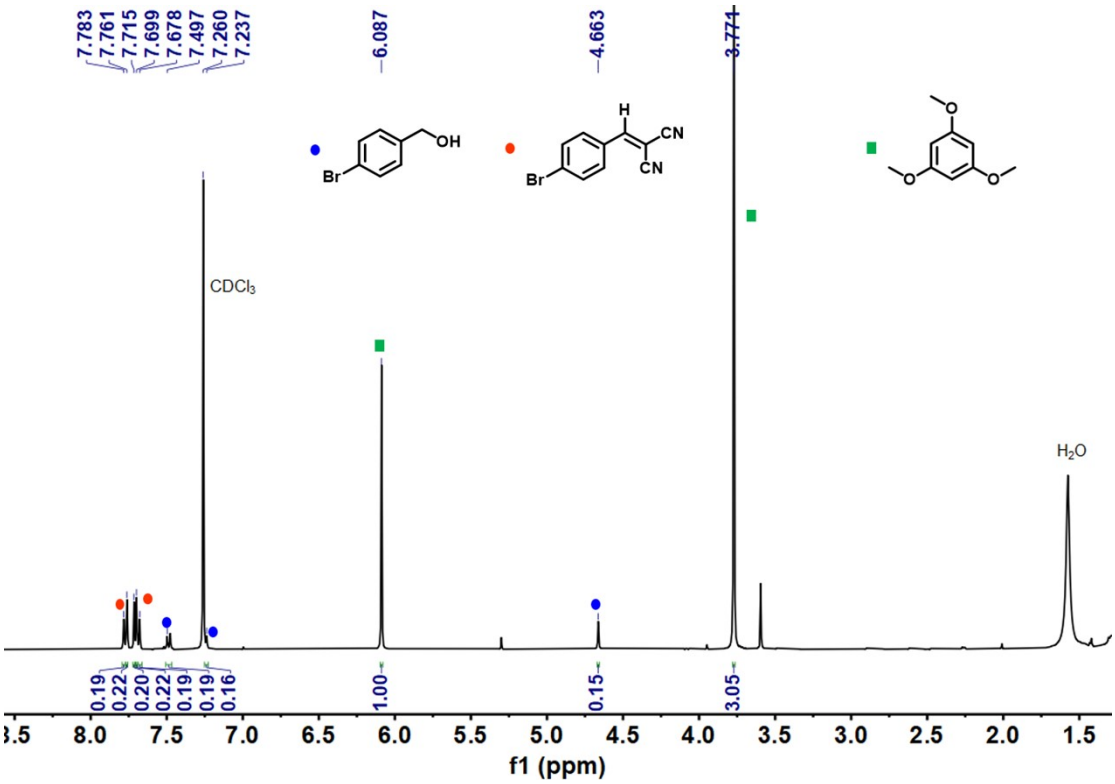

Figure S61. ^{1}H NMR spectra (400 MHz, 298 K, $CDCl_3$) of the crude product with the catalysis of cage **1** (10 mol% catalysis loading) and t-butyl alcohol (10 equiv., scavenger of ·OH). 1,3,5-trimethoxybenzene was used as internal standard. The yield was determined to be 93%.

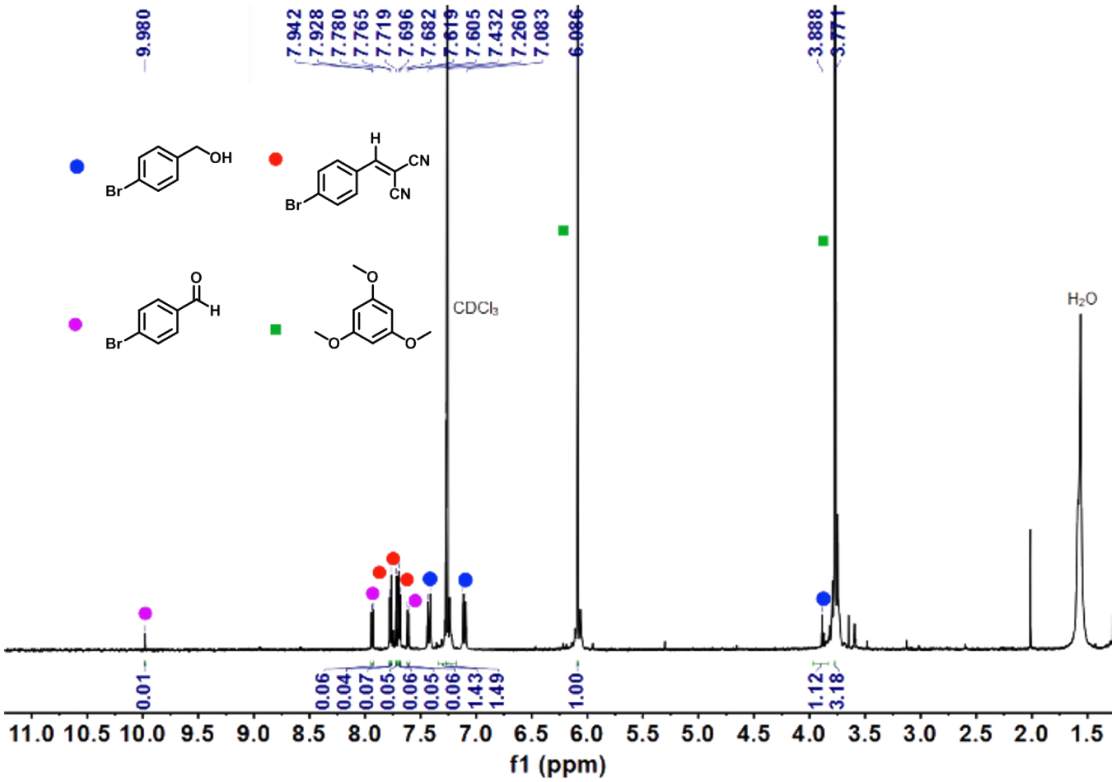

Figure S62. ^{1}H NMR spectra (400 MHz, 298 K, $CDCl_3$) of the crude product with the catalysis of cage **1** (10 mol% catalysis loading) and NaN_3 (10 equiv., scavenger of $^{1}O_2$).

1,3,5-trimethoxybenzene was used as internal standard. The yield was determined to be 8%.

Figure S63. ^{1}H NMR spectra (400 MHz, 298 K, $CDCl_3$) of the crude product with the catalysis of cage **1** (10 mol% catalysis loading) and 1,4-Benzoquinone **(**10 equiv., scavenger of $O_2^{\cdot-}$) . 1,3,5-trimethoxybenzene was used as internal standard. The yield was determined to be 18%.

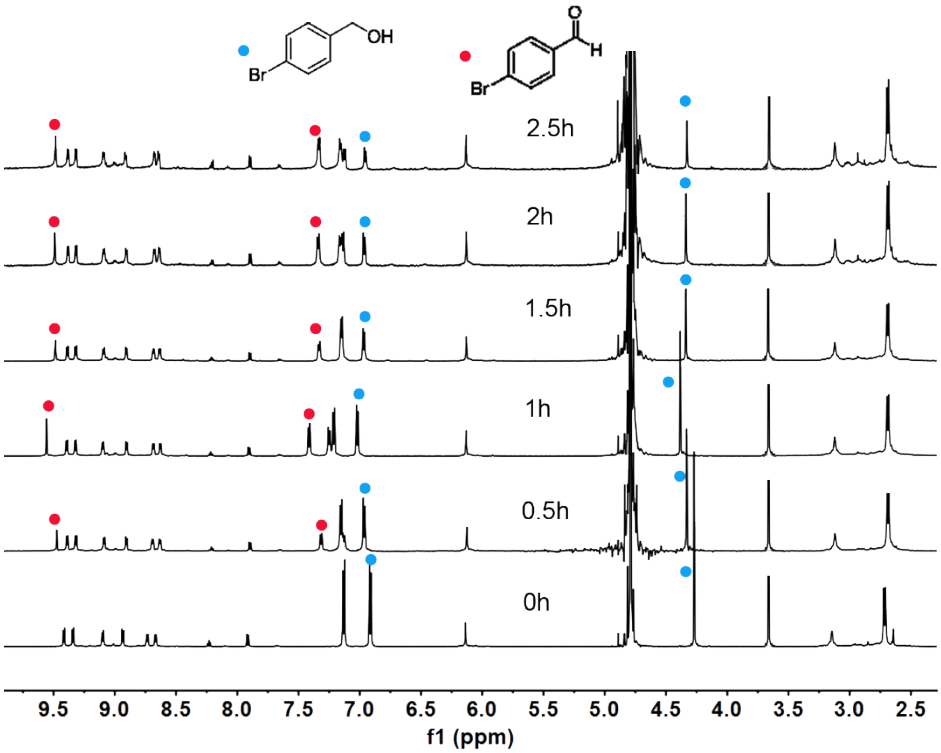

Figure S64. ^{1}H NMR spectra (600 MHz, 298 K, D_2O) of photooxidation of **3a** (10 equiv., under 6 W 395-nm LEDs), with the catalysis of cage **1** (10 mol% catalysis loading). 1,4- dioxane was used as an internal standard.

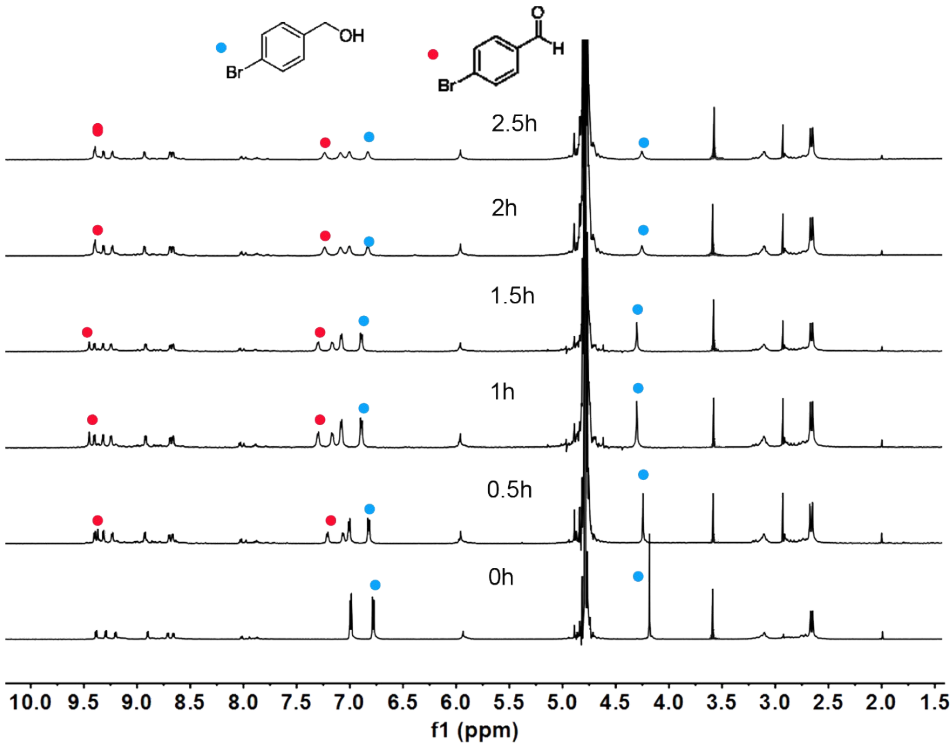

Figure S65. ^{1}H NMR spectra (600 MHz, 298 K, D_2O) of photooxidation of **3a** (10 equiv., under 6 W 395-nm LEDs), with the catalysis of cage **2** (10 mol% catalysis loading). 1,4- dioxane was used as an internal standard.

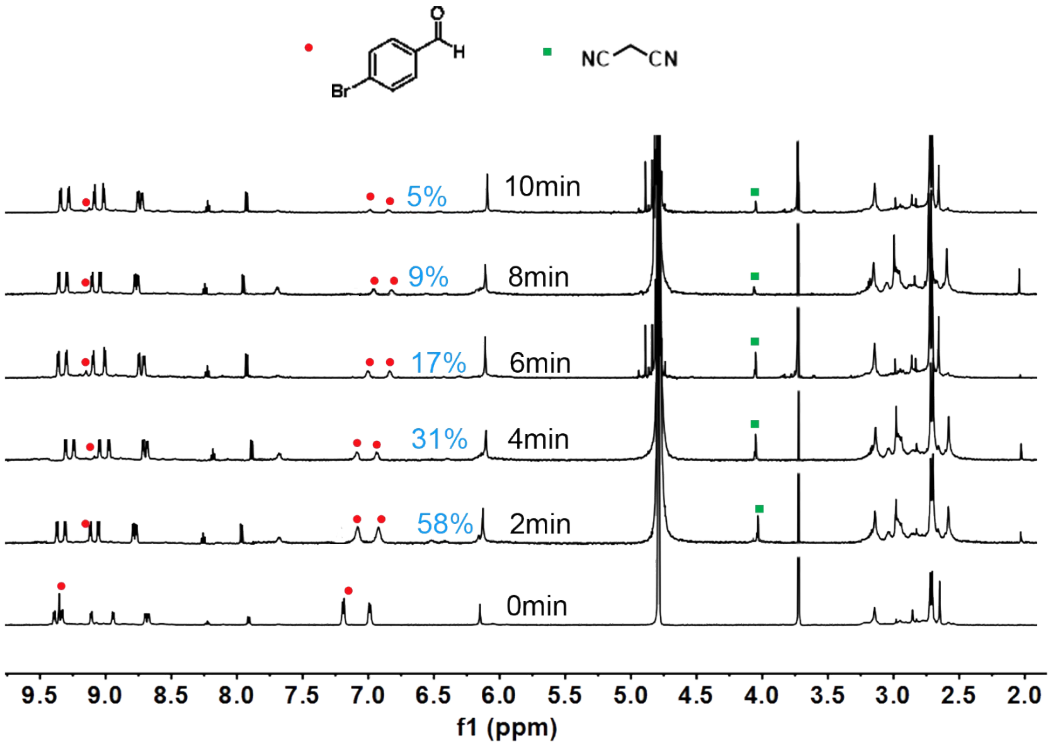

Figure S66. ^{1}H NMR spectra (600 MHz, 298 K, D_2O) of Knoevenagel condensation of 4-bromobenzaldehyde (10 equiv.), with the catalysis of cage **1** (10 mol% equiv. catalysis loading). 1,4- dioxane was used as an internal standard.

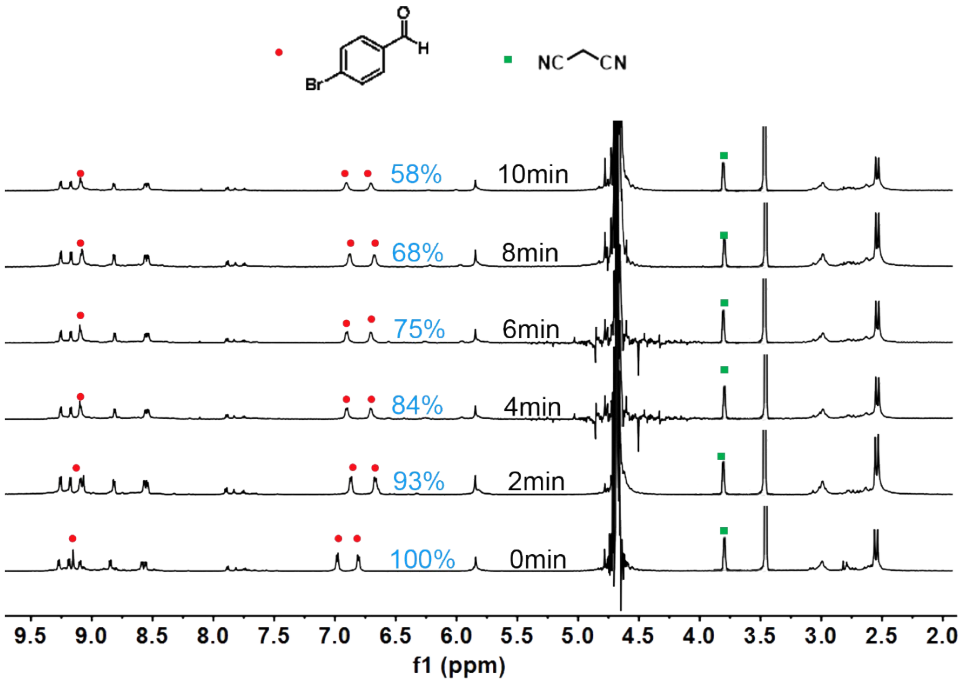

Figure S67. ^{1}H NMR spectra (600 MHz, 298 K, D_2O) of Knoevenagel condensation of 4-bromobenzaldehyde (10 equiv.), with the catalysis of cage **2** (10 mol% catalysis loading). 1,4-dioxane was used as an internal standard.

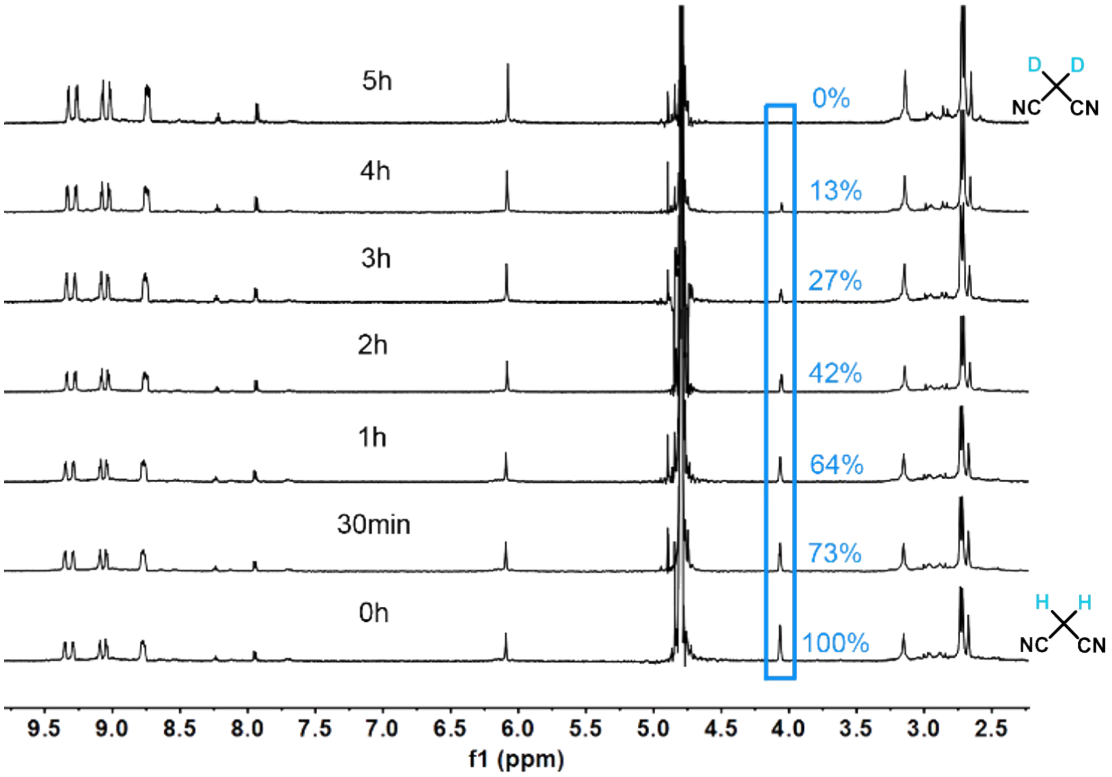

Figure S68. ^{1}H NMR spectra (600 MHz, 298 K, D_2O) of deuteration of **5** (100 equiv.), with the catalysis of cage **1** (10 mol% catalysis loading).

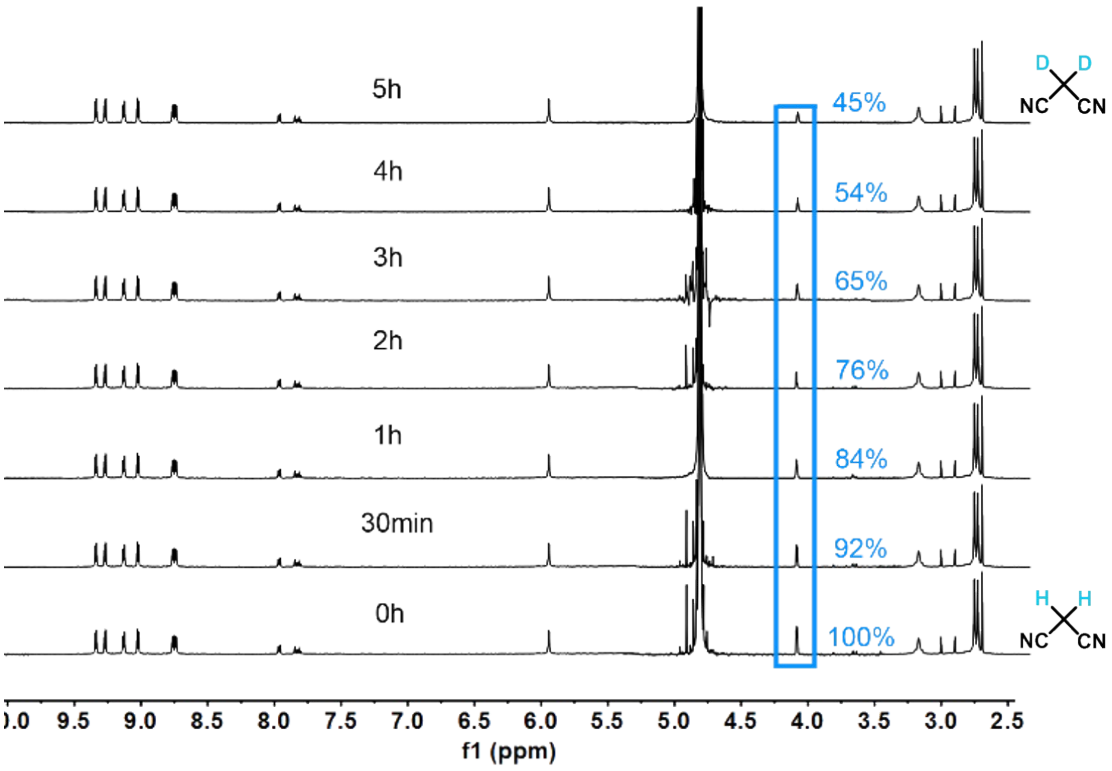

Figure S69. ^{1}H NMR spectra (600 MHz, 298 K, D_2O) of deuteration of **5** (100 equiv.), with the catalysis of cage **2** (10 mol% catalysis loading).

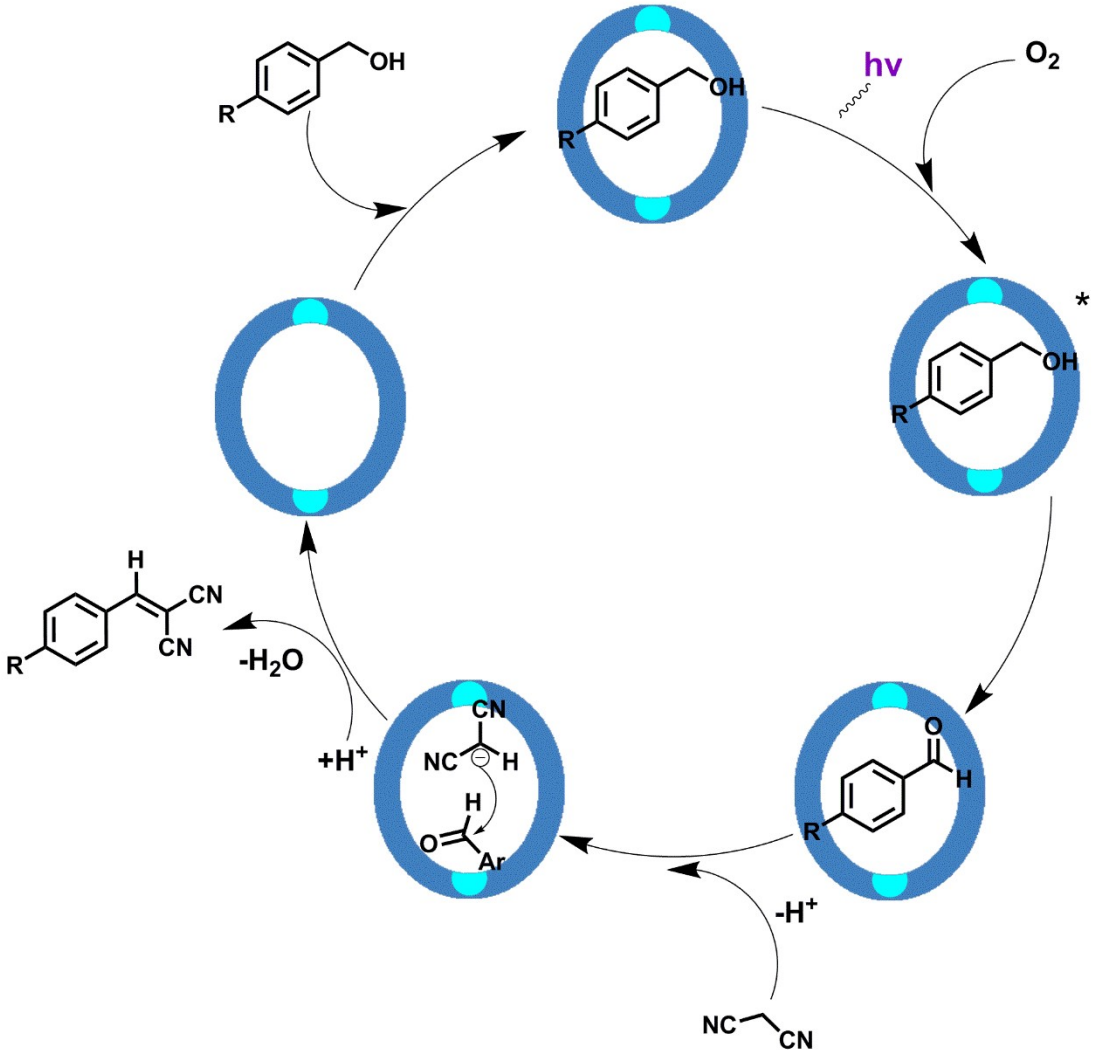

Figure S70. Proposed mechanism for a possible photooxidation-Knoevenagel condensation catalyzed by cage **1**.

7. Crystal data and structure refinement:

Table S2. Statistics vs resolution (taking redundancy into account).

resolution (Å)	# kept	# theory	# unique	% complete	average redundancy	mean F2	mean F2/sig(F2)	Rint	RsigmaB
inf-1.78	17963	3705	3696	99.8	4.9	6110.63	32.62	0.071	0.028
1.78-1.41	18554	3697	3696	100	5	2214.94	24.6	0.123	0.036
1.41-1.23	13375	3699	3696	99.9	3.6	1390.34	18.19	0.115	0.048
1.23-1.12	12637	3698	3696	99.9	3.4	856.5	12.42	0.133	0.072
1.12-1.03	12026	3700	3696	99.9	3.3	543.15	8.39	0.165	0.113
1.03-0.97	11394	3701	3696	99.9	3.1	426.24	6.59	0.2	0.156
0.97-0.92	10707	3709	3696	99.6	2.9	316.72	4.98	0.236	0.221
0.92-0.88	10107	3702	3696	99.8	2.7	229.41	3.76	0.287	0.312
0.88-0.85	9329	3706	3696	99.7	2.5	159.46	2.72	0.333	0.443
0.85-0.82	8565	3741	3701	98.9	2.3	104.75	1.95	0.401	0.647
inf-0.82	124657	37058	36965	99.7	3.4	1602.51	14.05	0.105	0.061

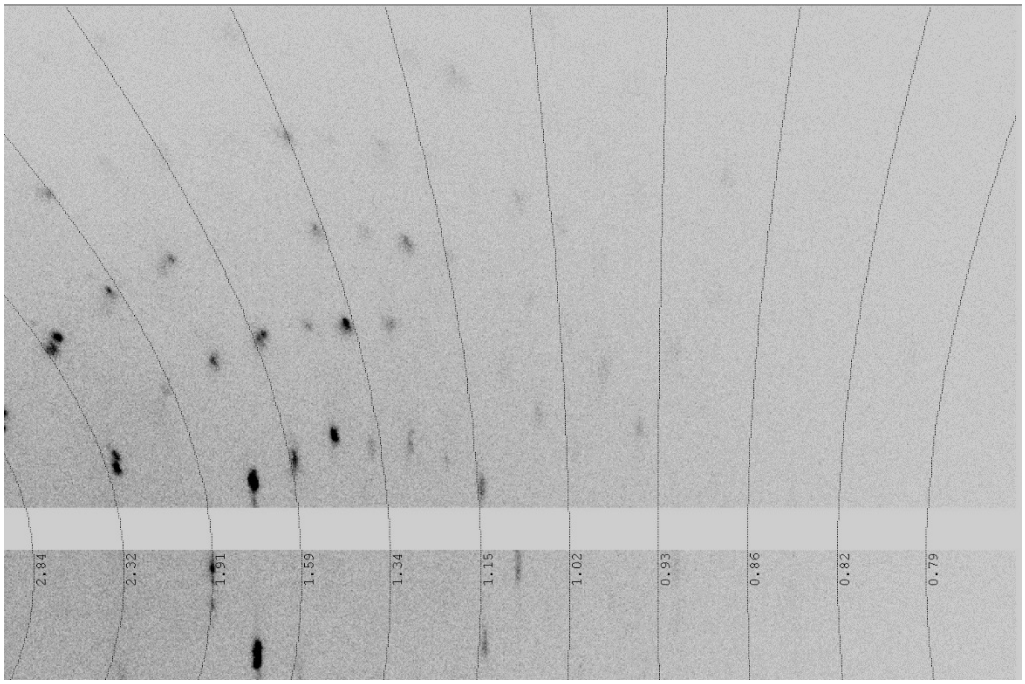

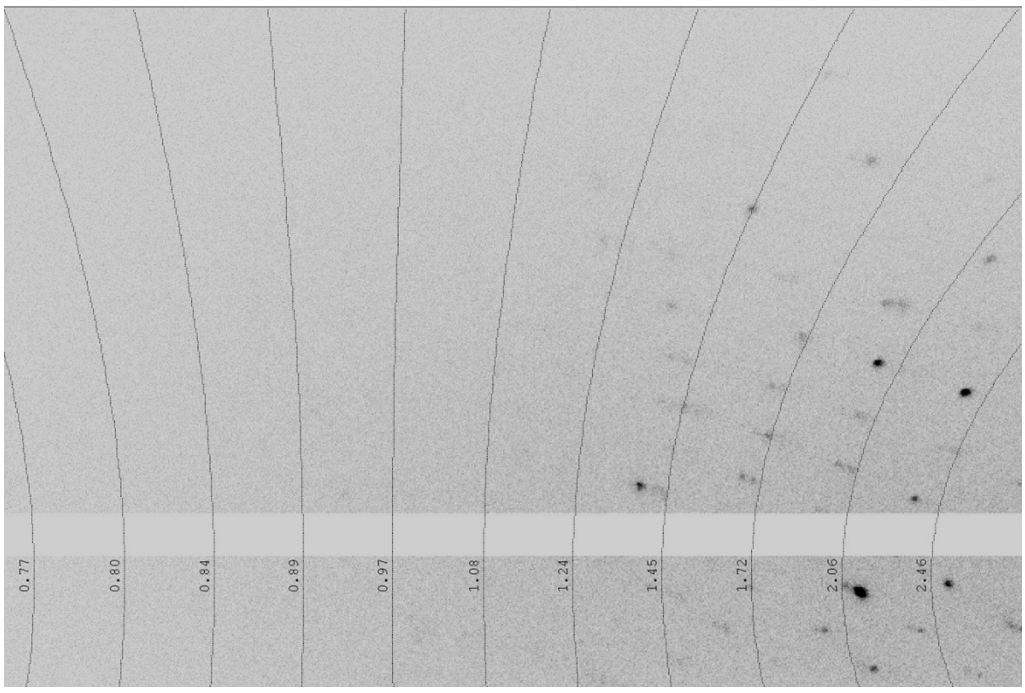

Figure S71. The diffraction image of cage **2** at the first run (up) and the last run (bottom), .

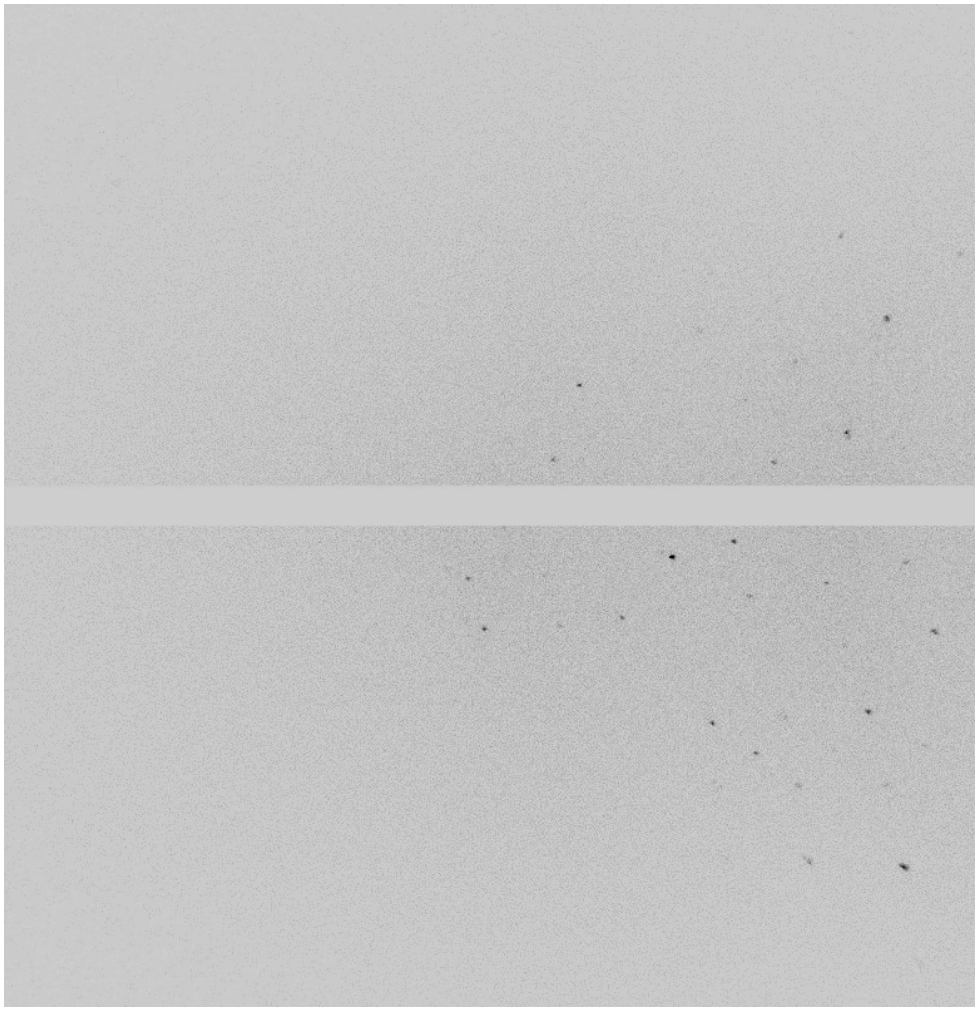

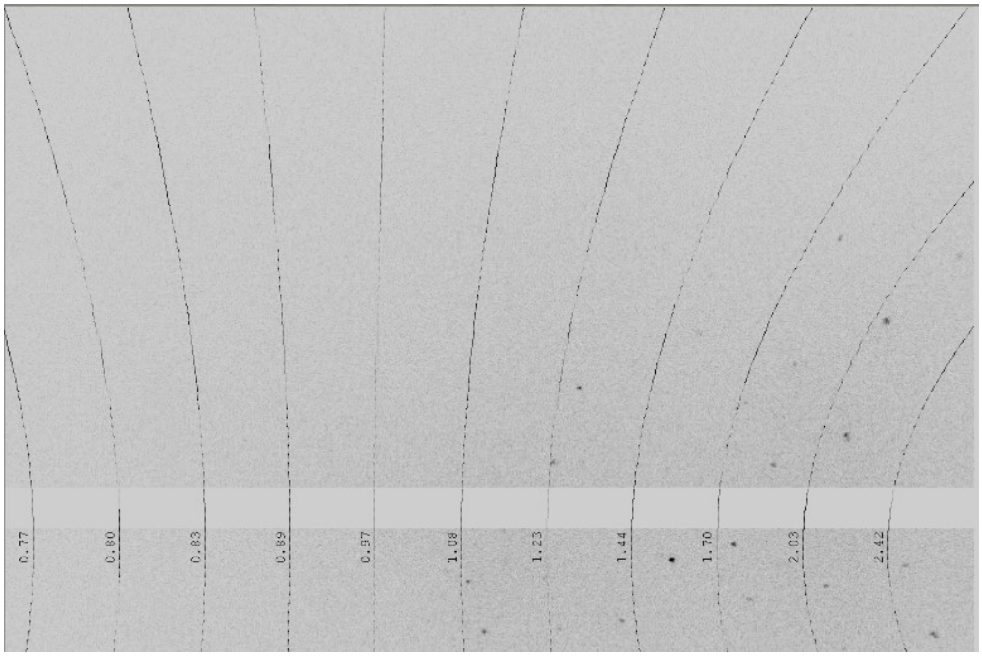

Figure S72. The diffraction image of ligand L^1 with the exposure time of 5 seconds, showing few reflections at greater than 1.08 Å resolution.

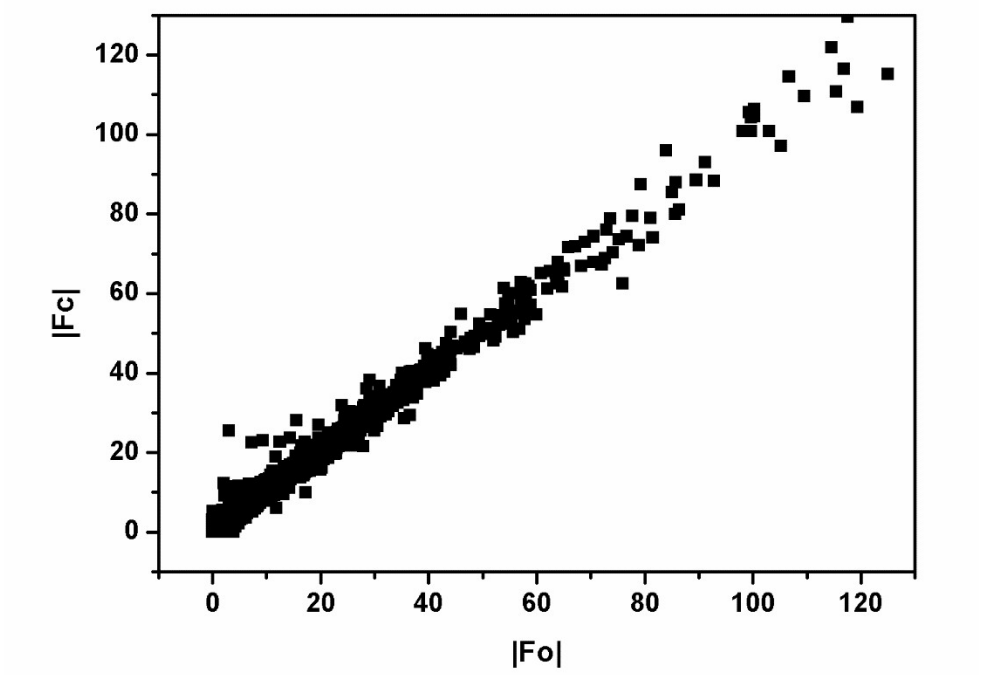

Figure S73. A plot of $|F_{obs}|$ vs $|F_{calc}|$ for the model of ligand L^1.

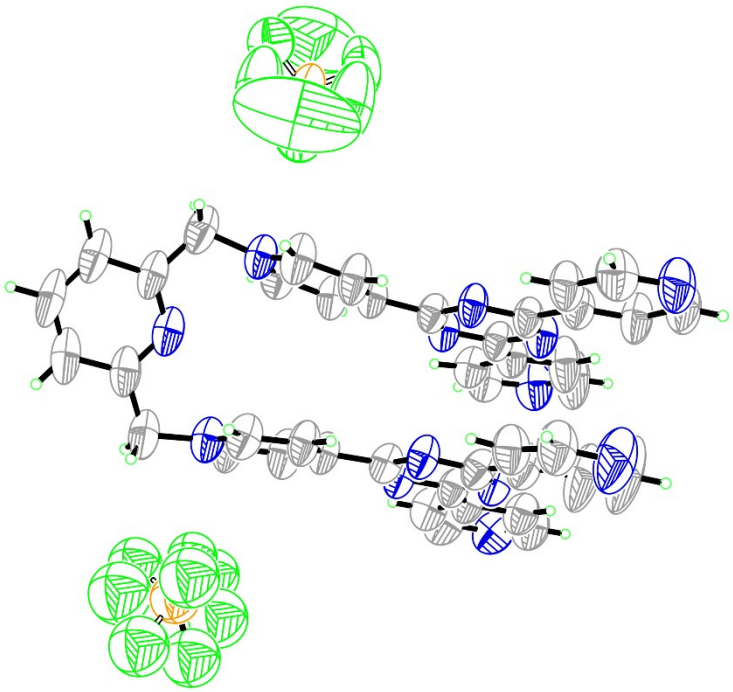

Figure S74. Ortep drawing of the asymmetric unit in the crystal structure of L^1 at 50% robability level.

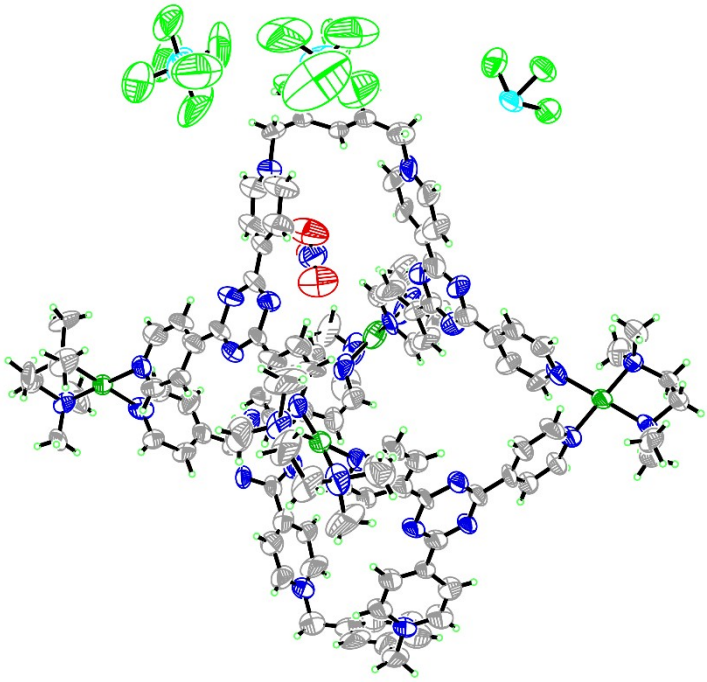

Figure S75. Ortep drawing of the asymmetric unit in the crystal structure of cage **2** at 50% robability level.

Table S3. Crystal data and structure refinement for ligand L^1.

Identification code	L^1	
Empirical formula	C43 H38 B2 F8 N13 O3.50	
Formula weight	966.48	
Temperature	293(2) K	
Wavelength	1.3405 Å	
Crystal system	Triclinic	
Space group	*P*-1	
Unit cell dimensions	a = 12.9685(6) Å	a= 104.732(4)°.
	b = 12.9815(6) Å	b= 108.372(4)°.
	c = 15.4846(8) Å	g = 98.682(4)°.
Volume	2315.6(2) $Å^3$	
Z	2	
Density (calculated)	1.386 Mg/m^3	
Absorption coefficient	0.620 mm^{-1}	
F(000)	994	
Crystal size	0.02 x 0.02 x 0.01 mm^3	
Theta range for data collection	2.761 to 38.344°.	
Index ranges	-11<=h<=11, -12<=k<=12, -14<=l<=14	
Reflections collected	11382	
Independent reflections	3799 [R(int) = 0.0533]	
Completeness to theta = 38.344°	98.9 %	
Refinement method	Full-matrix least-squares on F^2	
Data / restraints / parameters	3799 / 166 / 615	
Goodness-of-fit on F^2	1.070	
Final R indices [I>2sigma(I)]	R1 = 0.0855, wR2 = 0.2526	
R indices (all data)	R1 = 0.1025, wR2 = 0.2684	
Extinction coefficient	n/a	
Largest diff. peak and hole	0.304 and -0.347 $e.Å^{-3}$	

Table S4. Crystal data and structure refinement for cage **2**.

Identification code	**2**	
Empirical formula	C224 H256 F30 N66 O6 Pd8 Si5	
Formula weight	5530.58	
Temperature	100(2) K	
Wavelength	1.3405 Å	
Crystal system	Monoclinic	
Space group	$P2_1/c$	
Unit cell dimensions	a = 19.7341(8) Å	a= 90°.
	b = 58.059(2) Å	b= 114.463(4)°.
	c = 18.5454(7) Å	g = 90°.
Volume	19340.8(14) $Å^3$	
Z	2	
Density (calculated)	0.950 Mg/m^3	
Absorption coefficient	2.402 mm^{-1}	
F(000)	5636	
Crystal size	0.01 x 0.01 x 0.006 mm^3	
Theta range for data collection	2.138 to 56.910°.	
Index ranges	-24<=h<=22, -72<=k<=72, -21<=l<=23	
Reflections collected	129923	
Independent reflections	39474 [R(int) = 0.1088]	
Completeness to theta = 53.543°	99.9 %	
Refinement method	Full-matrix least-squares on F^2	
Data / restraints / parameters	39474 / 124 / 1528	
Goodness-of-fit on F^2	1.482	
Final R indices [I>2sigma(I)]	R1 = 0.1544, wR2 = 0.3960	
R indices (all data)	R1 = 0.1773, wR2 = 0.4092	
Extinction coefficient	n/a	
Largest diff. peak and hole	2.079 and -2.649 $e.Å^{-3}$	

8. Supplementary reference:

S1. Agilent Technologies,CrysAlisPro v. 1.171.36.28, ***2013***

S2. G. M. Sheldrick. *Acta Crystallogr. Sect. A*., **2008**, *64*, 112.

S3. A. L., Spek, *J. Appl. Crystallogr.*, **2003**, 36, 7-13.

S4. (a) H. Takezawa, T. Murase, G. Resnati, P. Metrangolo, and M. Fujita, *J. Am. Chem. Soc.* **2014**, *136*, 1786. (b) D. Yang, J. L. Greenfield, T. K. Ronson, L. K. S. von Krbek, L. Yu, and J. R. Nitschke, *J. Am. Chem. Soc.* **2020**, *142*, 19856. (c) K. Li , K. Wu, Y. L. Lu, J. Guo, P. Hu and C. Y. Su, *Angew. Chem. Int. Ed.*, **2022**, *61*, e202114070.